Speed Sensorless and MPPT Control of IPM Synchronous Generator for Wind Energy Conversion System

by

Nirav R. Patel

SUBMITTED IN PARTIAL FULFILLMENT OF THE

REQUIREMENTS FOR THE DEGREE OF

MASTER OF SCIENCE

AT

LAKEHEAD UNIVERSITY

THUNDER BAY, ONTARIO

May, 2013

Abstract

The popularity of renewable energy has experienced significant growth recently due to the foreseeable exhaustion of conventional fossil fuel power generation methods and increasing realization of the adverse effects that conventional fossil fuel power generation has on the environment. Among the renewable energy sources, wind power generation is rapidly becoming competitive with conventional fossil fuel sources. The wind turbines in the market have a variety of innovative concepts, with proven technology for both generators and power electronics interfaces. Recently, variable-speed permanent magnet synchronous generator (PMSG) based wind energy conversion systems (WECS) is becoming more attractive in comparison to the fixed-speed WECS. In the variable-speed generation system, the wind turbine can be operated at maximum power operating points over a wide speed range by adjusting the shaft speed optimally.

This thesis presents both wind and rotor speed sensorless control for the direct-drive interior permanent magnet synchronous generator (IPMSG) with maximum power point tracking (MPPT) algorithm. The proposed method, without requiring the knowledge of wind speed, air density or turbine parameters, generates optimum speed command for speed control loop of vector controlled machine side converter. The MPPT algorithm based on perturbation and observation uses only estimated active power as its input to track peak output power points in accordance with wind speed change and incorporates proposed sensorless control to transfer maximum dc-link power from generator.

In this work for the IPMSG, the rotor position and speed are estimated based on model reference adaptive system. Additionally, it incorporates flux weakening controller (FWC) for wide operating speed range at various wind speed and other disturbances. Matlab/Simulink based simulation model of the proposed sensorless MPPT control of IPMSG based WECS is built to verify the effectiveness of the system. The MPPT controller has been tested for variable wind speed conditions. The performance of the proposed WECS is also compared with the conventional control of WECS system. The proposed IPMSG based WECS incorporating the MPPT and sensorless algorithms is successfully implemented in real-time using the digital signal processor (DSP) board DS1104 for a laboratory 5 hp machine. A 5 hp DC motor is used as wind turbine to drive the IPMSG. The speed tracking performance and maximum power transfer capability of the proposed WECS are verified by both simulation and experimental results at different speed conditions.

Acknowledgements

I would like to express my most sincere gratitude to God and those people who have supported and helped me in the preparation of this thesis. Dr. M. N. Uddin, my thesis supervisor, has been vital in the completion of this thesis and success of the project. It is due to his constant inspiration and encouragement that I have gained a deeper understanding of engineering and made progress toward solving problems and improving my skills as a researcher. This work might not be possible without his guidance. I wish to thank my thesis committee members Dr. Krishnamoorthy Natarajan and Dr. Dimiter Alexandrov. I acknowledge the support from Lakehead University professors for their guidance to complete my thesis. I would like to give many thanks to my fellow graduate students, especially Bhavin Patel for his guidance throughout the last two years, and staff of Lakehead University.

Numerous people and innumerable instances, which I cannot enumerate in a single page, have helped me to accomplish this project. Finally I'd like to express sincere appreciation to my parents, Rukhiben and Rameshbhai Patel, and friends who have always been patient and supportive to me. I would like to appreciate all the circumstances around me, which have been so generous to this humble being.

Table of Contents

Table of Figures

List of Symbols

A	Swept area of the turbine blades
B_m	Friction damping coefficient
C_p	Wind turbine power coefficient
I_a	Armature current
I_a, I_b, I_c	a,b and c line currents
I_d	d-axis current
I_f	Field current
I_q	q-axis current
J	Rotor inertia constant
l	Tip speed ratio (directly proportional to rotor speed and inversely proportional to wind speed)
L_d	d-axis inductance
L_q	q-axis inductance
m	Mass
M_{ab}, M_{bc}, M_{ca}	Mutual inductances
P_n	Number of pole pairs
P_{Cu}	Iron loss

P_{dc}	Load power
P_{Fe}	Copper loss
P_m	Mechanical power available from wind
P_n	Number of poles
P_w	Kinetic energy per unit time
R_c	Core loss resistance
R_s	Stator resistance
S1-S6	IGBT switches
T_e	Developed electromagnetic torque
T_m	Mechanical torque provided by wind turbine
T_{opt}	Optimum Torque
V_a, V_b, V_c	a,b and c line voltages
V_{base}	Base wind component
V_d	d-axis voltage
V_{dc}	DC link load voltage
V_g	Gust wind component
V_m	Maximum stator phase voltage
V_n	Base noise wind component
V_q	q-axis voltage
V_r	Ramp wind component

V_s	Wind speed
β	Pitch angle
θ	Rotor position
ρ	Air density (1.2kg/m³ @ sea level and 20° C)
Ψ_a, Ψ_b, Ψ_c	Air gap flux linkage for the phase a, b, c, respectively
$\Psi_{am}, \Psi_{bm}, \Psi_{cm}$	Flux linkages in the three phase stator winding
ψ_d, ψ_q	d-q axis flux linkages
Ψ_m	Magnetic flux linkage
ω	Electrical angular speed
ω_r	Rotor speed
ω_{ref}	Reference rotor speed

List of Acronyms

AC	Alternative Current
CS	Constant Speed
DC	Direct Current
DD	Direct Drive
DFIG	Doubly Fed Induction Generator
DSP	Digital Signal Processor
EMF	Electromotive Force
FOC	Field Oriented Control
FWC	Flux Weakening Control
HAWT	Horizontal Axis Wind Turbine
IG	Induction Generator
IPMSG	Interior Permanent Magnet Synchronous Generator
IPMSM	Interior Permanent Magnet Synchronous Machine
MPPT	Maximum Power Point Tracking
MRAS	Model Reference Adaptive System
MTPA	Maximum Torque Per ampere
PE	Power Electronics
PI	Proportional Integral
PLL	Phase Lock Loop
PM	Permanent Magnet

PMSG	Permanent Magnet Synchronous Generator
PMSM	Permanent Magnet Synchronous Machine
PO	Perturbation and Observation
PWM	Pulse Width Modulation
RTI	Real Time Interface
SHE	Selected Harmonic Elimination
SMO	Sliding Mode Observer
SPMSM	Surface Mounted Permanent Magnet Synchronous Machine
SVM	Space Vector Modulation
THD	Total Harmonic Distortion
VAWT	Vertical Axis Wind Turbine
VSC	Voltage Source Converter
VSR	Voltage Source Rectifier
WECS	Wind Energy Conversion System
WT	Wind Turbine
WTG	Wind Turbine Generator

Chapter 1

Introduction

Recently, increasing concerns on energy crisis and environmental pollution caused by finite energy sources have promoted significant utilization of renewable sources. Solar, wind, hydro, bio-mass and geothermal are considered as renewable energy sources.

1.1 Research Motivation

Among various renewable energy sources, hydro energy has been used widely because it provides low cost per watt hour and predictable energy supply. However, it is only usable in limited areas. In addition, it has potentially large environmental impact; for example, flooding and dams. Another popular renewable energy source, solar energy has very low maintenance, simple installation and can be used everywhere. However, environmental impact of solar panel production and after use waste is an issue. Moreover, it also requires good sun exposure, which could be a concern during winter or rainy sessions. On the other hand, wind is an abundant renewable energy source that is available everywhere. Among these renewable energy sources, wind energy has received great attention as safe and clean renewable power source [1-7]. Wind energy is an indirect form of solar energy in contrast to the direct solar energy. Solar irradiation causes temperature differences on earth and which causes wind flow. Wind can reach much

higher power densities than solar irradiation: 10 kW/m^2 during a violent storm and over 25 kW/m^2 during a

Total Installed Capacity 2010-2012 [MW]

(a)
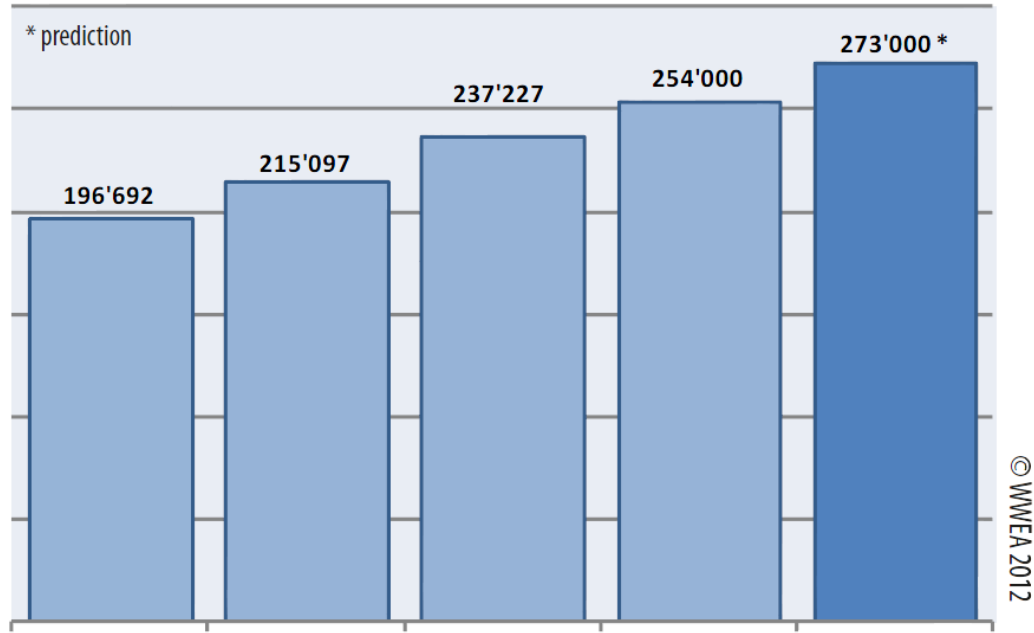
Total Installed Capacity 2011-2012 [MW]

* till end of May 2012   ** till end of April 2012
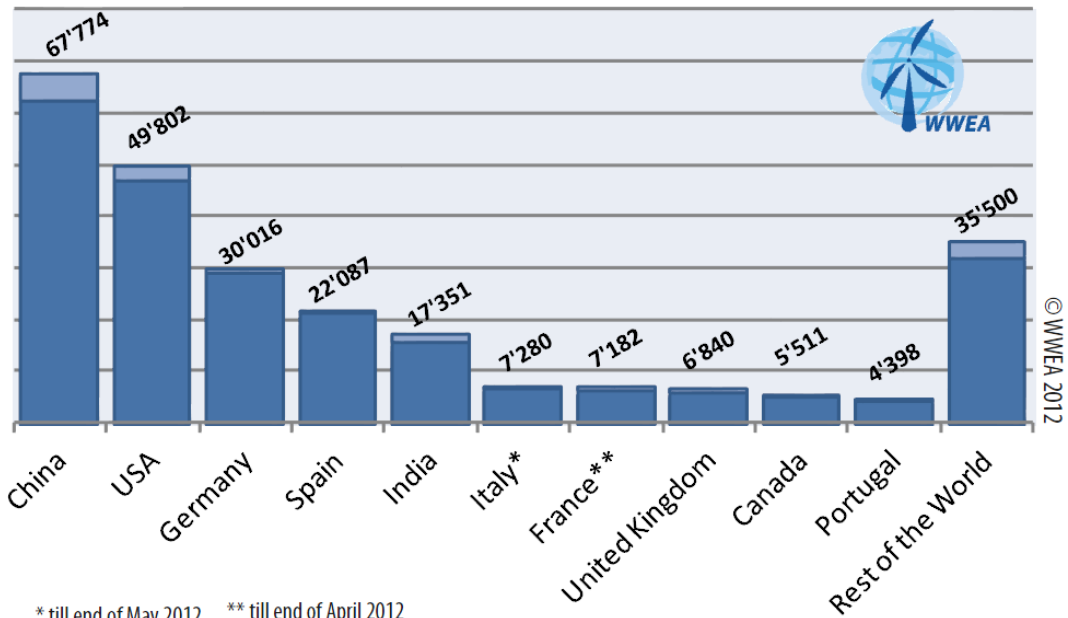
■ Capacity installed end 2011   ■ New capacity installed 1st half 2012

Fig. 1. 1 Total installed wind power capacity (a) in 2010-2012 (MW) around the world (b) in 2010-2012 (MW) in different countries [9].

hurricane, compared with the maximum terrestrial solar irradiance of about 1 kW/m^2 [8]. However, a gentle breeze of 5 m/s has a power density only 0.075 kW/m^2.

Wind energy is now achieving an exponential growth and has great potential in coming decades. According to world wind energy association, there has been 16,5 GW of new installations in the first half of 2012, after 18,4 GW in 2011. Worldwide wind capacity has reached 254 GW by June 2012, and 273 GW expected by the end of 2012 [9].

The wind energy conversion systems (WECS) are complex, nonlinear and are subject to parameters uncertainties and unknown disturbances [10]. For a fixed speed wind turbine generators (WTG), rotor speed is constant at varying wind speed which reduces overall efficiency considering power available in wind and extracted power. Using variable speed WTG where rotor speed is controlled optimally, maximum power can be extracted from wind. Hence, it is important to design a control technique which can track maximum power changing generator speed optimally for wide speed range. Moreover, the controller has to be WT parameter independent.

Control, monitoring, and protection of WTG usually require the information of wind speed and generator rotor position. These can be measured by well-calibrated mechanical sensors, such as anemometers and rotor position sensors. However, the use of these mechanical sensors increases the cost and failure rate of the WTG systems. According to [11], sensor failures contribute to more than 14% of failures in WTG systems and more than 40% of failures are related to the failure of sensors and the consequent failures of the control or electrical systems. Repairing the failed components requires additional cost and leads to a significant loss in electric

power production. It is important to design proper controller to track maximum power point of wind turbine (WT) without relying on wind speed or rotor position sensors. In order to reduce overall operating cost and expand rotor operating speed range, high efficiency power electronic converters need to be implemented and sophisticated control algorithms should be developed to extract optimal power at all atmospheric conditions.

1.2 Literature Survey on WECS

Wind energy harvesting has been a very long tradition. Some historians suggest that wind mills were used over 3000 years ago. Until the early twentieth century wind power was used to provide mechanical power to water pump, boats, ships and grinding mills. At the beginning of the last century the first wind turbines appeared and technology was improved step by step from the early 1970s. By the end of the 1990s, wind energy has come back as one of the most important sustainable energy resources, partly because of the increasing price of the oil, security concerns of nuclear power and its environmental issues [8].

1.2.1 Wind Energy Conversion

The sun heats up air masses in the atmosphere. The spherical shape of the Earth, the Earth's rotation and seasonal and regional fluctuations of the solar radiance cause spatial air pressure differentials. These are the source of air movements. Wind resources are particularly high in coastal areas because wind can move unhindered across the smooth surface of the sea. Furthermore, temperature differences between water and land cause local compensating streams. The sunlight heats the land more quickly than the water during the day. The results are pressure differentials and compensating winds in the direction of the land.

Wind energy systems convert the kinetic energy of the wind into the electrical energy. The kinetic energy produced by a moving object $E_{kinetic}$ is expressed by the following equation [8]:

$$E_{kinetic} = \frac{1}{2}mv_s^2 \qquad (1.1)$$

Where, m and v_s are mass and wind velocity of the object respectively.

The power (P_w) is this kinetic energy per unit time (joules /sec or watts).

$$P_w = \frac{1}{2}\dot{m}v_s^2 \qquad \text{(Assuming } v_s \text{ is constant)} \qquad (1.2)$$

Here, $\dot{m}$ is the mass of air flowing per unit time, thus it can be defined as,

$$\dot{m} = \rho A v_s \qquad (1.3)$$

where, v_s - wind velocity; m - mass of air; A - swept area of the turbine blades; ρ- density of air (1.225 kg/m^3 @ sea level and 20° C)

So, mechanical power of due to wind flow can be written as,

$$P_w = \frac{1}{2}\rho A v_s^3 \qquad (1.4)$$

When using wind rotors to extract wind power (i.e., wind turbine), it's not 100% efficient. In 1919, a German physicist Albert Betz found limit of power conversion factor 16/27ths (i.e., 59.3%) of the kinetic energy into mechanical power (P_m). This conversion factor is known as C_p constant or Betz limit, and is a theoretical maximum coefficient of power for any wind turbine.

This constant is a measurement of how efficiently the wind turbine converts the energy in the wind into electrical energy.

The power coefficient can be utilized in the form of a look-up tables or in form of a function. The second approach is presented below, where the general function defining the power coefficient as a function of the tip-speed ratio and the blade pitch angle is defined as [12],

$$C_P(\lambda, \beta) = C_1 [C_2 \frac{1}{\mu} - C_3 \beta - C_4 \beta^x - C_5] e^{-C_6(\frac{1}{\mu})}$$

1.5)

$$\frac{1}{\mu} = \frac{1}{\lambda + 0.08\beta} - \frac{0.035}{1 + \beta^3}, \qquad \lambda = \frac{\omega_r R}{v_s}, \qquad \omega_r = \frac{\omega}{P}$$

(1.6)

where, C1= 0.5 , C2= 116 , C3= 0.4 , C4= 0 , C5= 5, C6= 21; β - pitch angle; ω_r- shaft speed [rad/s], ω- electrical angular velocity [rad/s], R - rotor radius [m]; v_s - wind speed [m/s], **l** -tip speed ratio, and P- pole pairs of the wind generator.

Wind speed model is given by the following equation:

$$v_s(t) = v_b(t) + v_r(t) + v_g(t) + v_n(t)$$

(1.7)

where, v_b-base wind component; v_r- ramp wind component; v_g- gust wind component; v_n- base noise wind component.

Therefore mechanical power available from wind turbine is given by,

$$P_m = \frac{1}{2}\rho A v_s^3 C_P(\lambda, \beta)$$

(1.8)

and mechanical torque is given by,

$$T_m = \frac{\pi}{2} \rho C_p(\lambda, \beta) \frac{R^2 v_s^3}{\omega_r}$$

(1.9)

6

Here C_p is a function of tip speed ratio **l** and pitch angle β, which can be seen in Fig. 1.2. At zero pitch angle maximum power can be extracted from wind. Fig. 1.3 shows mechanical power as a function of wind speed at different rotor speed.

In Fig 1.4 output power is shown as a function of C_p at various wind speed. At cut in speed WT starts producing usable power. By tracking maximum C_p, the maximum power can be obtained up to rated wind speed of the turbine. Above the rated speed, WT power will remain constant at the rated value (maximum), until the wind speed reaches the cut-out speed. If speed keeps increasing above the cut-out speed, WT failure could occur. In this condition, some control technique, such as flux weakening control, is necessary for WT's safe operation.
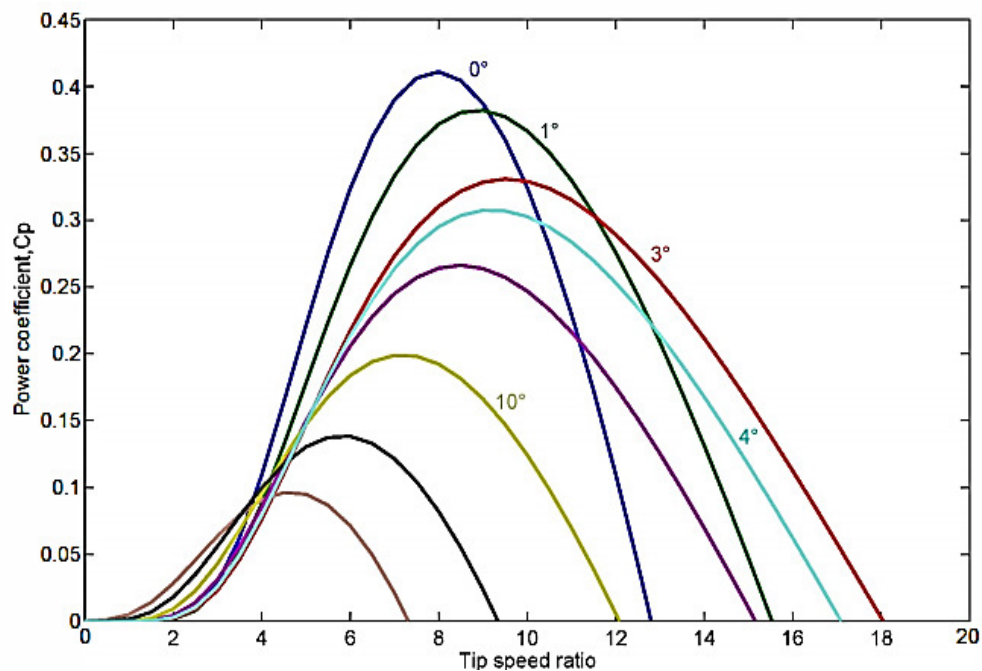
Fig. 1. 2 Power coefficient Cp as a function of the tip speed ratio λ and the pitch angle β.
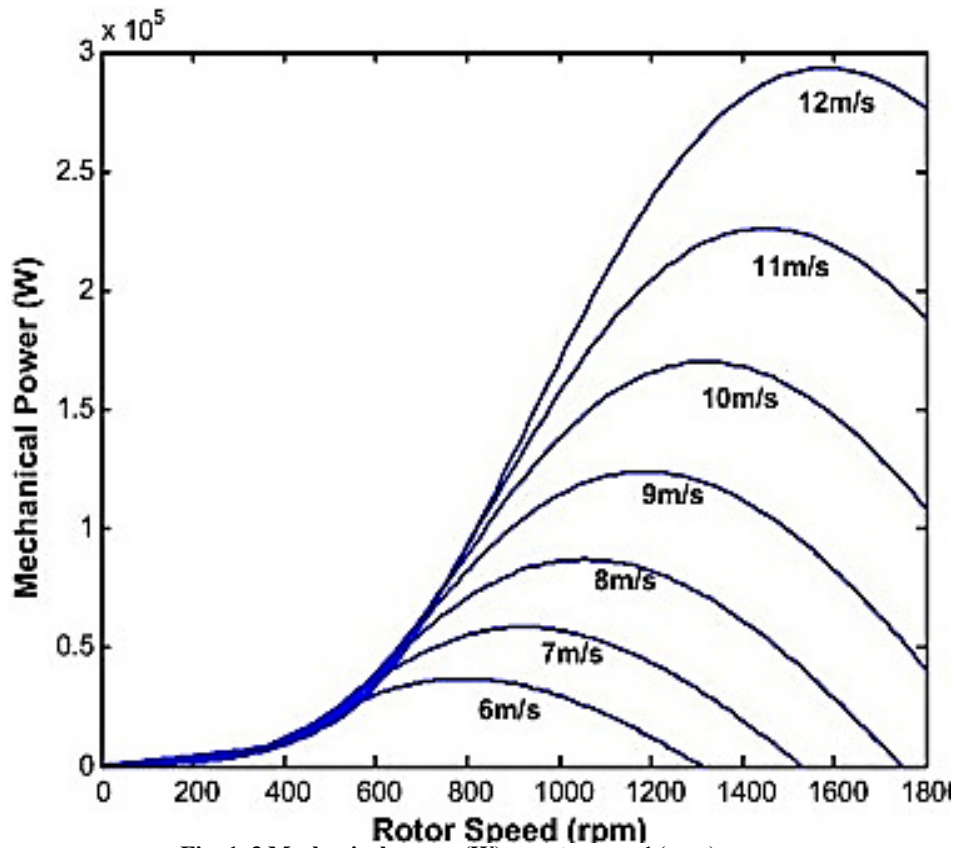
Fig. 1. 3 Mechanical power (W) vs rotor speed (rpm).
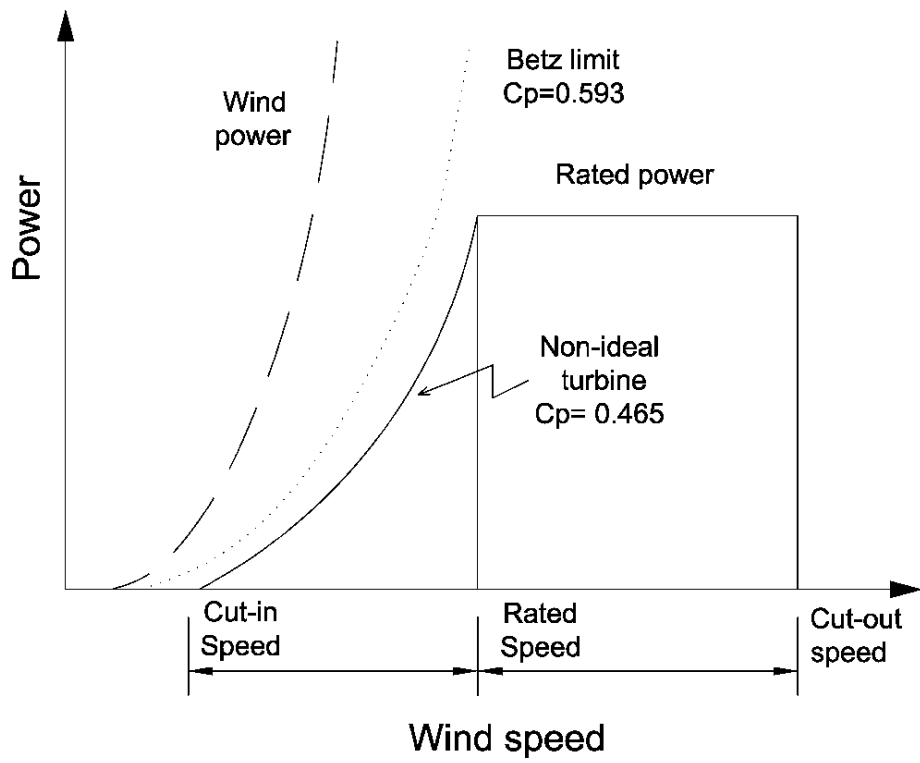
Fig. 1. 4 Wind speed vs variation of turbine power with wind speed.

8

1.2.2 Wind Energy Conversion System (WECS) Overview

In the WECS, captured wind energy by wind turbine is converted into electrical energy using generator. The WECS is a complex system because it includes concepts form aerodynamics and mechanical, control and electrical engineering. The WECS is composed of wind turbine blades, an electric generator, a power electronic converter and the corresponding control system. As shown in Fig 1.5-1.6, there are different WECS configurations based on using synchronous or asynchronous machines, and stall-regulated or pitch regulated systems. However, the functional objective of these systems is the same: converting the wind kinetic energy into electric power and injecting this electric power into a utility grid. To make WECS more efficient, combination of different control techniques from engineering fields have been implemented in past few decades [13-42]. In WECS, energy conversion is mainly divided into four categories [13, 16, 28]:

(a) Fixed speed wind turbine with an asynchronous squirrel cage induction generator (IG) connected to the grid.

(b) Variable speed wind turbine with a doubly fed induction generator (DFIG) and blade pitch control.

(c) Variable speed wind turbine using a permanent magnet synchronous generator that is connected to the grid through a full-scale frequency converter. This is called direct drive (DD) wind turbine.

(d) Brushless generator with gear and connected to the grid through a full scale freq. converter.

(a)

(b)

(c)

(d)
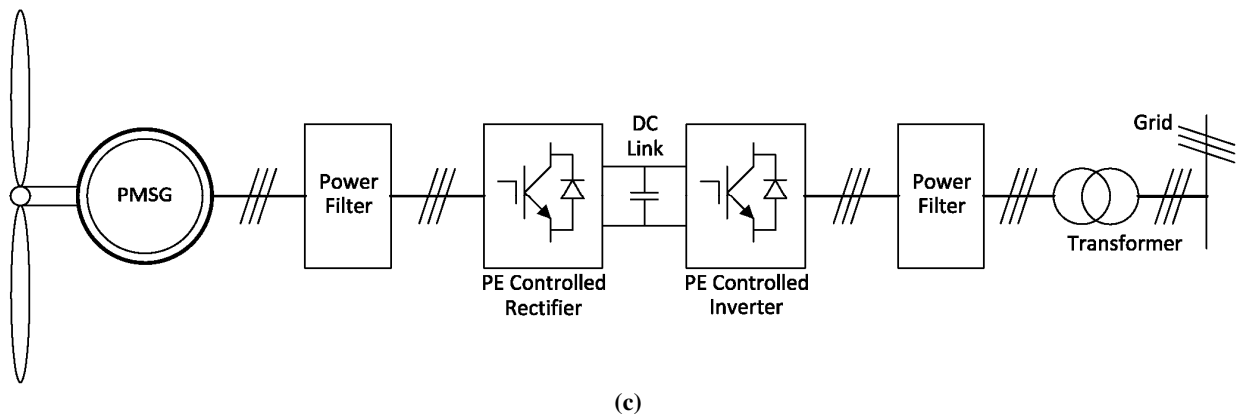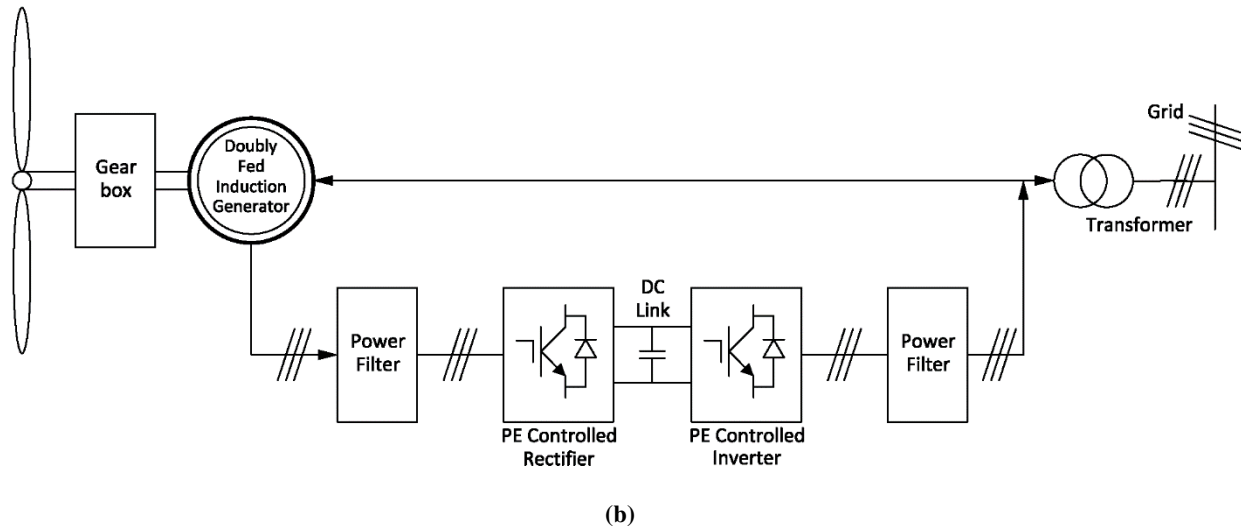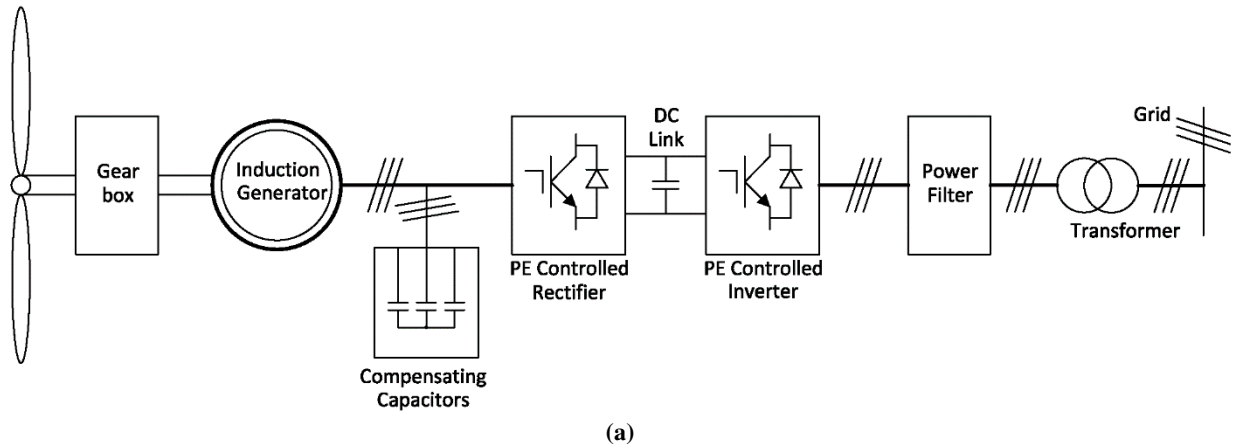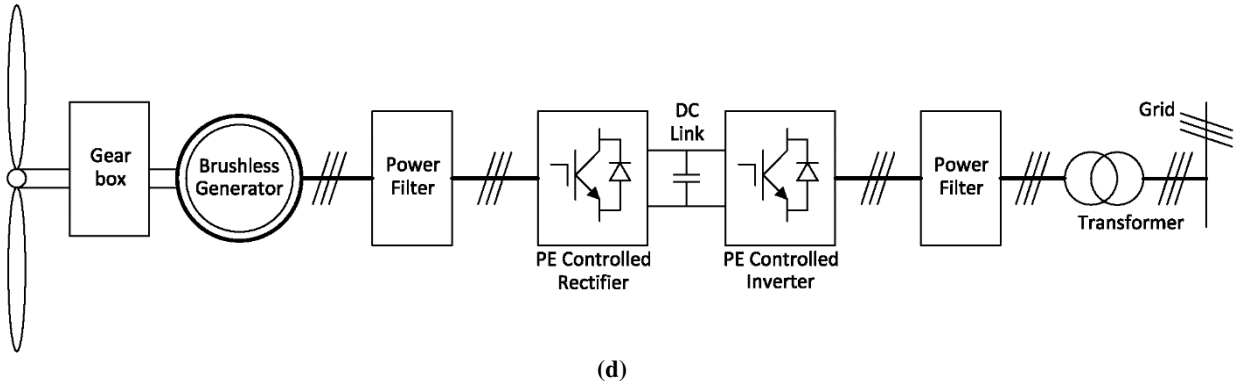
Fig. 1. 5 WECS categories (a) fixed speed wind turbine with an asynchronous squirrel cage IG (b) variable speed wind turbine with a DFIG (c) variable speed wind turbine using PMSG (d) brushless generator with gear box.
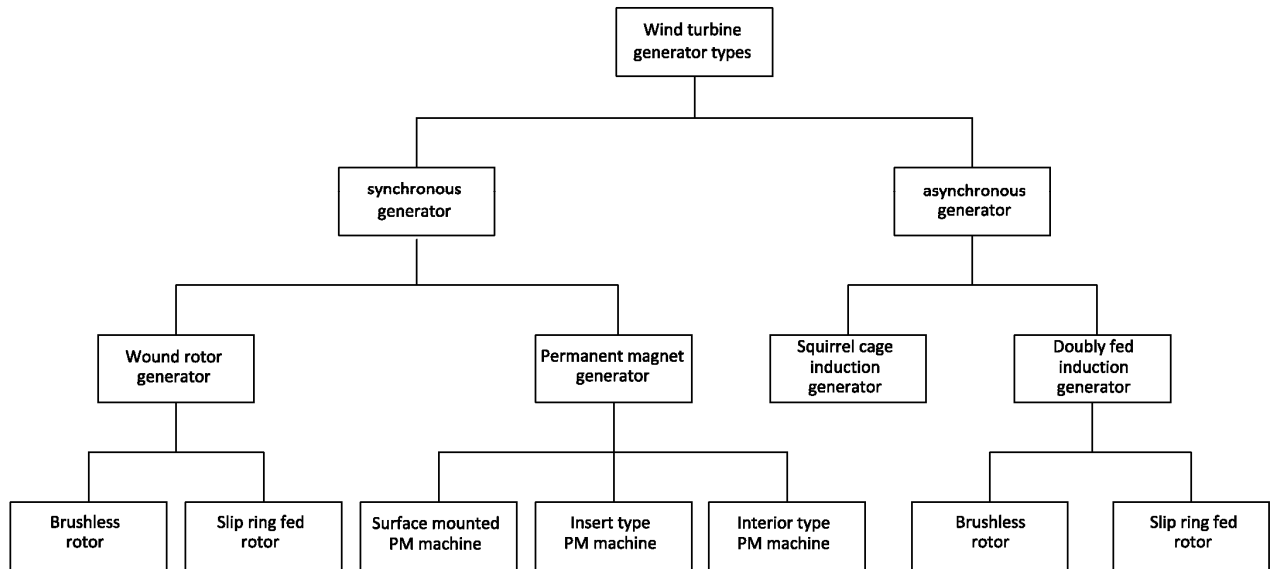
Fig. 1. 6 Wind turbine generator types.

In fixed speed wind turbines, IGs are very commonly used. The wind turbine system in Fig. 1.5(a) is using IG, which almost independent of torque variation operating at a fixed speed with 2-3% slip condition. The power is limited aerodynamically either by stall, active stall or by pitch control. All three systems are using a soft-starter in order to reduce the inrush current and thereby limit flicker problems on the grid. They also need a reactive power compensator to reduce the reactive power demand from the turbine generators to the grid. Those solutions are

attractive due to low cost, but they are not able to control the active power very fast. Fig 1.7 shows the typical models of constant speed WT with gear box and direct drive WT.

<center>(a)   (b)</center>
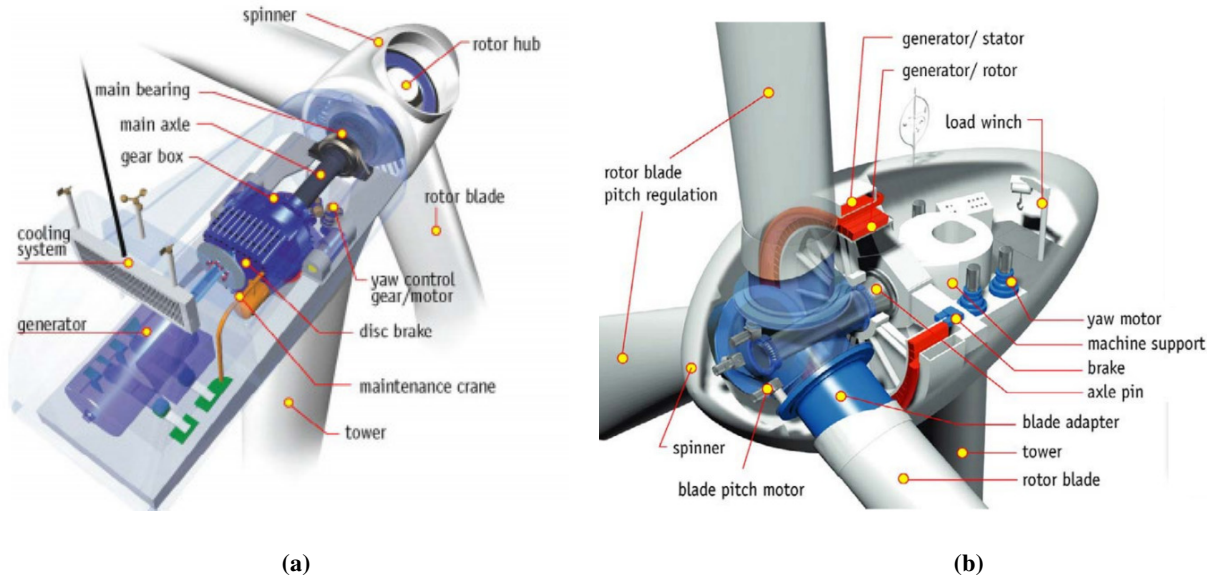
Fig. 1. 7 Sketch of (a) a constant speed WT with gear box (b) direct drive WT [13].

In contrast to direct grid connected IG, indirect grid connected wind turbines (including wind turbines with DFIG - Fig 1.5(b)) are much more efficient because they could run at variable speed condition. Additionally, these turbines can control reactive power to improve efficiency for the electrical grid. The disadvantage for using the DFIG wind turbine is that the generator uses slip rings. Since slip rings must be replaced periodically, and so the use of DFIGs need frequent maintenance and require long term costs than other brushless generators [16]. The PMSG connected to the grid by a full power back to back converter has become an attractive alternative to the DFIG. This concept has several advantages such as the feasibility of direct drive of the wind turbine with a PMSG of high number of poles, avoiding the use of a gearbox; the high efficiency and high power density of PMSG; and the capability of the front end converter to operate under network disturbances. Furthermore, the absence of a gearbox and the lack of moving contacts on the PMSG increase the reliability and decreases the maintenance

requirements. With the advance of power electronics, PMSGs have drawn increased interest to wind turbine manufacturers due to its advantages over other variable speed WTGs [29]. The details about PMSG are discussed in the next chapter.

Table 1: COMPARISON OF FOUR WIND TURBINE GENERATOR CONCEPTS,

+ STRENGTH,-WEAKNESS [13].

		CS	DFIG	GFC	DD
Cost, size and weight		+	+/-	+/-	-
Suitability for 50 and 60 Hz grid		-	-	+	+
Audible noise from blades		-	+	+	+
Energy yield	Variable speed	-	+	+	+
	Gearbox	-	-	-	+
	Generator	+	+	+	-
	Converter	+	+/-	-	-
Reliability and maintenance	Brushes	+	-	+	- (PM: +)
	Gearbox	-	-	-	+
	Mechanical loads	-	+	+	+
	Complexity	+	-	-	-
Power quality	'Flicker'	-	+	+	+
	V&f control possible	-	+	+	+
	Harmonics	+	-	-	-
Grid faults	Fault currents	+	-	-	-
	Fault ride-through	+	+/-	+	+
	Restoring voltage	-	+/-	+	+

The comparison among four WTGs are shown in Table-1, where CS indicates constant speed with gearbox and induction generator, DFIG indicates variable speed with gearbox, doubly-fed induction generator and partly rated converter, GFC PM indicates variable speed with gearbox, permanent-magnet generator or induction generator and full converter, and DD indicates variable speed direct-drive permanent-magnet generator and full converter.

As seen in Table 1, both GFC and DD based WTGs can obtain better grid-fault ride through characteristics than the DFIG and to avoid the brushes of the DFIG.

This thesis mainly focuses on the control strategies of variable speed wind turbine using DD PMSG where interior permanent magnet synchronous generator (IPMSG) is used for

13

simulation and real time experiment. The power gain using variable speed wind turbine against fixed speed which varies from 2% to 38% [22]. The variance depends on ability of controller to track the maximum power point of WT.

Wind Turbine Rotor Types

As shown in Fig. 1.8, mainly wind energy is converted to electricity using two basic turbine types determined by which way the turbine spins. Wind turbines that rotate around a horizontal axis are more common.
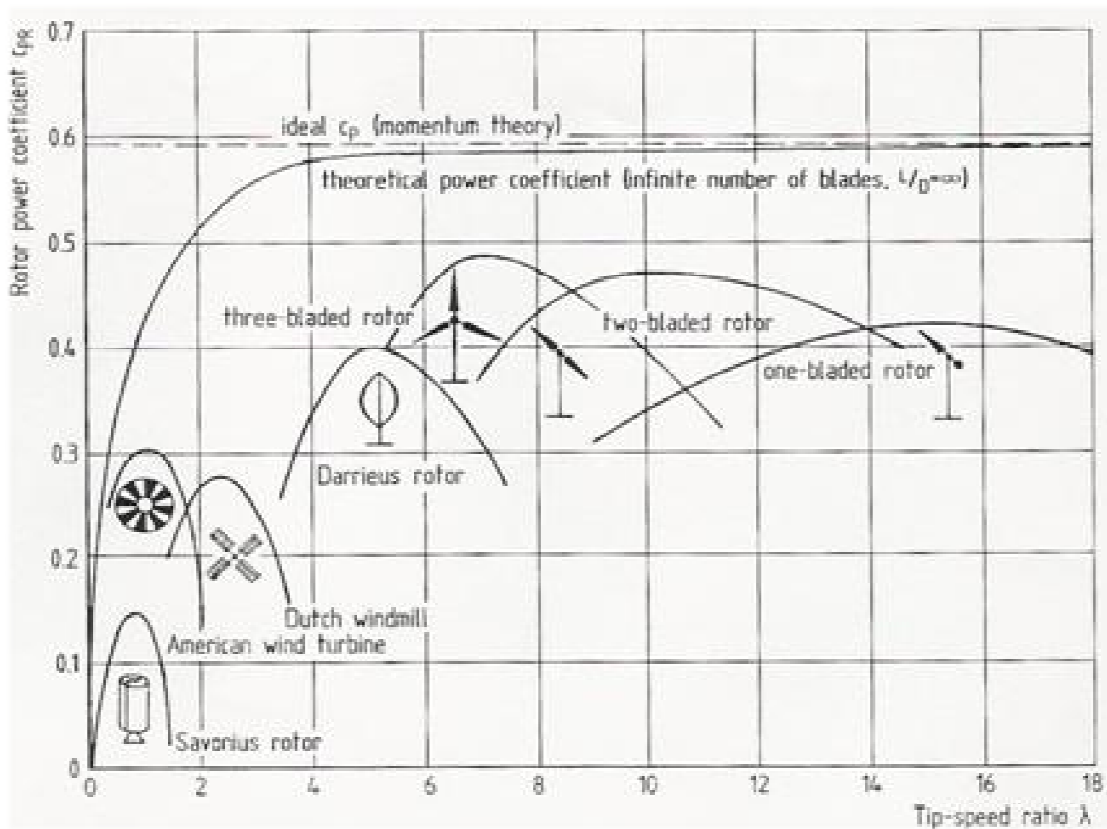
Fig. 1. 8 Wind turbine rotor types.

(1) Horizontal Axis Wind Turbine (HAWT)

(a) 3 bladed Horizontal Axis Wind Turbine

Horizontal axis wind turbines are the more common style for commercial wind turbine. The HAWT has blades that look like a propeller and spin on a horizontal axis. The most popular turbine at the time is the 3 bladed HAWT as shown in Fig 1.9.

The HAWT has high efficiency, since the blades always move perpendicularly to the wind, receiving power through the whole rotation; however, they require heavy construction to support the heavy blades, gearbox, and generator housed in a nacelle on top of a large mast. The HAWT have to be angled into the wind's path, so that the wind's direction is perpendicular to the rotor plane. When the turbine is angled into the wind, the lift force from the aerodynamic profiles will make the rotor turn. The advantages and disadvantages of HAWT as compared to Vertical Axis Wind Turbine (VAWT) are summarized below.

Advantages of the HAWT:

- Higher efficiency
- Lower cost-to-power ratio

Disadvantages of the HAWT:

- More complex design required due to the need for yaw or tail drive
- Generator and gearbox should be mounted on a tower, which makes the maintenance relatively more difficult

Fig. 1. 9 Three bladed horizontal Axis wind turbine [9].

(2) Vertical Axis Wind Turbine (VAWT)

Vertical axis wind turbines have the main rotor shaft arranged vertically. As shown in Fig 1.10 1.11, the main advantage of this arrangement is that the wind turbine does not need to be pointed into the wind. This is an advantage on sites where the wind direction is highly variable or has turbulent or swirling winds. A VAWT is typically located nearer to the ground, making it easier to maintain the moving parts. There are mainly two types of VAWT, which are briefly discussed below.

(a) Darrieus wind turbine

The Darrieus wind turbine was patented by Georges Jean Marie Darrieus, a French aeronautical engineer in 1931.The Darrieus rotor is a VAWT provided with two or more blades having an aerodynamic airfoil. The blades are normally bent into a chain line and are connected to the hub at the upper and lower side.

They have good efficiency, but produce large torque ripple and cyclical stress on the tower, which contributes to poor reliability. They also generally require some external power

source, or an additional Savonius rotor to start turning, because the starting torque may be too low to overcome the startup torque threshold of the generator.
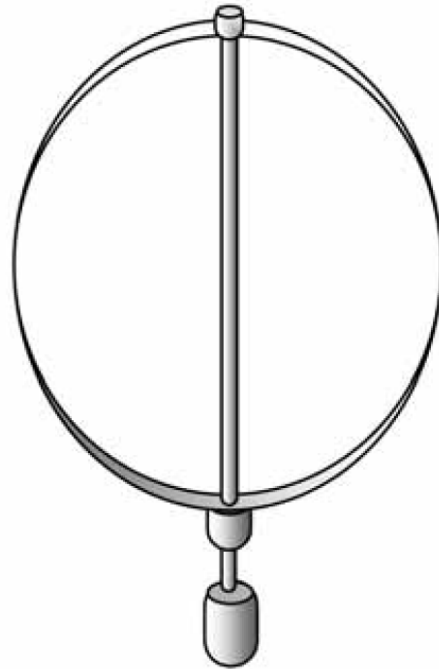
Fig. 1. 10 Darrieus wind turbine [8].

(b) Savonius wind turbine

Savonius wind turbine was invented by the Finnish engineer Sigurd J. Savonius in 1922. The Savonius rotor consists of two hollow, half cylinders displaced from each other. Generally the halves overlap by about one third of their diameter. The Savonius rotor can be constructed from simple material using common tools. Savonius rotor concept never became popular, until recently, probably because of its low efficiency. Its maximum power coefficient can reach up to 0.25 only [8].
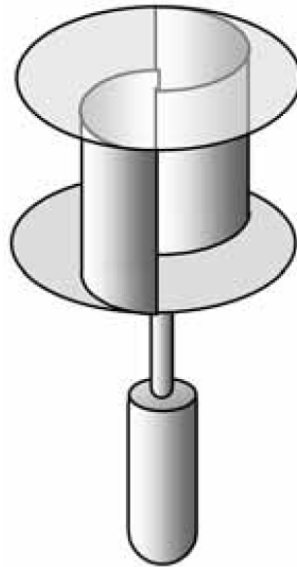
Fig. 1. 11 Savonius wind turbine [8].

Typical advantages of VAWT:

- Easy maintenance for ground mounted generator and gearbox,

- Receive wind from any direction (No yaw control required), and

- Simple blade design and low cost of fabrication.

Disadvantages of VAWT:

- Lower efficiency (the blades lose energy as they turn out of the wind),

- Difficulty in controlling blade over-speed, and

- Oscillatory component of the aerodynamic torque is high.

1.2.3 WECS control

The amount of power transferred from turbine to the grid side through PMSG, rectifier/ inverter set depends on the control algorithm for converters. Therefore, sophisticated control algorithms should be developed to transfer maximum power or to minimize the losses in the IPMSG. Moreover, controller should operate the PMSG over wide operating speed range as

wind speed is very unpredictable. Researchers have reported some maximum power transfer controllers or algorithms for PMSG based WECS [13-55].
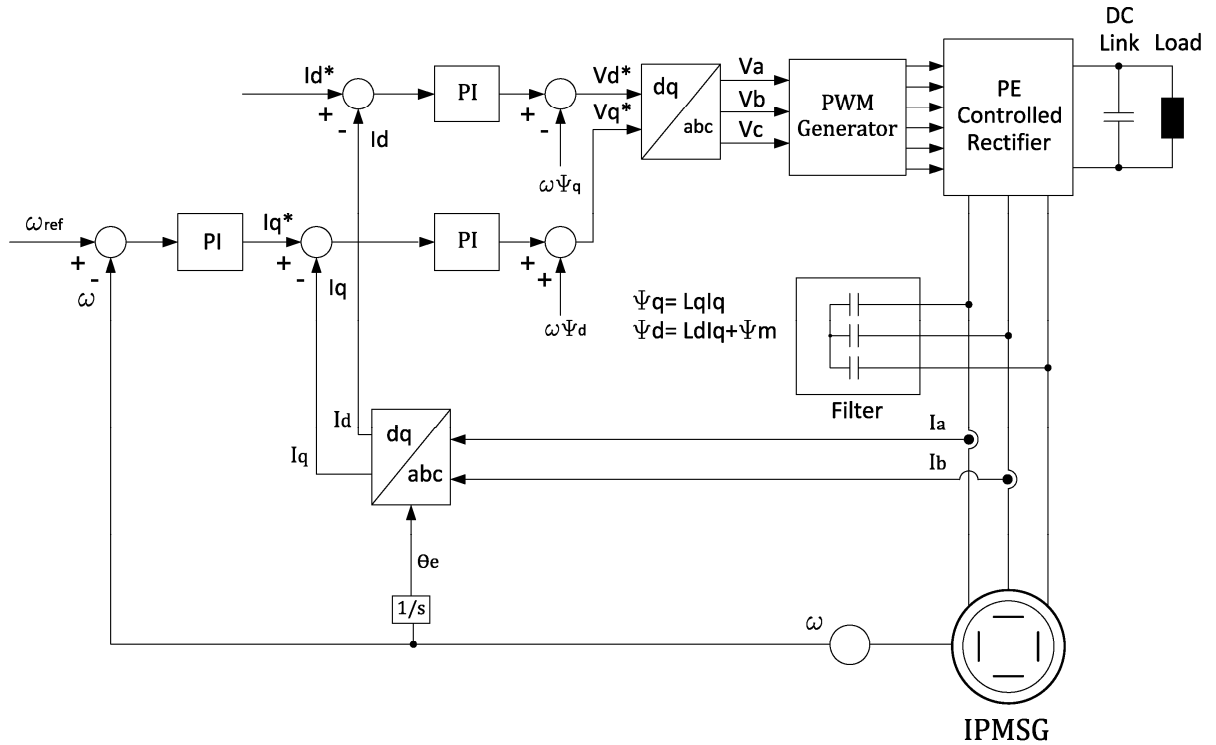
Fig. 1. 12 A typical closed loop vector control scheme of IPMSG.

1.3.1 Power extraction strategies:

A typical closed loop vector control scheme of the IPMSG is shown in Fig. 1.12. From Eqns. (1.5)-(1.8), it can be seen that C_p is only control variable which can maximize available turbine power. In fixed speed WT, C_p is a function of pitch angle, wind speed and generator rotational speed (ω_r). When WT is connected with power electronics interface for control, pitch angle is set to zero to get maximum C_p value as shown in Fig. 1.2. Some researchers have proposed control strategies to produce optimum reference speed (ω_{ref}) to extract maximum power from WT. There exist different strategies to get $\omega_{ref,}$ where some of them are wind speed sensor dependent [1, 2, 7, 11, 24]. The wind speed sensors are not a reliable option in harsh weather condition. Some control methods estimate wind speed; however, many of them require the

19

knowledge of air   density and mechanical parameters of WECS [6, 12, 15, 21, 22, 29, 42-48]. With changing weather conditions, their controller output may vary. Moreover, rotating parts of WECS may change their characteristics which could be an issue on performance over longer period of time. Therefore, a lot of research efforts are focused on developing maximum power point tracking (MPPT) controllers independent of wind speed senor and turbine parameters; for example, hill-climb search type algorithm, optimum power search algorithm, etc. [19, 23, 30, 49-55]. This algorithms can be very effective and can track optimum power online. Here, most of the researchers who designed MPPT algorithms, did not show turbine power coefficient C_p graph in their simulation results which explains maximum power tracking at different wind speed. In [5], C_p graph is shown to explain MPPT, however, system operation is only shown for very narrow wind speed operation. Some of them show the efficiency of generator for the maximum power tracking operation of the system; however, their control doesn't use any loss minimization algorithm [55].   In [5, 11, 56, 57], intelligent control such as fuzzy logic and neural network logic based power tracking have been presented. This controllers could provide good performance in WECS as they don't need exact parameters of the system. However, these control techniques may increase complexity of the system, and add an extra calculation burden on hardware side. Sometimes it could lead to run time errors and hence, prevent the system use for real world applications.

1.3.2 Position and speed estimation:

Traditionally the rotor position is obtained from a shaft-mounted optical encoder or Hall sensors. However, it is desirable to eliminate such sensors in PMSM drives to reduce system costs and total hardware complexity, to increase the mechanical robustness and reliability, to reduce the maintenance requirements, [59-83].

Authors reported different position and speed sensorless strategies in [59, 61, 80]. The rotor position and angular speed of the IPMSM can be estimated by various methods. Position estimation can be mainly divided into two categories. Non-adaptive methods and adaptive methods. Non- adaptive methods use measured currents and voltages as well as fundamental machine equations for estimation. On the other hand, adaptive estimation methods compare the error between the measured output of the real system and the calculated estimated output of machine model, and adapts the parameters of the model with the aim to minimize the error between the real system and the model. The process of the adaptation is desired to be stable and robust.

The simplest fundamental model methods are based on rotor flux position estimation, by integrating the back-EMF [81]. It's very simple but fails to estimate the rotor position at low and zero rotor frequency. Low speed operation is critical in practical applications, since the estimated rotor flux can be very sensitive to stator resistance variations, and inaccuracies. Among the existing sensorless approaches, sliding mode has been recognized as a potential control approach for electric machines. Previous studies show that sliding mode observers (SMO) have attractive advantages of robustness to disturbances and low sensitivity to parameter variations [10, 66-68, 71, 72]. In [72] authors used sliding mode controller to estimate the induced back-EMF, rotor position and speed. A sliding mode observer was built based on the electrical dynamic equations. The back EMF information was obtained from the filtered switching signals relative to current estimation error. To design the switching gain over a wide speed range based on this observer model would be a challenging job.

The sensorless control methods presented in [73-75] based on Phase Locked Loop (PLL) is simple, and easy to implement. In [64, 76-77], sensorless schemes that are based on the

application of flux observers (such as Kalman filter) have poor performance at low speed and can be too complex and expensive to be used in practical systems. Signal injection schemes [63, 69, 79] can be more efficient, at low and zero speed, than any other sensorless estimation scheme. In [69] authors investigated a high frequency signal injection method in such a way that carrier-frequency voltages were applied to the stator windings of PMSM, producing high-frequency currents whose magnitude varies with rotor position. The sensed currents were then processed with a heterodyning technique that produced a signal approximately proportional to the difference between the actual and the estimated rotor position. However, all these techniques require high bandwidth and high precision measurement, and fast signal processing capability, which may increase the complexity and cost of control system. The injected high-frequency voltages may also cause more torque ripple, shaft vibration and audible noise.
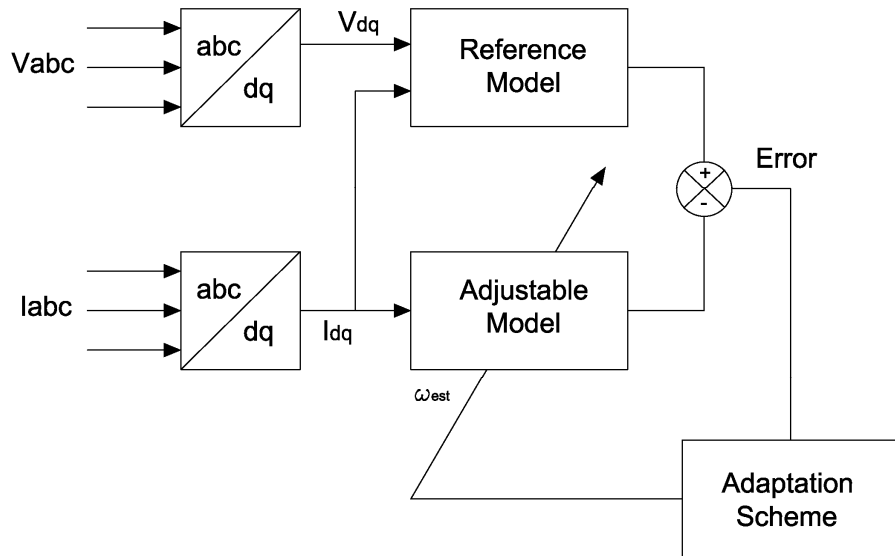
Fig. 1. 13 Model Reference Adaptive System for speed estimation.

The Model Reference Adaptive System (MRAS) scheme offers simpler implementation and require less computational effort compared to other methods, and it is widely accepted for speed estimation. The MRAS method uses two models: one independent of rotor speed

(Reference Model) and the other dependent on rotor speed (Adjustable Model), both having same output (flux 'Ψ_m' or back-EMF 'E'). The error of these actual and estimated outputs is fed to the adaptation mechanism which outputs the estimated rotor speed (ω) as shown in Fig. 1.13. This estimated ω is used to tune the adjustable model till error is zero at which the estimated speed is same as the actual speed. MRAS method suffers from parameter dependence and pure integrator related problems in reference model. To overcome this problem, an alternative MRAS structure based on stator current error using PMSM motor itself as a reference model is employed [12, 82, 83]. This structure is shown in Fig.1.13 where the stator current model with stator current output is used as adaptive model. The error between the actual and estimated output currents is fed to an adaptation mechanism which is a PI or Sliding Mode Controller. The gains of this adaptation mechanism are calculated through Popov's Hyperstability criterion. As MRAS is not very sensitive to the parameters of machine, it is a widely applicable method.

1.3.3 Flux Weakening control (FWC):

In order to extend the operating speed range of PMSMs, the armature currents partially demagnetize the magnets achieving field weakening [84]. However, this approach involves the risk of irreversible demagnetization of the PMs and generates significant heat due to the I^2R losses. Above the normal operating point temperature, d-axis flux could demagnetize the permanent magnets (PM). To avoid this effect, author in [85] suggested to connect groups of the stator winding in different configurations so that the induced voltage is adjusted accordingly. In [86] flux control techniques are developed for both below and above rated speed condition of IPMSM. Comprehensive design methods were reviewed in [87]. It proposes a magnetic structure termed the consequent-pole PM (CPPM) machine which has inherent field weakening capability. This machine combines the fixed excitation of the rare earth permanent magnet with the variable

flux given by a field winding located on the stator. So, air-gap flux can be controlled over a wide range with a minimum of conduction losses and without demagnetization risk for the PM pieces.

The efforts discussed above were made on the different types of PM machine design, which has increased manufacturing cost due to the additional windings and/or complicated rotor structure. On the other hand, many control strategies and algorithms have been developed for flux-weakening operation of PMSM and published during the last decade [88-91]. In [88], authors investigated a current-regulated flux-weakening method by introducing a negative current component to create direct-axis flux in opposition to that of the magnetic flux, resulting in a reduced air-gap flux. This armature reaction effect was used to extend the operating speed range of PMSM and relieve the current regulator from saturation that can occur at high speeds. In [89], author proposed FWC for surface-mounted permanent Magnet (SPM) machines which did not require a knowledge of the machine or system parameters and was relatively simple design. In [90], the flux-weakening is achieved by look-up table. The method is accurate and easy to plan, but it needs a lot of test data, and the portability is poor. In [91] a review on the state-of-the-art on flux-weakening control strategies for PMSMs are provided.

1.3 Objective of Thesis

The objectives of this thesis are to design, simulate and implement the control strategies for variable speed WECS incorporating the MPPT algorithm for direct driven IPMSG. The MPPT algorithm is designed based on a perturbation and observation algorithm. It is derived based on active input power only and independent of wind speed. Thus, it makes the system wind speed sensorless. In particular, the proposed objectives are as follows:

- To develop a new adaptive MPPT technique to transfer the maximum mechanical power from WT to the dc-link.

- To incorporate wind speed sensorless approach with the proposed WECS.

- To incorporate the rotor position sensorless technique based on MRAS approach.

- To incorporate the field weakening technique to operate the machine over wide speed range

- To simulate the overall IPMSG based WECS incorporating the proposed algorithms.

- To implement the proposed IPMSG based WECS in real-time using DSP board DS1104.

1.4 Thesis Organization

The present report consists of 6 chapters. Chapter 1 covers an overview of WECS. It starts with an introduction to the subject. The advantages and disadvantages of the different types of wind turbines and the two main kinds of wind energy systems are discussed. The literature review, and objectives are also presented in this Chapter.

Chapter 2 provides general overview of the proposed WECS. The system components are also described briefly. The modeling of Interior permanent magnet machine is presented. A brief description of Space Vector Modulation (SVM) strategy to control the rectifier switches is also provided.

In Chapter 3, a conventional control strategy for WECS has been discussed with simulation results. The proposed novel adaptive MPPT algorithm with flux control is presented in this Chapter. The performance of the proposed MPPT and FWC based WECS is investigated in simulations.

Chapter 4 presents the developed rotor speed sensorless technique based MRAS approach. The performance of the proposed MRAS based WECS is investigated in simulations.

Chapter 5 describes the real-time implementation of the 5 HP IPMSG drive system in laboratory using dSPACE DS1104 DSP board. The experimental results of the MPPT based rotor position sensorless control of IPMSG are shown in this Chapter. The detailed real-time implementation procedures for both hardware and software are also discussed.

Finally, Chapter 6 presents summary/conclusions of this work and suggestions for future work. The thesis concludes with references and appendices.

Chapter 2

Modeling of Wind Energy Conversion

System

2.1 General Overview of the Proposed WECS

The block diagram of the specific direct-drive wind energy conversion system (WECS) considered in this thesis is shown in Fig. 2.1. Area inside of dotted line in this figure shows the scope of this thesis. A variable speed WT drives permanent magnet synchronous generator (PMSG) which is connected to the dc-link through a controlled rectifier. As this system doesn't use gear box, it is called direct drive WECS. The absence of a gearbox and the lack of moving contacts on the PMSG increase the reliability and decreases the maintenance requirements. With the advance of power electronics, PMSGs have drawn increased interest to wind turbine manufacturers due to its advantages over other variable speed WTGs, which are discussed later in this Chapter.
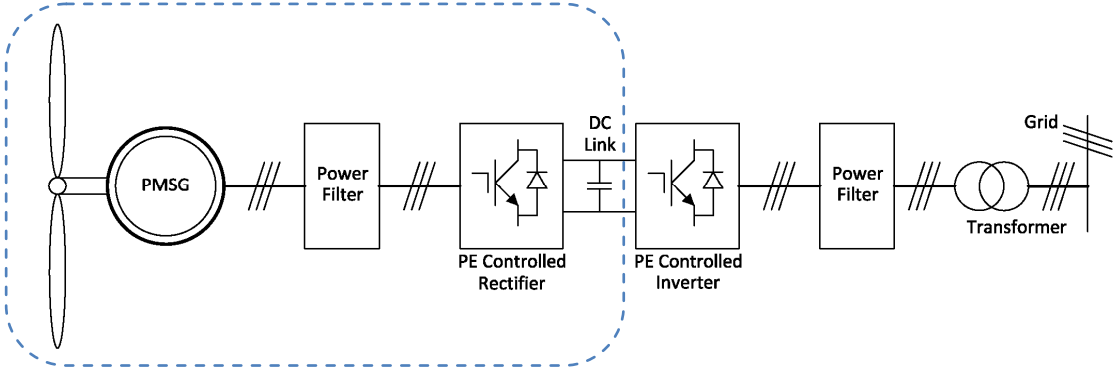
Fig. 2. 1 Block diagram of the proposed WECS.

In simulation, wind turbine is designed according to the mathematical model, whereas in real-time implementation a variable speed DC motor is used in place of wind turbine to provide mechanical torque. Using the mechanical torque IPMSG produces 3-phase AC power which is converted to DC power using controlled rectifier. In this thesis, first the control technique is developed to extract maximum power from wind to turbine output. Then another technique is developed for the rectifier to track maximum power transfer from WT to the dc-link. Moreover, the field weakening technique is also incorporated to operate the generator above the rated speed condition.

2.2 Park's and Clarke's Transformations

The AC machine voltage equation depends on the flux linkages which are function of rotor speed. If ψ_m is the constant flux linkage provided by the permanent magnets, then the flux linkages in the three phase stator winding due to PM of the rotor can be given as,

$$\begin{bmatrix} \psi_{am} \\ \psi_{bm} \\ \psi_{cm} \end{bmatrix} = \psi_m \begin{bmatrix} \sin(\theta) \\ \sin(\theta - \dfrac{2\pi}{3}) \\ \sin(\theta + \dfrac{2\pi}{3}) \end{bmatrix} \tag{2.1}$$

where Ψ_{am}, Ψ_{bm} and Ψ_{cm} are the flux linkages in the three phase stator winding due to PM of the rotor and θ is the rotor position. So total air gap flux linkage for three phases are the summation of the flux linkage for the corresponding phase current, mutual flux linkage for the currents in other phases and the flux linkages in the three phase stator winding due to PM of the rotor. The equations for the air gap flux linkage for three phases are given as,

28

$$\begin{bmatrix} \psi_a \\ \psi_b \\ \psi_c \end{bmatrix} = \begin{bmatrix} L_{ab} & M_{ab} & M_{ac} \\ M_{ba} & L_{bb} & M_{bc} \\ M_{ca} & M_{cb} & L_{cc} \end{bmatrix} \begin{bmatrix} i_a \\ i_b \\ i_c \end{bmatrix} + \psi_m \begin{bmatrix} \sin(\theta) \\ \sin(\theta - \dfrac{2\pi}{3}) \\ \sin(\theta + \dfrac{2\pi}{3}) \end{bmatrix} \qquad (2.2)$$

where Ψ_a, Ψ_b and Ψ_c are the air gap flux linkage for the phase a, b, c, respectively; L_{aa}, L_{bb}, L_{cc} are the self-inductances and M_{ab}, M_{bc}, M_{ca} are the mutual inductances, respectively and θ is rotor position. The phase voltage is the voltage drop in each phase plus the voltage drop due to the rate of change of flux linkage. The voltage equations of the three phases of the IPMSM can be defined as:

$$v_a = r_a i_{\mathrm{a}} + \frac{d\psi_a}{dt} \qquad (2.3)$$

$$v_b = r_b i_{\mathrm{b}} + \frac{d\psi_b}{dt} \qquad (2.4)$$

$$v_c = r_c i_{\mathrm{c}} + \frac{d\psi_c}{dt} \qquad (2.5)$$

where v_a, v_b, v_c are the three phase voltages, i_a, i_b, i_c are the three phase currents and r_a, r_b, r_c are the three phase stator resistances. These equations can be written in matrix form as,

$$\begin{bmatrix} v_a \\ v_b \\ v_c \end{bmatrix} = \begin{bmatrix} r_a & 0 & 0 \\ 0 & r_b & 0 \\ 0 & 0 & r_c \end{bmatrix} \begin{bmatrix} i_a \\ i_b \\ i_c \end{bmatrix} + \frac{d}{dt} \begin{bmatrix} \psi_a \\ \psi_b \\ \psi_c \end{bmatrix} \qquad (2.6)$$

v_a, v_b and v_c depends on the flux linkage components which are functions of rotor position θ and hence functions of rotor speed ω. Therefore, the coefficients of the voltage equations are time

varying except when the machine is motionless. In order to keep away from the difficulty of calculations, all the equations have to be changed to the synchronously rotating rotor reference frame where the machine equations are no longer dependent on the rotor position. These transformations can be achieved in two steps using Clarke's and Park's transformation equations [92]. In the first step, v_a, v_b and v_c will be transformed from the three phase stationary a-b-c frame into two phase stationary α-β frame and in the second step, from the stationary α-β frame to the synchronously rotating d-q frame. The transformed phase variables in the stationary d-q-0 axis can be written in matrix form as:

$$
\begin{bmatrix} x_a \\ x_b \\ x_c \end{bmatrix} = \begin{bmatrix} \cos(\theta) & \sin(\theta) & 1 \\ \cos\left(\theta - \dfrac{2\pi}{3}\right) & \sin\left(\theta - \dfrac{2\pi}{3}\right) & 1 \\ \cos\left(\theta + \dfrac{2\pi}{3}\right) & \sin\left(\theta + \dfrac{2\pi}{3}\right) & 1 \end{bmatrix} \begin{bmatrix} x_\beta \\ x_\alpha \\ x_0 \end{bmatrix}
$$

(2.7)

The corresponding inverse relation can be written as:

$$
\begin{bmatrix} x_\beta \\ x_\alpha \\ x_0 \end{bmatrix} = \frac{2}{3} \begin{bmatrix} \cos(\theta) & \cos(\theta - \dfrac{2\pi}{3}) & \cos(\theta + \dfrac{2\pi}{3}) \\ sin(\theta) & \sin(\theta - \dfrac{2\pi}{3}) & \sin(\theta + \dfrac{2\pi}{3}) \\ \dfrac{1}{2} & \dfrac{1}{2} & \dfrac{1}{2} \end{bmatrix} \begin{bmatrix} x_a \\ x_b \\ x_c \end{bmatrix}
$$

(2.8)

where, x_a, x_b and x_c are the a, b and c phase quantities, respectively, x_α, x_β and x_0 are the α -axis, β -axis and zero sequence components, respectively. The matrix element x may represent either voltage or current.

The rotor location or rotor position angle θ is defined as:

$$\theta = \int_0^t \omega(\delta)d(\delta) + \theta(0) \tag{2.9}$$

where, δ is a dummy variable.

For balanced three phase, zero sequence component (x_0) does not exist, and it is convenient to set initial rotor position $\theta(0) = 0$ so that the q-axis coincides with a-phase. Under these conditions Eqns. (2.7) and (2.8) can be written, respectively, as:

$$\begin{bmatrix} x_a \\ x_b \\ x_c \end{bmatrix} = \begin{bmatrix} 1 & 0 \\ -\dfrac{1}{2} & -\sqrt{\dfrac{3}{2}} \\ -\dfrac{1}{2} & \sqrt{\dfrac{3}{2}} \end{bmatrix} \begin{bmatrix} x_\beta \\ x_\alpha \end{bmatrix} \tag{2.10}$$

and

$$\begin{bmatrix} x_\beta \\ x_\alpha \end{bmatrix} = \begin{bmatrix} \dfrac{2}{3} & -\dfrac{1}{3} & -\dfrac{1}{3} \\ 0 & -\dfrac{1}{\sqrt{3}} & -\dfrac{1}{\sqrt{3}} \end{bmatrix} \begin{bmatrix} x_a \\ x_b \\ x_c \end{bmatrix} \tag{2.11}$$

The relative position of the stationary α-β frame and the synchronously rotating d-q frame is shown in Fig. 2.2. With the help of Fig. 2.2 the stationary α-β frame can be converted to the synchronously rotating d-q frame as:

$$\begin{bmatrix} x_q \\ x_d \end{bmatrix} = \begin{bmatrix} \cos\theta & -\sin\theta \\ \sin\theta & \cos\theta \end{bmatrix} \begin{bmatrix} x_\beta \\ x_\alpha \end{bmatrix} \tag{2.12}$$

The inverse relation can be written as:

$$\begin{bmatrix} x_\beta \\ x_\alpha \end{bmatrix} = \begin{bmatrix} \cos\theta & \sin\theta \\ -\sin\theta & \cos\theta \end{bmatrix} \begin{bmatrix} x_q \\ x_d \end{bmatrix} \tag{2.13}$$

In order to derive the d-q axis model of IPMSM drive, the following four assumptions are made:

a) The eddy current and hysteresis losses are negligible.

b) The induced emf is sinusoidal.

c) The saturation is neglected.

d) The stator resistance of the three phases are balanced.
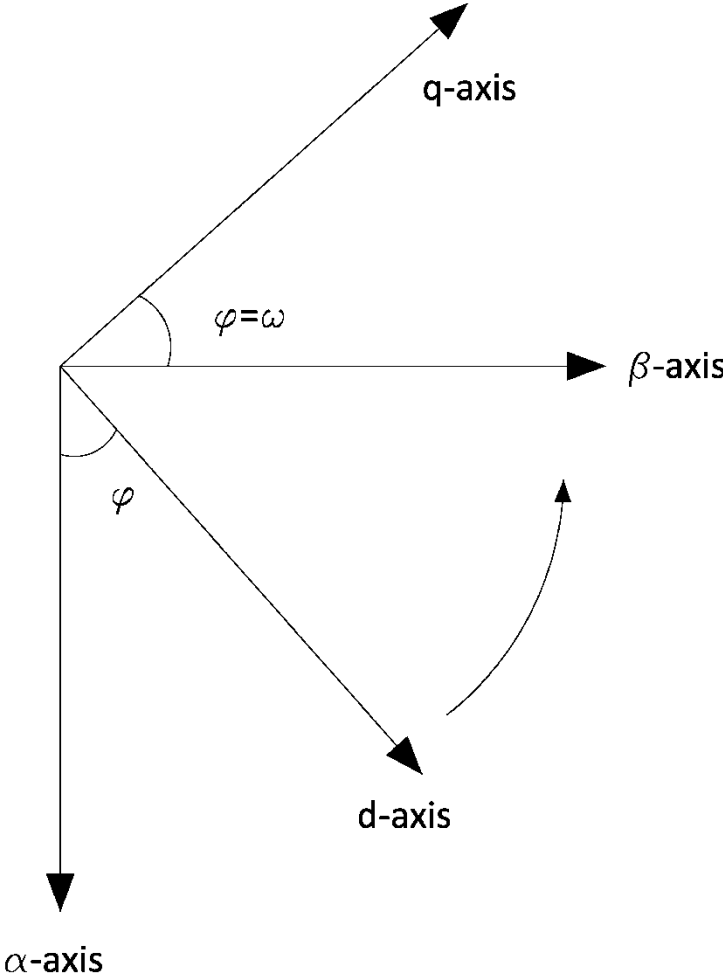
Fig. 2. 2 Relative position of stationary α-β axis to the synchronously rotating d-q axis.

2.3 Introduction to Permanent Magnet Synchronous Machines

Recently, the PMSG has received much attention in wind energy application because of its several advantages such as high efficiency, high power density, less maintenance robustness over the conventional ac machines utilized for WECS [17]. Furthermore, the PMSGs do not need additional power for rotor excitation as the flux is supplied by the permanent magnets.

Current improvement of PMSG is directly associated to the recent achievement in high energy permanent magnet materials. Ferrite and rare earth/cobalt alloys such as neodymium-boron-iron (Nd-B-Fe), samarium-cobalt (Sm-Co) are widely used as magnetic materials. Rare earth/cobalt alloys have a high residual induction and coercive force than the ferrite materials. But the cost is also relatively high. So rare earth magnets are usually used for high performance variable speed drive as high torque to inertia ratio is desirable

The classification for PMSM can be done based on some different principle such as design of the machine, driving power circuit configuration, position of magnet in the rotor, current regulation and the principal machine control method. The performance of a PMSM drive varies with the magnet material, placement of the magnet in the rotor, configuration of the rotor, the number of poles, EMF waveform and the presence of dampers on the rotor [93, 94]. Depending on magnet configuration, it can be categorized into three divisions.

(a) Surface mounted PM machine:

In this type of PM machine, the PMs are typically glued or banded with a non-conducting material to the surface of the rotor core as shown in Fig.2.4 (a). This type of machine is not suitable for high speed.

(b) Inset type PM machine:

In this type of PM machine, the PMs are typically glued directly or banded with a non-conducting material inside the rotor core as shown in Fig.2.4 (b). This type of machine is not suitable for high speed.

(c) Interior type PM machine:

In this type of PM machine, the PMs are imbedded in the interior of the rotor core as shown in Fig.2.4 (c). Interior magnet designs offer q-axis inductance larger than the d-axis inductance. The saliency makes possible a degree of flux weakening, enabling operation above nominal speed at constant voltage and should also help to reduce the harmonic losses in the machine. This kind of PM machine has the same advantages of inset machine as well as the advantages of mechanical robustness and a smaller magnetic air gap. Therefore, the interior type PM synchronous machine (IPMSM) is more suitable for high speed operations.
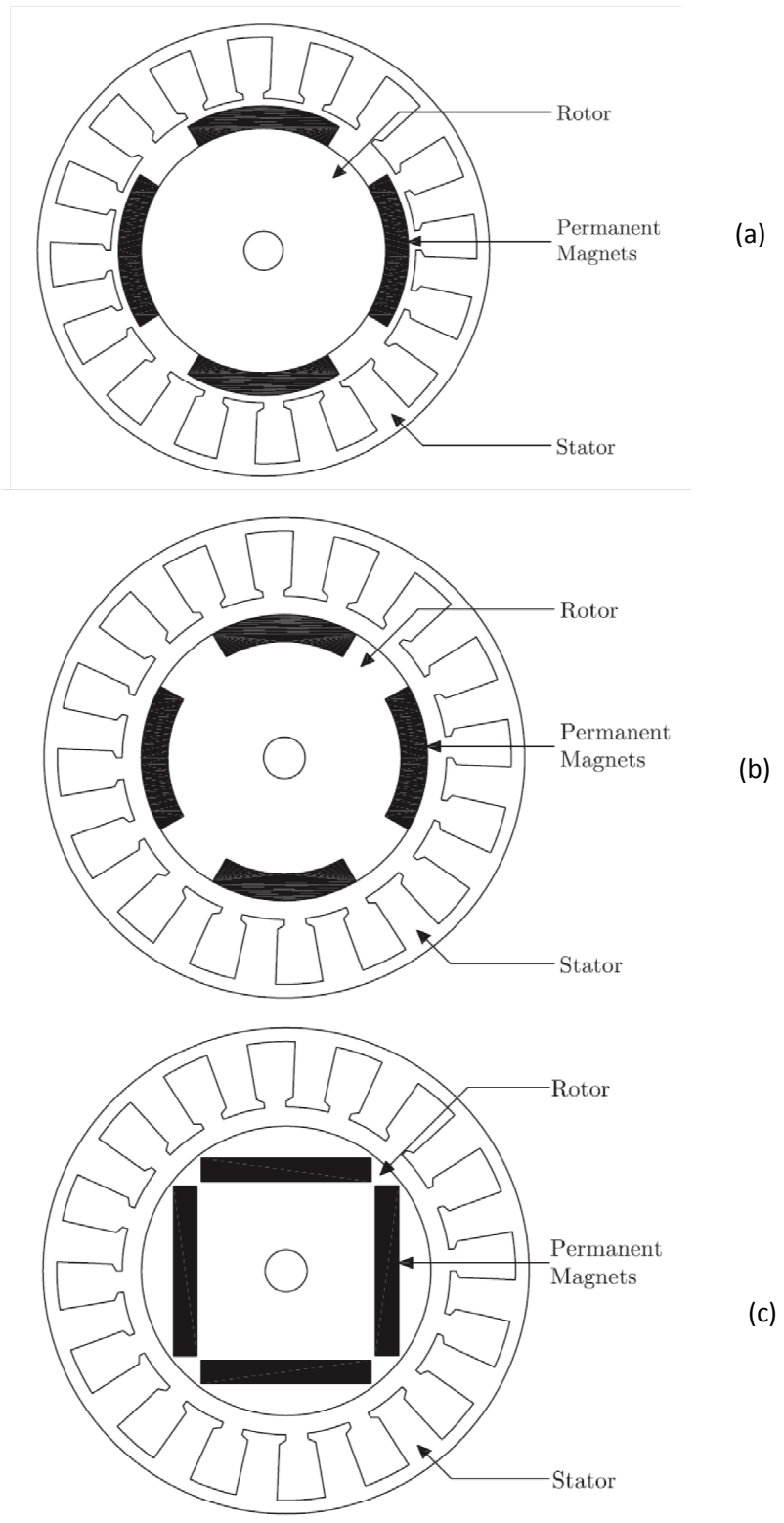
Fig. 2.3 cross section of 4 pole of PMSM, (a) surface mounted, (b) inset and, (c) interior type.

An interior permanent magnet (IPM) synchronous generator can produce more energy compared to surface PMSG which is used in this thesis to make the system more efficient. IPMSG can offer high efficiency and high-controllability generation by utilizing the reluctance torque as well as magnetic torque as both d- and q- axis components of stator current contribute to the torque development process. Therefore, in this thesis the IPMSG is considered for WECS.

2.4 Mathematical Model Development

These voltage equations depend on the flux linkage components which are function of rotor position θ and the coefficients of the voltage equations are time varying except when the machine is motionless. In order to keep away from the difficulty of calculations, all the equations have to be changed to the synchronously revolving rotor reference frame where the machine equations are no longer dependent on the rotor position. These transformations can be accomplished in two steps using Park's transformation equations.
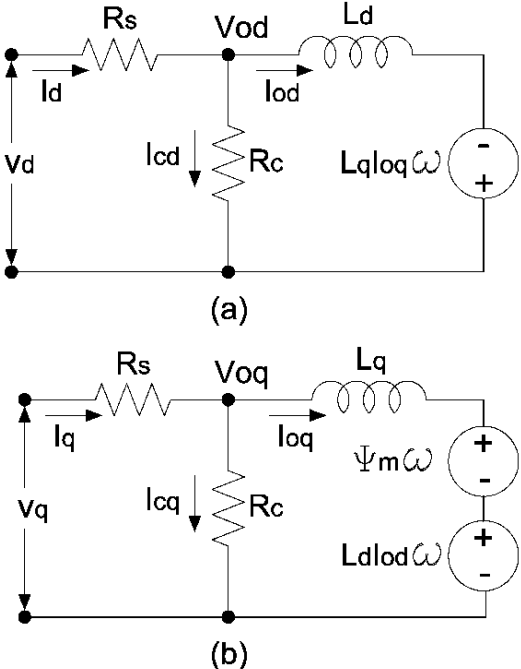
Fig. 2. 4 Equivalent circuits of IPMSM (a) d-axis equivalent circuit. (b) q-axis equivalent circuit.

$$v_q = i_q R_s + \frac{d\psi_q}{dt} + \omega\psi_d \qquad (2.14)$$

$$v_d = i_d R_s + \frac{d\psi_d}{dt} - \omega\psi_q \qquad (2.15)$$

where v_d, v_q are d-q axis voltages and i_d, i_q are d-q axis currents, ψ_d, ψ_q are d-q axis flux linkages and R is the stator resistance per phase and ω is the electrical angular velocity. ψ_d and ψ_q can be written as,

$$\psi_q = L_q i_q \qquad (2.16)$$

$$\psi_d = L_d i_d + \psi_m \qquad (2.17)$$

where, L_d and L_q are d- q-axis self-inductances.

so eq. 2.14 and 2.15 becomes

$$v_d = i_d R_s + L_d \frac{di_d}{dt} - \omega L_q i_q \qquad (2.18)$$

$$v_q = i_q R_s + L_q \frac{di_q}{dt} + \omega L_d i_d + \omega\psi_m \qquad (2.19)$$

When using lumped mass model as given in equation below for WT generator shaft system, the motion equation of IPMSG can be expressed as:

$$J \frac{d\omega_r}{dt} = T_m - T_e - B_m \omega_r \qquad (2.20)$$

where, J - total moment of inertia of the wind turbine (Kg.m^2), B_m- Viscous damping coefficient (Kg.m^2/s), T_m- input mechanical torque (Nm) given by,

$$T_m = P_m / \omega_r \tag{2.21}$$

$$\omega_r = 2\omega / P_n \tag{2.22}$$

where, ω_r is rotor speed (rad/sec), P_n - Number of poles of IPMSG

Electrical torque (T_e) equation is given by:

$$T_e = \frac{3}{2} \frac{P_n}{2} \{ \psi_m i_{oq} + (L_d - L_q) i_{od} i_{oq} \} \tag{2.23}$$

Considering core loss resistance (R_c), the IPMSM's dynamic model can be represented mathematically in d-q synchronous rotating frame as [38].

$$v_d = R_s i_{od} + \left(1 + \frac{R_s}{R_c} \right) \left[L_d \frac{di_{od}}{dt} - \omega L_q I_{oq} \right] \tag{2.24}$$

$$v_q = R_s i_{oq} + \left(1 + \frac{R_s}{R_c} \right) \left[L_q \frac{di_{oq}}{dt} - \omega (L_d I_{od} + \psi_m) \right] \tag{2.25}$$

Where i_{od} and i_{oq} are d-axis demagnetizing and q-axis torque generating currents respectively, i_{cd} and i_{cq} are d-q axis core loss currents respectively.

Copper and core losses are the two losses in IPMSM. Eddy current losses are caused by the flow of induced currents inside the stator core and hysteresis losses are caused by the continuous variation of flux linkages and frequency of the flux variation in the core. On the other hand copper loss, P_{Cu} is due to current flow through the stator windings. Based on Fig. 2.4 the copper loss P_{Cu} and iron loss P_{Fe} in steady state are expressed as follows:

$$P_{cu} = \frac{3}{2} R_s (i_d^2 + i_q^2) = \frac{3}{2} R_s \left\{ i_{od} - \left(\frac{\omega L_d i_{oq}}{R_c} \right) \right\}^2 + R_s \left\{ i_{oq} + \left(\frac{\omega (\psi_m + L_d i_{od})}{R_c} \right) \right\}^2 \tag{2.26}$$

$$P_{Fe} = \frac{3}{2} R_c (i_{cd}^2 + i_{cq}^2) = \frac{3}{2} R_c \left(\frac{\omega \sigma L_d i_{oq}}{R_c} \right)^2 + \frac{3}{2} R_c \left(\frac{\omega^2 (\psi_m + L_d i_{od})}{R_c} \right)^2 \quad (2.27)$$

where, σ is Lq/Ld. The efficiency of WECS is defined as,

$$\eta = \frac{P_o}{P_m} 100 \ \% \quad (2.28)$$

$$P_o = V_{dc} I_{dc} \quad (2.29)$$

where, P_m is the output power of WT, P_o is DC-link power, and V_{dc} and I_{dc} are DC-link voltage and current respectively.

2.5 Vector Control of IPMSM

Vector control is the most popular control technique of AC machine. In d-q reference frames, the expression for the electromagnetic torque of the smooth-air-gap machine is similar to the expression for the torque of the separately excited DC machine. In the case of PM machine, the control is usually performed in the reference frame (d-q) attached to the rotor flux space vector. In case of dc motor, the developed torque is given by,

$$T_e = K I_f I_a \quad (2.30)$$

where I_a is the armature current, I_f is the field current and K is a constant. Both I_a and I_f are orthogonal and decoupled vectors. So the control becomes easier for separately excited dc motor. In case of PM machine the first term of torque Eqn. (2.30) represents the magnet torque produced by the permanent magnet flux and q axis current and the second term represents the reluctance torque produced by the interaction of q and d axis inductances and the d-q axis

currents. Most of the researchers consider the command d-axis current, i_d=0. So that the torque equation becomes linear with i_q and control task becomes easier.

With $i_d = 0$, T_e becomes,

$$T_e = \frac{3P}{2}\psi\, i_q = K_t i_q$$

(2.31)

However with the assumption of i_d=0, as per Eqn. (2.31), the flux cannot be controlled in an IPMSM. Without a proper flux control, machine cannot be operated above the rated speed while maintaining voltage and current within the rated capacity of the machine/converter. In the proposed work, the flux will be properly controlled so that the machine can be controlled efficiently below and above the rated speed. Thus, the IPMSM can be controlled like a separately excited DC motor where i_q controls the torque and i_d controls the flux.

Using phasor notation and taking the d axis as the reference phasor, the steady state phase voltage V_a can be derived from steady state d-q axis voltage using equation (2.14) and (2.15) as,

$$V_a = V_d + jV_q$$

$$= R_s I_a - \omega_r L_q i_q + j\omega_r L_d i_d + j\omega_r \psi_m$$

(2.32)

where, the phase current is:

$$I_a = -i_d + ji_q$$

(2.33)

In the case of IPM machine, the d axis current is negative and it demagnetizes the main flux provided by the permanent magnets. Thus in order to take the absolute value of i_d we can rewrite the equation as,

$$V_a = R_s I_a - \omega_r L_q I_q - j\omega_r L_d i_d + j\omega_r \psi_m \qquad (2.34)$$

Based on equation (2.40), the basic vector diagram of the IPMSM is shown in Fig.2.5. The stator current vector can be controlled by controlling the individual d-q current components.
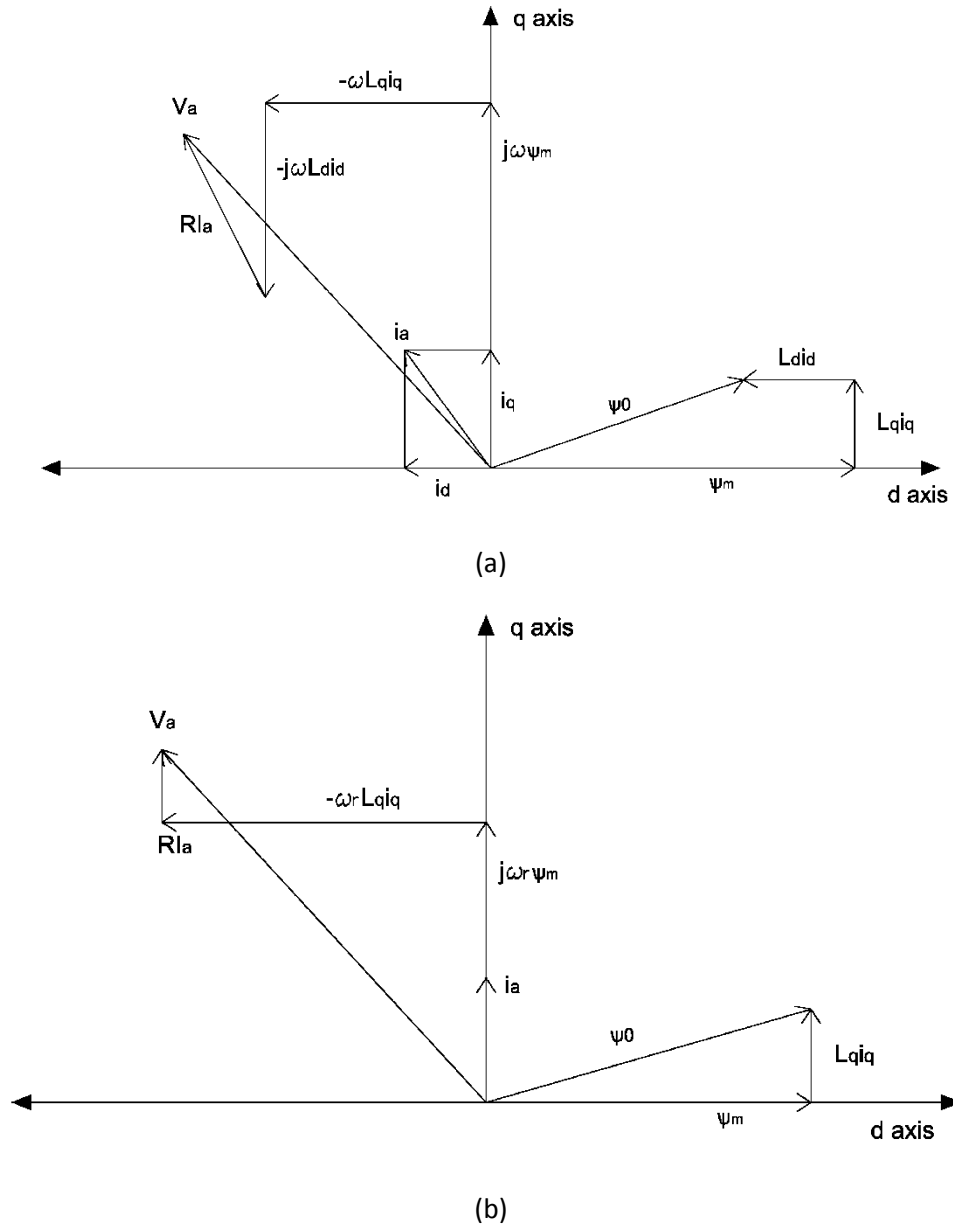

(a)

(b)

Fig. 2. 5 Vector diagrams of the IPMSM: (a) general vector diagram, (b) modified with id=0 diagram.

2.6 Space-Vector Pulse Width Modulation of the Voltage Source Converter

A 3-phase controlled rectifier circuit to convert the ac output voltage of IPMSG to a fixed dc voltage is shown in Fig. 2.6. The rectifier switches (S1-S6) can be controlled using well-known pulse width modulation technique (PWM).
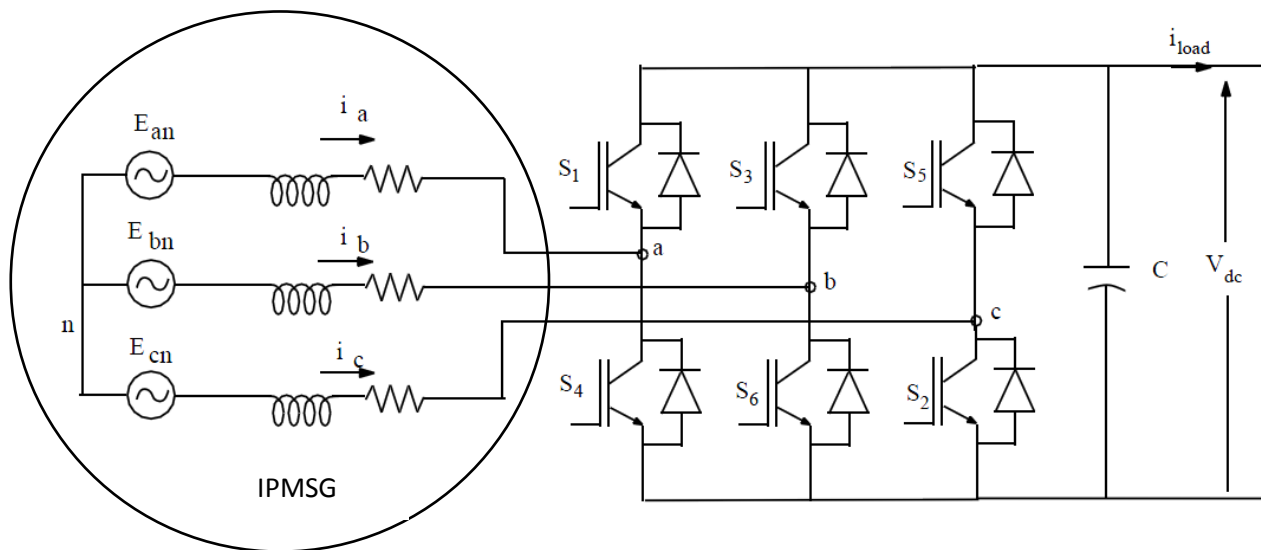
Fig. 2. 6 Simplified representation of three-phase PWM rectifier.

Pulse width modulation has been studied extensively during the past decades. Many different PWM methods have been developed to achieve the following aims: wide linear modulation range; low switching loss; low total harmonic distortion (THD) in the spectrum of switching waveform; and easy implementation and low computation time [95]. There are many possible PWM techniques have proposed in past decades. The classifications of PWM techniques can be given as follows:

- o   Sinusoidal PWM (SPWM)
- o   Selected harmonic elimination (SHE) PWM

- Minimum ripple current PWM

- Space vector PWM (SVM)

- Random PWM

- Hysteresis band current control PWM

- Sinusoidal PWM with instantaneous current control

- Delta modulation

- Sigma-delta modulation

The space-vector PWM method is an advanced, low computation PWM method and is possibly the best among all PWM techniques for variable frequency drive applications [96]. It uses the space-vector concept to compute the duty cycle of the switches.

Fig. 2.7 shows the topology of the typical three-phase PWM rectifier circuit. There are six switching regions, which are determined by the angle of phase input voltages. The upper and lower switches in each phase are always operated complementary. Switches of two phases are driven by PWM mode while ones of another phase are always turned on or off during each region. Table 2.1 summarizes the switching schemes and the available voltage vectors in each region. The voltage space vector diagram and the switching logics of upper switches (S1, S3, and S5) for each voltage vector can be seen in Table 2.1.
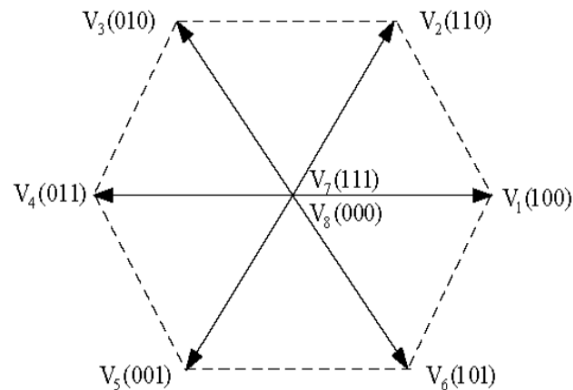
Fig. 2. 7 Voltage space vector diagram.

Table 2.1: SWITCHING SCHEME AND AVAILABLE VOLTAGE VECTORS IN EACH REGION [97]

Region	S1	S2	S3	S4	S5	S6	Available Voltage Vectors
1	PWM	PWM	OFF	ON	PWM	PWM	V5,V6,V1,V8
2	ON	OFF	PWM	PWM	PWM	PWM	V6,V1,V2,V7
3	PWM	PWM	PWM	PWM	OFF	ON	V1,V2,V3,V8
4	PWM	PWM	ON	OFF	PWM	PWM	V2,V3,V4,V7
5	OFF	ON	PWM	PWM	PWM	PWM	V3,V4,V5,V8
6	PWM	PWM	PWM	PWM	ON	OFF	V4,V5.V6,V7

2.7 Concluding Remarks

This Chapter has provided a general overview of proposed WECS system. The detail mathematical model of IPMSM has been derived. The vector control technique for IPMSM has also been introduced in this Chapter. An overview of space-vector pulse width modulation technique to control the rectifier switches has also been provided.

Chapter 3

Power Extraction Strategies and Control Techniques

Electricity is an integral part in the development of modern society and life without electricity is unimaginable in developed countries. In many countries, with increased population and necessities, demand of electricity has been increasing rapidly and at the same time conventional power sources are limited. Renewable energy sources are becoming a good solution to these issues. Among the renewable energy sources, wind energy is one of the fastest growing, cost effective and environmental friendly way of electricity generation. However, it is important to extract the maximum power available from variable wind conditions.

In wind energy conversion system output power is maximum at particular rotor speed for a given wind speed. Fig. 3.1 shows the power coefficient C_P vs tip speed ratio (λ). It is seen that the maximum C_p can be obtained at the specific TSR value. To further explain this concept, Fig. 3.2 shows the typical WT and generator power curve at different rotor speed for different wind velocities. Maximum turbine power ($P_{m\ max}$) and generator power ($P_{e\ max}$) are the maximum power points at different rotor speed with changing wind. It is desired that the maximum power controller follows that generator power curve at variable wind speed. As shown in Eqns. (1.6 and

1.7), mechanical output power is a function of TSR, so maximum power is extracted at optimum TSR. Rotor speed is a controllable variable in TSR equation. The rotor speed can be controlled mechanically or electrically. It can be achieved by changing pitch angle of the turbine rotor (mechanically) or changing load on the generator (electrically). With unpredictable wind speed change, mechanical control is not feasible. Mechanical elements suffers from considerable faults and increasing maintenance expenses [5]. To make the control efficient and robust, generator terminal voltage needs to be controlled using some power converter such a way that rotor speed corresponds to optimum TSR with changing wind speed. The load at the generator can be changed by controlled rectifier converter as discussed in Chapter 2.

Several types of control schemes such as duty cycle control, look up table for optimum rotor speed and optimum TSR have been proposed to improve the performance of wind power extraction [1, 2, 7, 6, 12, 15, 19-26]. However, these schemes depend on wind turbine characteristics (torque, power and power coefficient curves) or wind speed either before or during execution. Wind turbine components tend to change their characteristics over the time; moreover, some of these strategies are customized for a particular turbine. In addition, they don't take atmospheric change in air density into consideration which plays significant part in the aerodynamics of the turbine.

Control strategy independent of WT characteristics, such as perturbation and observation (PO) method is very flexible and accurate [23]. Optimum power search algorithm proposed in this work tracks peak power points in P-ω (power-speed) curve corresponds to dP/dω = 0. In [5] neural network based MPPT algorithm and in [11] back propagation neural network based MPPT algorithm are proposed.
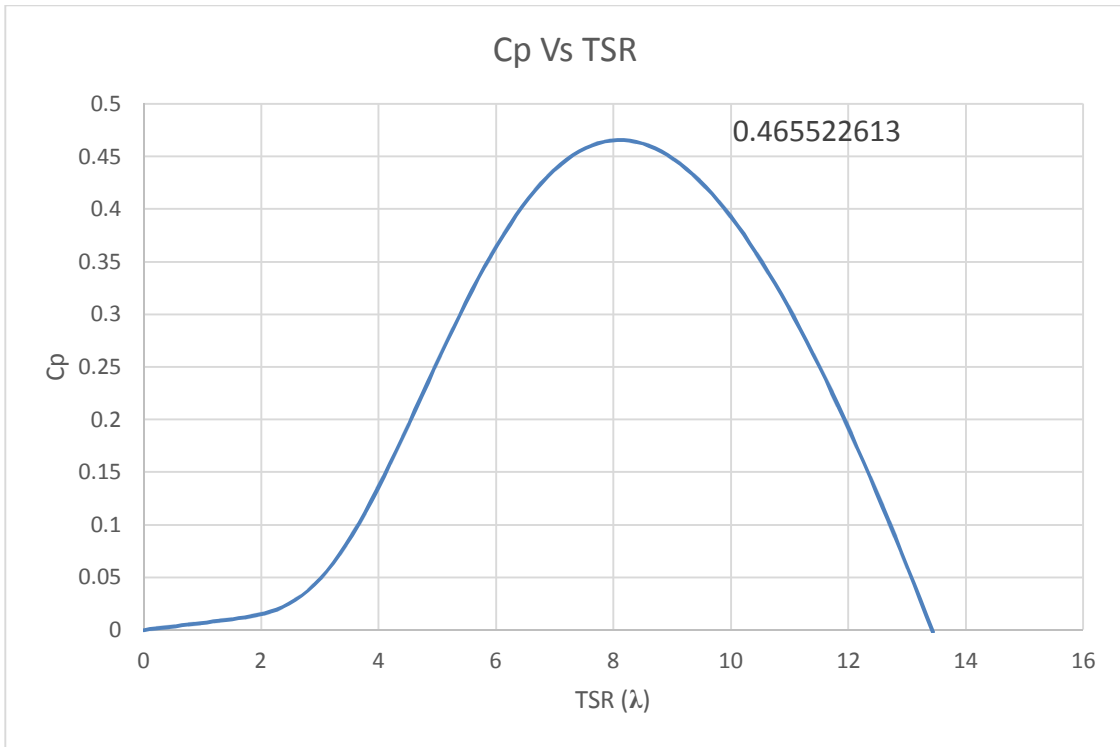
Fig. 3. 1 Power coefficient C_P as a function of the tip speed ratio λ and the pitch angle β at different wind Velocities.
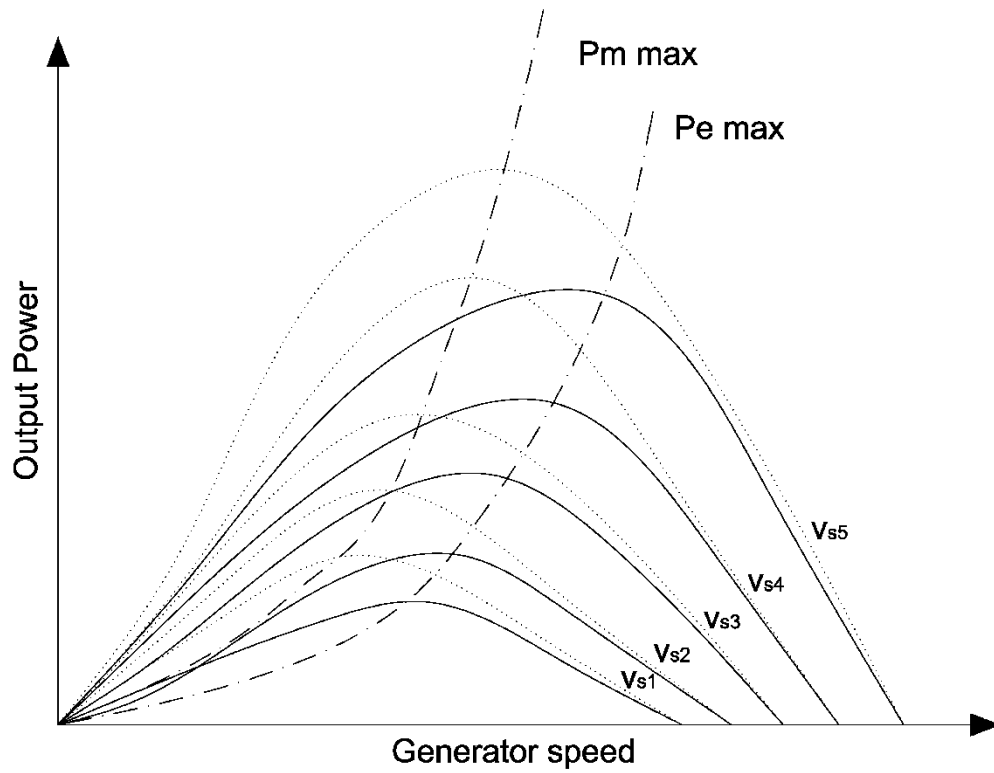

Fig. 3. 2 Generator Power-Speed characteristics at various wind velocities ('….' -turbine power; '___'-generator power)

47

With changing wind speed, rotor speed needs to be controlled optimally to extract the maximum power from WT. The proposed MPPT algorithm computes optimum speed based on change in output power direction. It conforms that power curve (P-ω) corresponds to dP/dω = 0 follows the maximum power point as shown in Fig. 3.3.
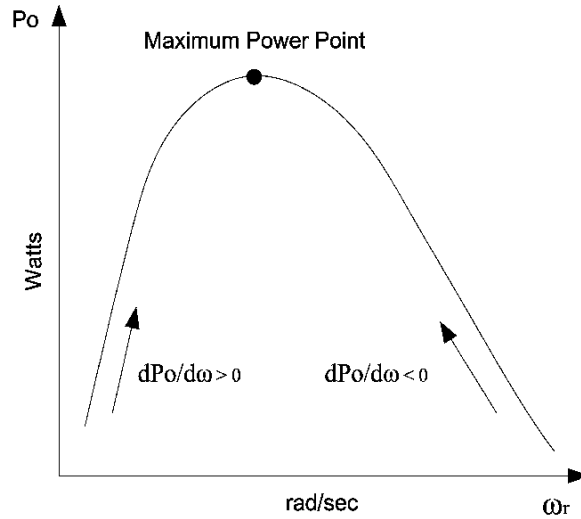

Fig. 3. 3 Hill climb search algorithm for MPPT.

3.1 Conventional Control of WT

The block diagram of conventional MPPT based control of IPMSG is shown in Fig. 3.4. In conventional MPPT control the optimum torque (T_{opt}) of the IPMSG can be found using eqn. (3.1) [12, 27] which is a function of WT mechanical parameters and the optimum value of C_p ($C_{p\ opt}$). Generally, it is considered constant to extract maximum power for specific WT. For example, in Fig 3.1 it was 0.465.

In this method, if the rotor speed is higher than the optimum, the generator torque is higher than that of the turbine, decelerating the system. Inversely, if the rotor speed is lower than the optimum, the generator torque is lower than that of the turbine, accelerating the system.

48

Therefore, by the use of this simple rule, the convergence to the maximum power point in steady state is obtained.
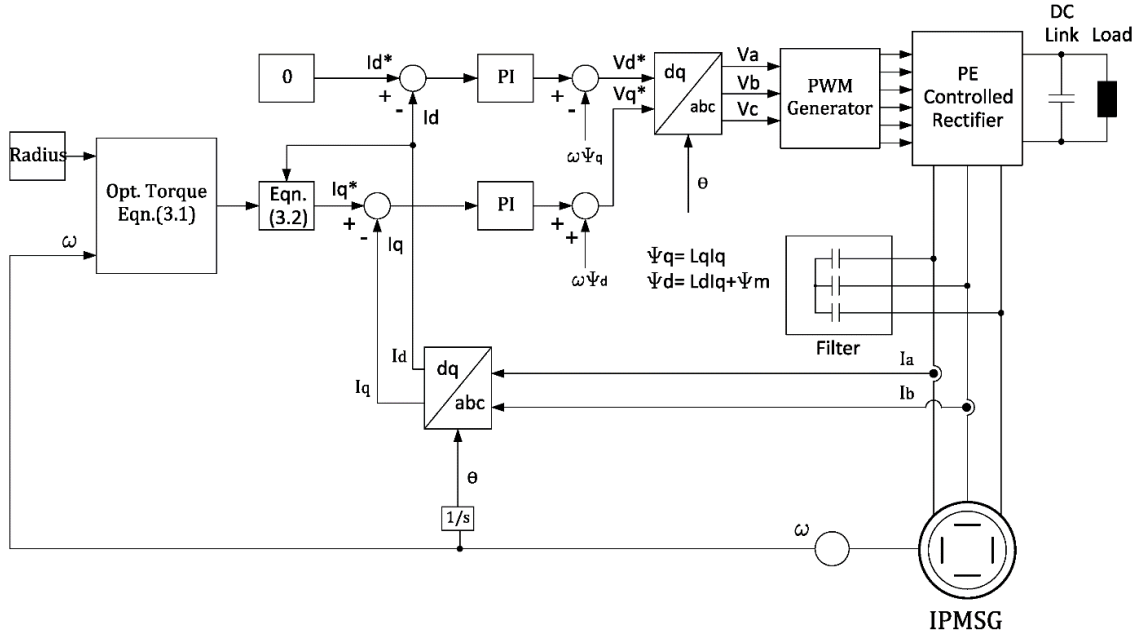

Fig. 3. 4 Conventional MPPT control of IPMSG.

$$T_{opt} = \frac{\pi}{2} \rho C_{p\_opt} \frac{R^5 \omega_r^2}{\lambda_{opt}^3} \tag{3.1}$$

The optimum i_q can be found from T_{opt} as follows:

$$i_{q\_opt} = \frac{\frac{2}{3P} T_{opt}}{\psi + (L_d - L_q) i_d} \tag{3.2}$$

The main disadvantage of this method is the reference signal depends on a priori information of wind turbine characteristics. To provide turbine independent control, an algorithm based control can be used. Perturbation and observation method is an online optimization algorithm, which is used in this thesis for maximum power extraction. This concept is explained as follows.

3.2 Proposed MPPT Algorithm

The proposed adaptive MPPT controller uses perturbation and observation (PO) based algorithm. Estimated power output P_e is calculated based on sensed currents and voltages. This power is sampled to check the changes in direction and difference between previous and current value (ΔP_e). ΔP_e is checked if it's within the adequate range, then the optimum speed reference value remains same.

The flow chart for the proposed MPPT algorithm based PO method is shown in Fig 3.5. X is the control variable, which is considered as rotor speed for this thesis. According to the direction of ΔP_e and ΔX, sign is assigned for optimum step change in speed which is shown in Table 4.1.

Table 4.1: Sign deciding table for control variable step:

ΔPe	ΔX	Sign ΔXstep
+	+	+
+	-	-
-	+	-
-	-	+

The sign is multiplied with ΔP_e and variable 'K' to find optimum ΔX. Here, K is a function of X which is designed in such a way that it gives larger value of ΔX at low and high value of X. The following function is developed to adapt the coefficient K with the value of X based on trial and error in simulation so that the MPPT algorithm converges faster.

$$K = -2 * e^{(-0.00002*(x-300)^2))} + 2.01 \tag{3.3}$$

Optimum speed reference is found by adding ΔX to previous value of X. As shown in Fig. 3.6 optimum speed is tracked to extract maximum power at different wind speeds. The curve connecting to A-B-C shows the path of maximum power points.
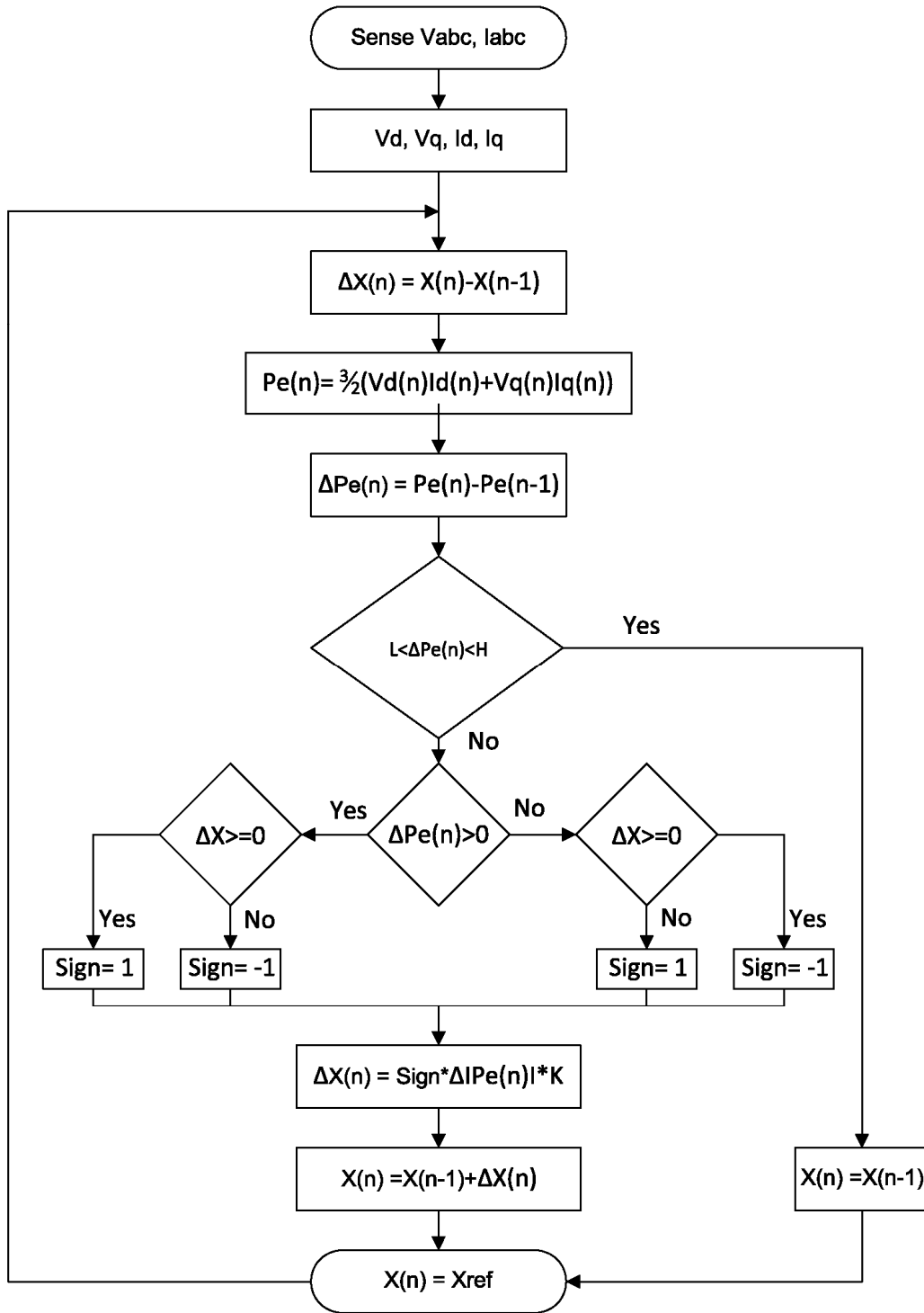
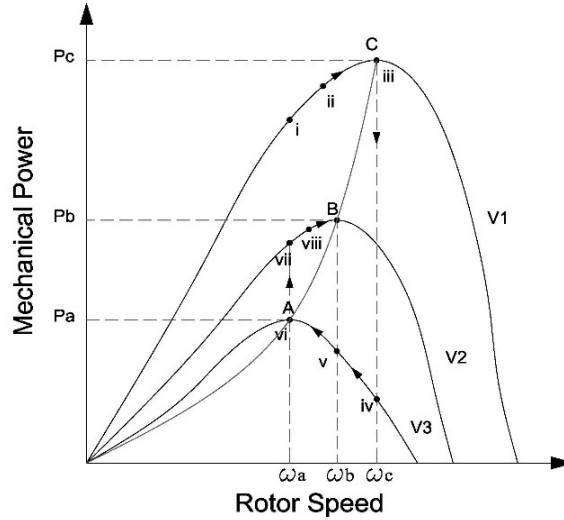**Fig. 3. 5 Proposed MPPT control of IPMSG.**

Fig. 3. 6 Change of operating point for MPPT.

3.3 Overall Control of the Proposed WECS System

The block diagram of the control structure for the proposed WECS with MPPT algorithm and flux weakening control (FWC) algorithm is shown in Fig. 3.7. The phase currents and voltages are converted into d-q axis quantities to control torque and the flux of IPMSG respectively. The reference speed ω^* is generated based on newly developed MPPT algorithm, which is compared with actual speed of IPMSG. The speed error is processed through speed controller which gives the q-axis command current i_q^* as output. To control generator flux, d-axis command current i_d^* is controlled by maximum torque per ampere if the speed is below rated speed, and FWC if it is above rated. Obtained d-q axis command voltages from i_d^* and i_q^* generates PWM signals for generator side controlled rectifier. On dc-link resistive load is connected across low pass filter. Capacitive bank is connected between IPMSG and controlled rectifier to filter out voltage spikes generated by rectifier.
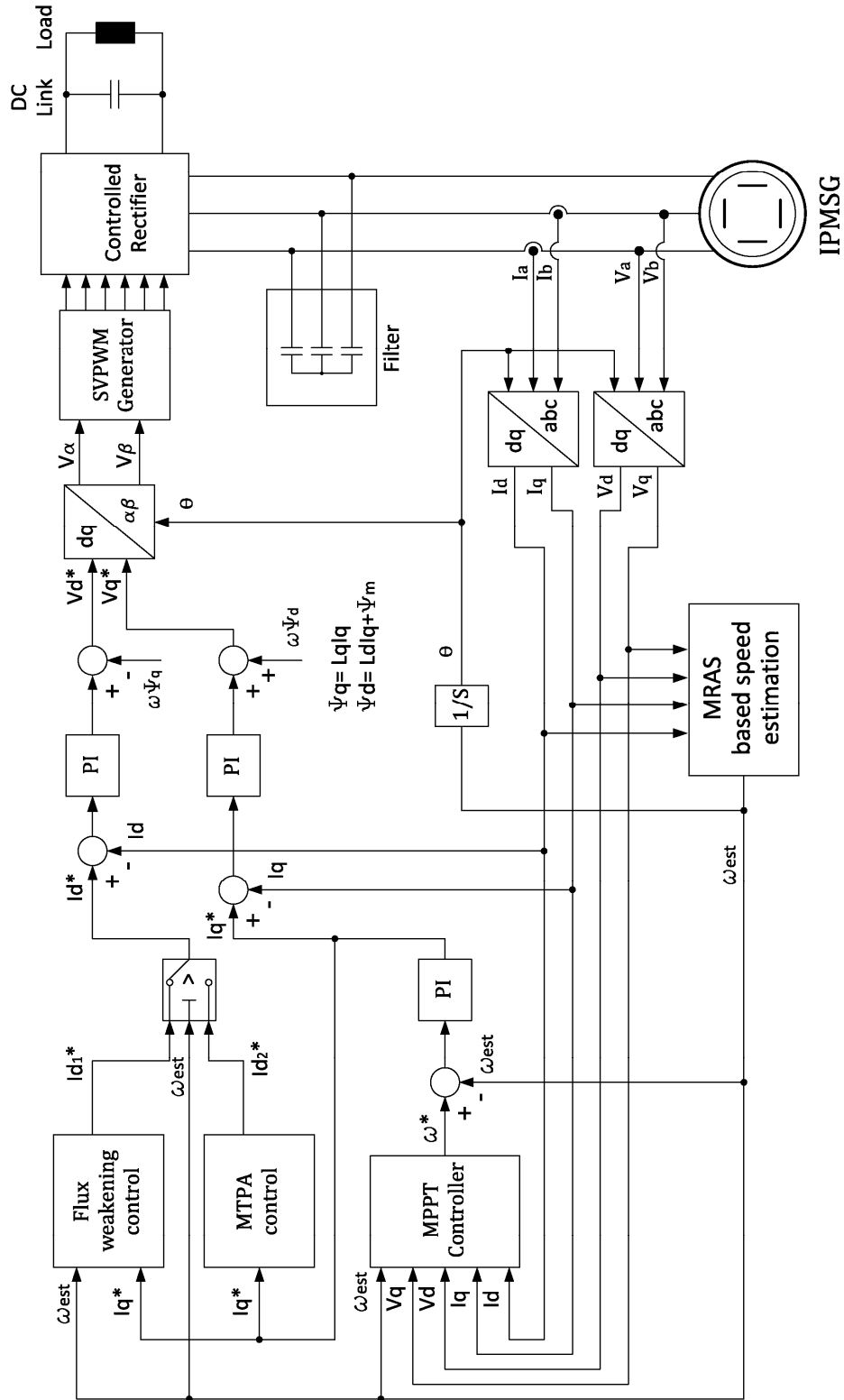
52

Fig. 3. 7 Proposed WECS configuration and control structure.

3.4 Flux Controller Design

Precise control of the high performance IPMSG over a wide speed range is an engineering challenge. Traditionally in the design of the controller, $i_d = 0$ is taken to make the control task easier with this assumption the flux supplied by the permanent magnet remains constant. Moreover, the assumption of $i_d = 0$ leads to a non-optimum efficiency and sometimes instability of the IPMSM even below the base rotor speed. The speed is inversely proportional to the flux due to permanent magnet and proportional to the back EMF. In order to operate the machine above the base speed within the rated voltage capacity of the generator and the rectifier, the field flux must be weakened. In the case of the IPMSG, direct control of the field flux is not possible. However, the field flux can be weakened by the demagnetizing effect of the d-axis stator current i_d. Above the base speed as the voltage and the current remain fixed to their maximum value, the power remains constant. The operation above the base speed is called the constant power mode. Recently, researchers [84-91] have reported some work in the flux weakening control technique of the IPMSM. The proposed flux control scheme incorporates the maximum torque per ampere (MTPA) operation in the constant torque region i.e., below the base speed and the flux-weakening operation in the constant power region i.e., above the base speed. The power capacities of the machine and the converter are also considered. The efficiency of the above mentioned control techniques of IPMSM drive system is evaluated by simulation results.

The first term of developed torque Eqn. (2.23) represents the magnet torque component due to the rotor permanent magnet flux ψ_m and the second term represents the reluctance torque due to the complex interaction of d-q axis currents and inductances of the IPMSM. In the case of the IPMSM, i_d is negative and the q-axis inductance L_q is greater than the d-axis inductance L_d,

so the reluctance torque component is an additional advantage for the IPMSM in terms of performance and cost. To make the torque equation linear and the control task easier, usually i_d is set to zero. However, in an actual IPMSM nonlinear drive, the assumption of $i_d = 0$ leads to erroneous results due to the saturation of the current regulator particularly at high speeds. In the proposed technique i_d is not considered zero. The value of i_d is calculated from i_q maintaining the armature voltage and current within the capacity of the generator and the converter.

The stator phase voltage and current can be related to the d-q axis voltages and currents as per Eqns. (2.32 and 2.33). The maximum value of the stator phase voltage and current are V_m and I_m, respectively. Below the base speed, with the assumption of keeping the absolute value of stator current I_a constant at its maximum value I_m, i_d can be calculated in terms of i_q for MTPA. This is obtained by differentiating Eqn. (2.23) with respect to i_q and setting the differentiating result to zero as [86],

$$i_d = \frac{\psi_m}{2(L_q - L_d)} - \sqrt{\frac{\psi_m^2}{4(L_q - L_d)^2} + (i_q)^2} \qquad (3.4)$$

Above the base speed, the steady-state current i_d can be calculated in terms of i_q in order to maintain the absolute value of stator voltage V_a constant at its maximum value of V_m. This is obtained from Eqns. (2.14, 2.15 and 2.32) by neglecting the voltage drop across the stator resistance as [86],

$$i_d = -\frac{\psi_m}{L_d} + \frac{1}{L_d} \sqrt{\frac{(V_m')^2}{P^2 \omega^2} - L_q^2 (i_q)^2} \qquad (3.5)$$

where V_m' is the corresponding maximum stator phase voltage.

$$V_{m}{}' = \sqrt{\left(v_{do}\right)^2 + \left(v_{qo}\right)^2} \qquad (3.6)$$

$$v_{do} = -P_n \omega i_q L_q \qquad (3.7)$$

$$v_{qo} = P_n \omega i_d L_d + P_n \omega \psi_m \qquad (3.8)$$

The typical torque-speed characteristic curve over a wide range of speed is shown in Fig.3.8. Eqn. (3.5) represents an ellipse in the d-q plane, which indicates that an increase in rotor speed results in smaller ranges for the current vector. By appropriately controlling id, the amplitude of the terminal voltage is adjusted to V_m.
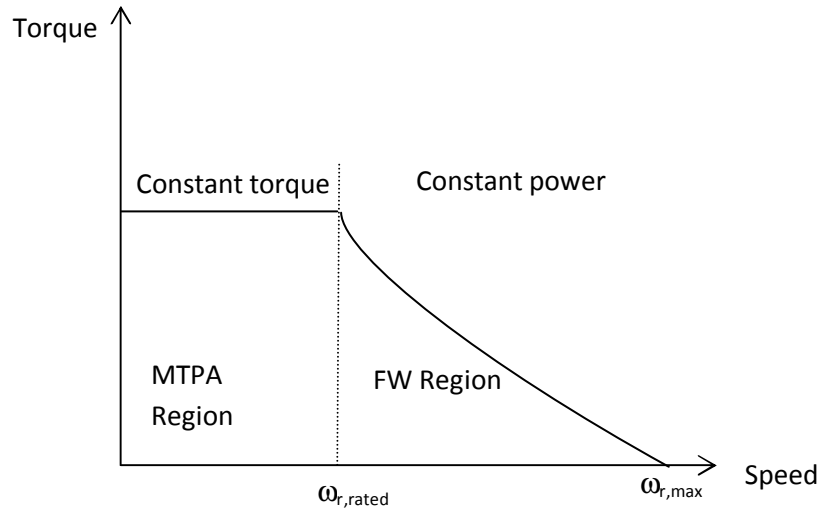
Fig. 3. 8 Typical torque-speed characteristic curve over wide range of speed.

It is seen from Eqns. (3.4) and (3.8) that in case of $i_d = 0$, the magnitude of the terminal voltage V_a increases with an increase in machine speed ω or the q-axis current i_q. Therefore, the saturation of the current regulator occurs at high speeds for a given torque when the generator terminal voltage approaches V_m. This may cause instability of the drive for $i_d = 0$ control. From Eqn. (3.5) the maximum attainable speed for a given set of maximum stator voltage and current can be calculated as,

$$\omega_{\max} = \frac{\sqrt{V_m^2 - R_s^2 I_m^2}}{P\left(\psi_m - L_d I_m\right)} \qquad (3.15)$$

In the case of the conventional $i_d = 0$ control technique, the maximum attainable speed can be calculated in order to maintain the maximum voltage limitation of the rectifier as,

$$\omega_{\max} = \frac{V_m}{P_n \psi_m} \qquad (3.16)$$

3.5 Simulation Results

The effectiveness of the proposed IPMSG incorporating the Novel MPPT and flux control technique is investigated first in simulation using Matlab/Simulink. The wind turbine is modeled based on Eqns. (1.5)-(1.9). The parameters for IPMSG used in simulation are shown in Appendix A. All waveforms are respect to time unless they're specified. To test the efficiency of MPPT and stability of the WECS system, two types of wind profiles are used in simulation. In the first section, wind with sudden disturbance is applied to check step change and steady state conditions. The second section, real wind speed profile is designed according to Eqn. (1.7) to test the system with real wind variation.

In the wind turbine modeling, it can be seen for Eqns. (1.5)-(1.9) that produced turbine torque is a function of generator speed. As the initial generator speed is zero, a constant torque is given to generator for the startup. When enough torque is built by the WT to drive the generator, constant torque is switched to WT torque. In some results of this section, this switching can be seen as a disturbance during initial transient state.

3.5.1 Sudden Disturbance in Wind Speed

In this section, system performance due to step changes in wind speed is investigated while the dc-link is loaded with 20Ω resistor. Wind speed is varied from 8m/s to 17m/s in a stepwise manner as shown in Fig. 3.12 (a) [1-3, 5, 7]. Fig. 3.12 (b) shows the corresponding speed response of IPMSG. It is seen from this figure that the generator speed follows the wind speed smoothly. Fig. 3.13 (a) and 3.14 (a) show three phase currents and voltages responses respectively. It is seen from these Figures that the generator currents and voltages are proportional with the wind speed, which verifies that the algorithms are working properly. Fig 3.13(b) and 3.14(b) show the zoom-in view of the steady-state currents and voltages respectively. This verifies the balanced operation of the generator.

Figs. 3.13 (a) and (b) show dc-link voltages and currents with step changes in wind speed, respectively. It is seen from these Figures that the proposed WECS is transferring more power to the dc-link when wind speed increases.

Fig. 3.14 shows how the dc-link & wind turbine powers track with the variation in wind speed according to proposed MPPT algorithm. The WT power is the input power to the generator and hence, the difference between the turbine power and dc-link power is the losses in the generator, converter and filters.

Fig 3.15 shows the variation of overall efficiency of the WECS system with step changes in wind speed. The efficiency is calculated by the ratio of dc-link power and WT power. It is found that the efficiency is maintained almost constant over wide speed range.

To conform the maximum power tracking, the C_p graph is shown in Fig. 3.16. As mentioned in earlier Eqns. (1.5-1.8), C_p is only controllable variable to extract maximum power.

The maximum C_p that can be achieved by proposed system is 0.465. The simulation results verify the analytical results shown in Fig. 3.1. Thus, the proposed WECS ensures the extraction maximum power from wind to the turbine output.

Fig. 3.17 shows the tracking of the power coefficient (C_p) with variation in TSR corresponding to changes in wind speed. It is clearly seen that the controller is tracking the C_p so that it can extract maximum power with step changes in wind speed. Thus, the C_p value was maintained constant. At different speed which was shown in Fig. 3.16.

Fig. 3.18 shows the tracking of dc-link power at different rotor speeds according to MPPT algorithm. It is clearly seen that the algorithm can track the maximum power condition almost smoothly. Thus, the algorithm ensures the stability of the overall WECS while tacking the maximum power transfer from turbine to dc-link. Furthermore, it verifies the analytical results shown in Fig. 3.2.

It can be seen from Fig. 3.19 that both the turbine power and dc-link power for the proposed control system is higher than those of the conventional controller based WECS. Thus, it verifies the effectiveness of transfer more power to the dc-link and power from wind especially, at high wind speed condition.

Fig 3.20 shows the variation in C_p for conventional control scheme. It is found that the conventional control cannot maintain C_p constant at different wind speeds, whereas the proposed control can maintain constant C_p corresponding maximum power extraction as shown in Fig 3.16
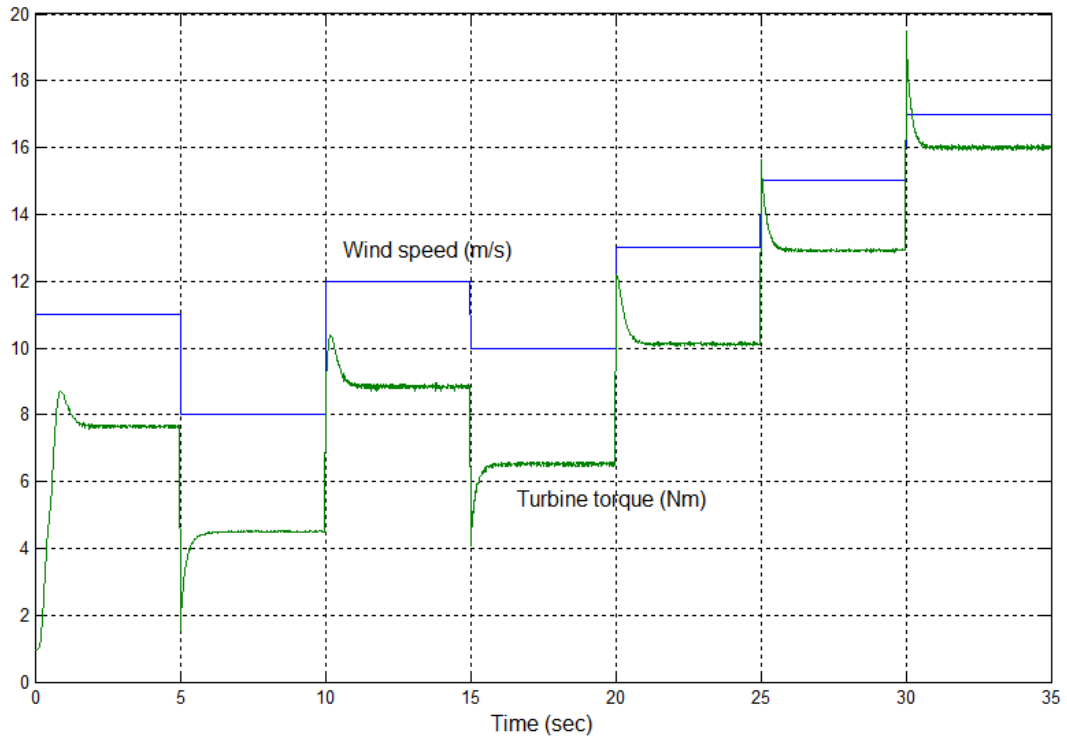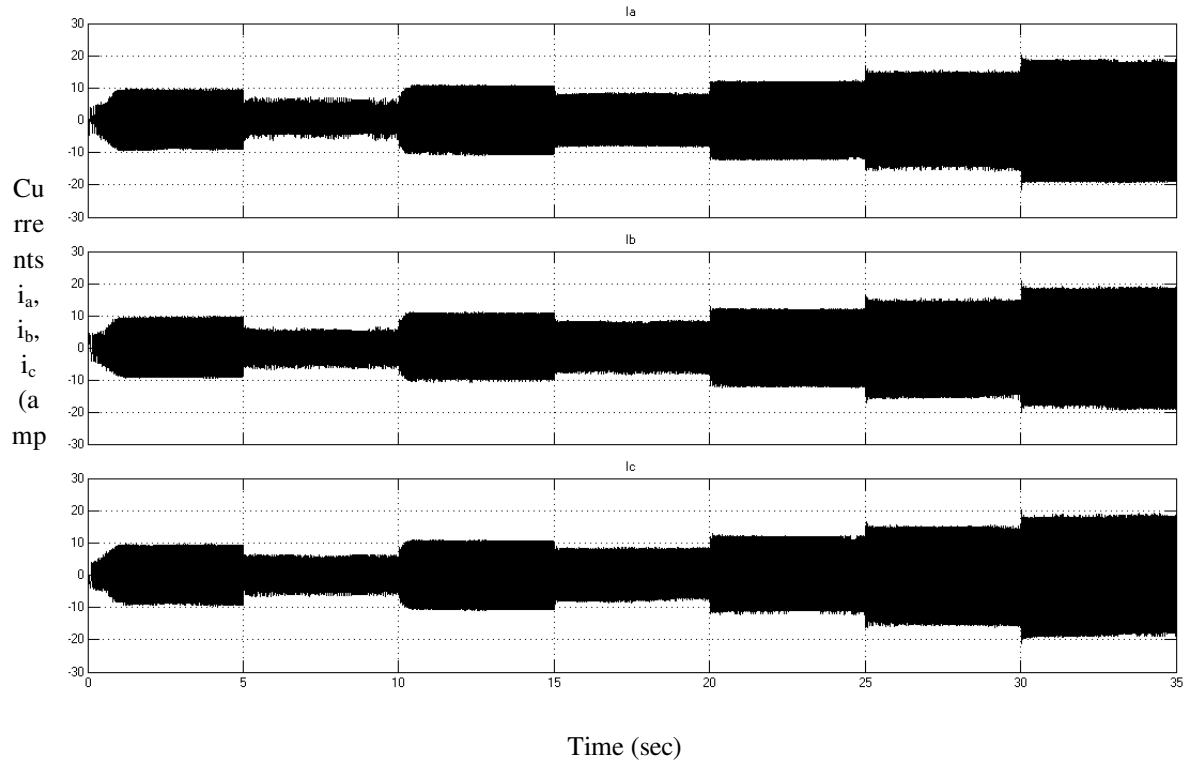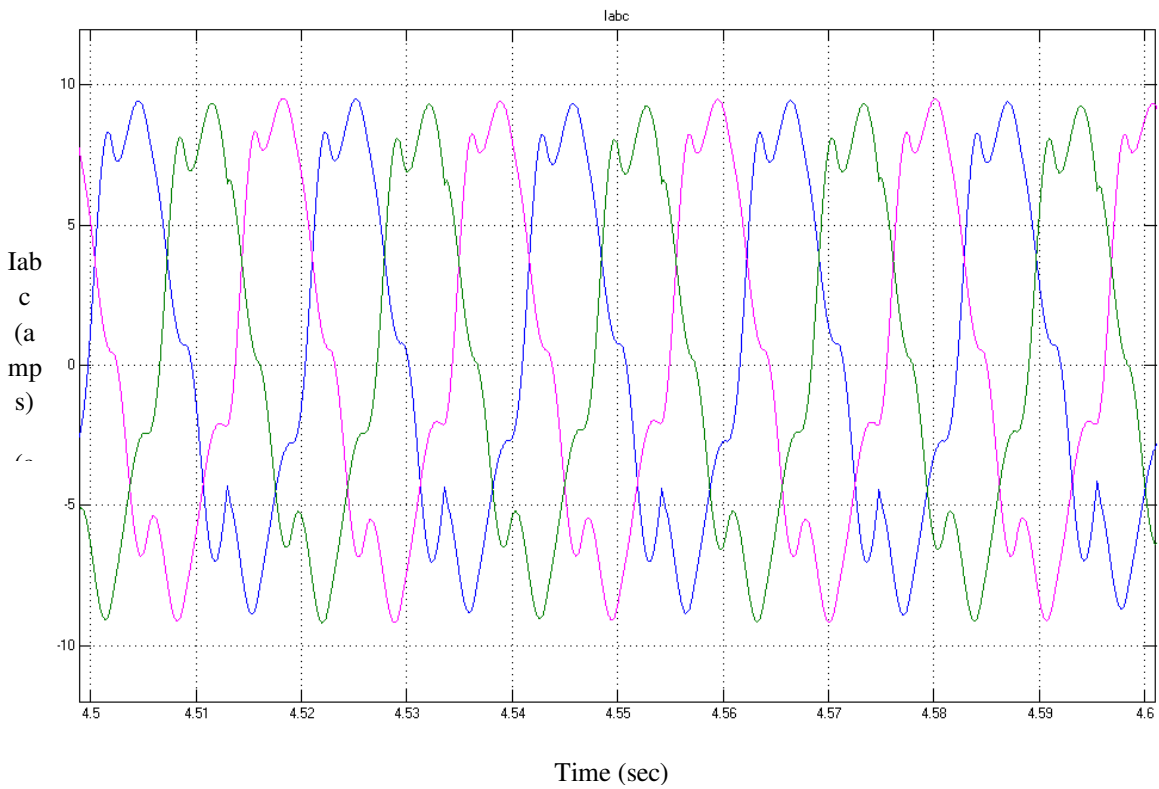
(a)
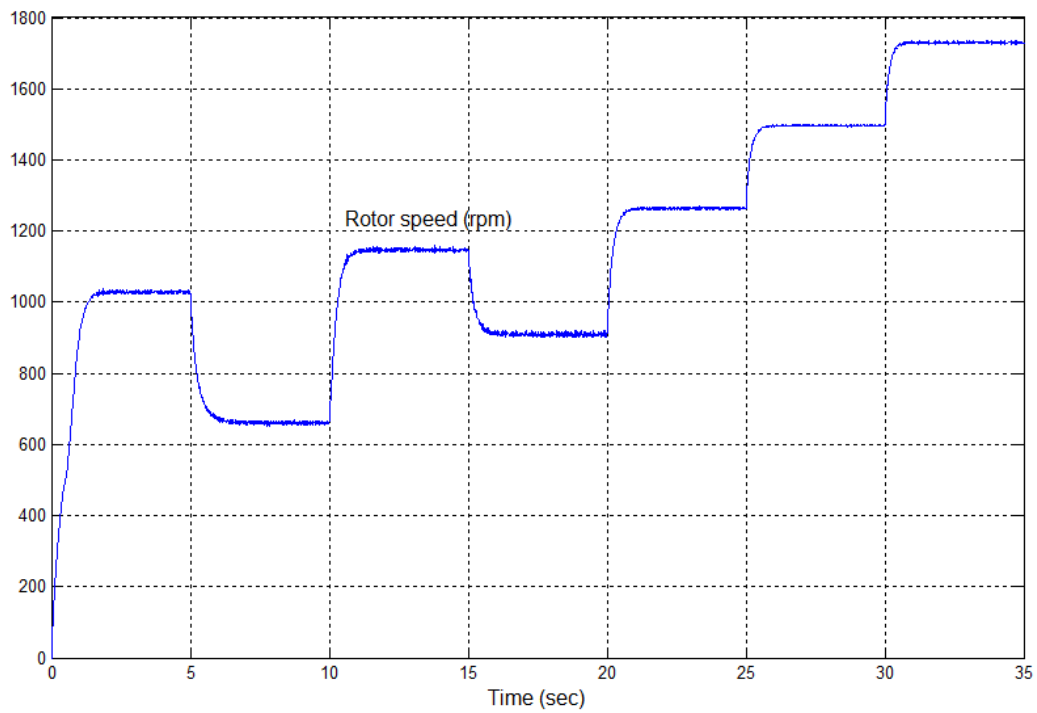
(b)

Fig. 3. 9 .   Responses of the proposed IPMSG based WECS for step changes of wind speed: (a) wind speed (m/s) and turbine torque (N.m) (b) rotor speed (rpm).
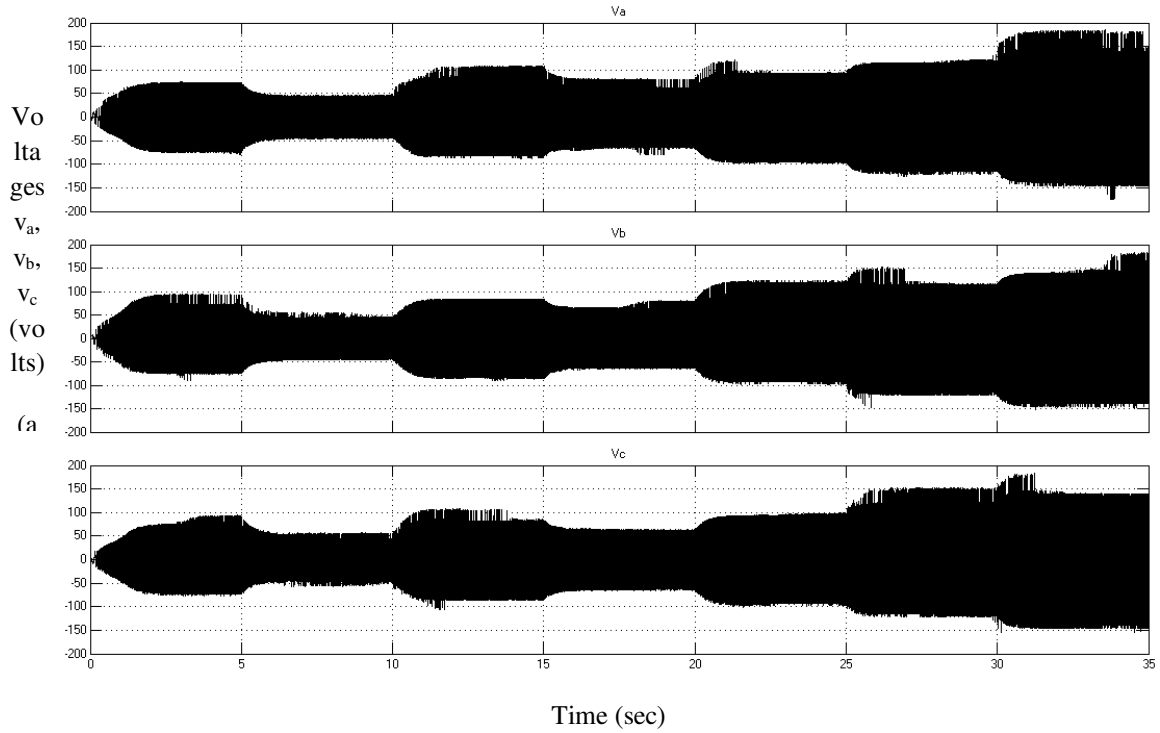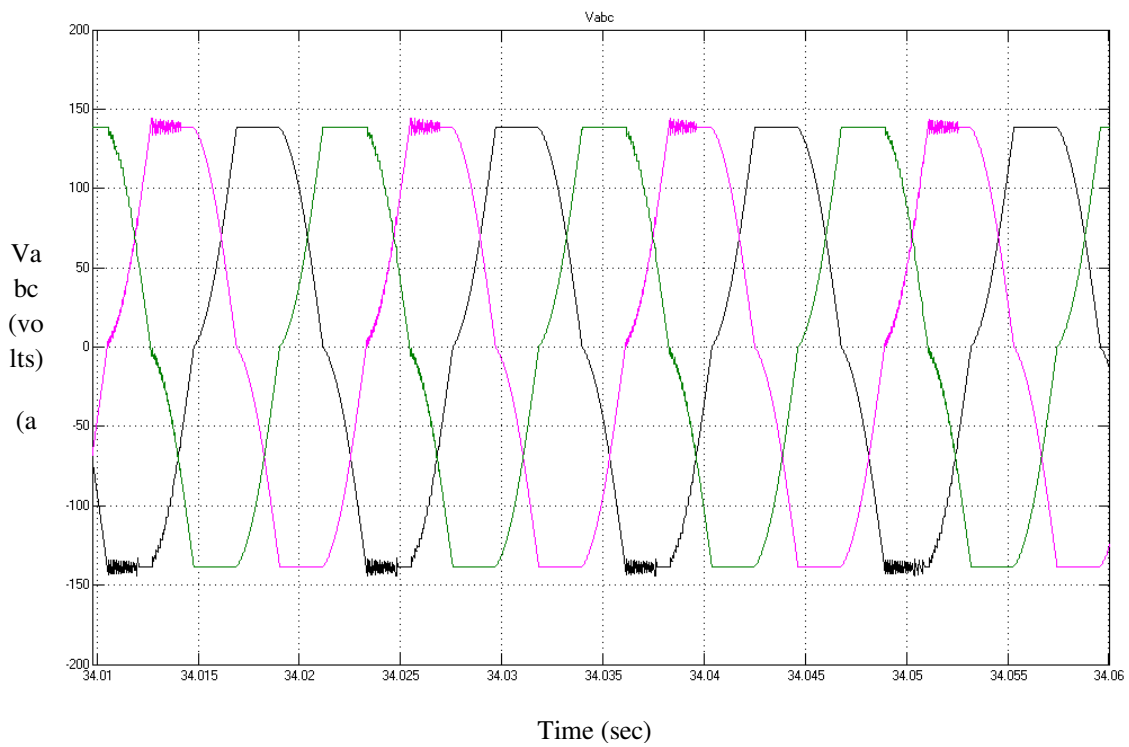
(a)

(b)

Fig. 3. 10 Responses with step changes in wind speed: (a) steady state three phase currents (a) zoom-in view of the steady state 3 phase currents.
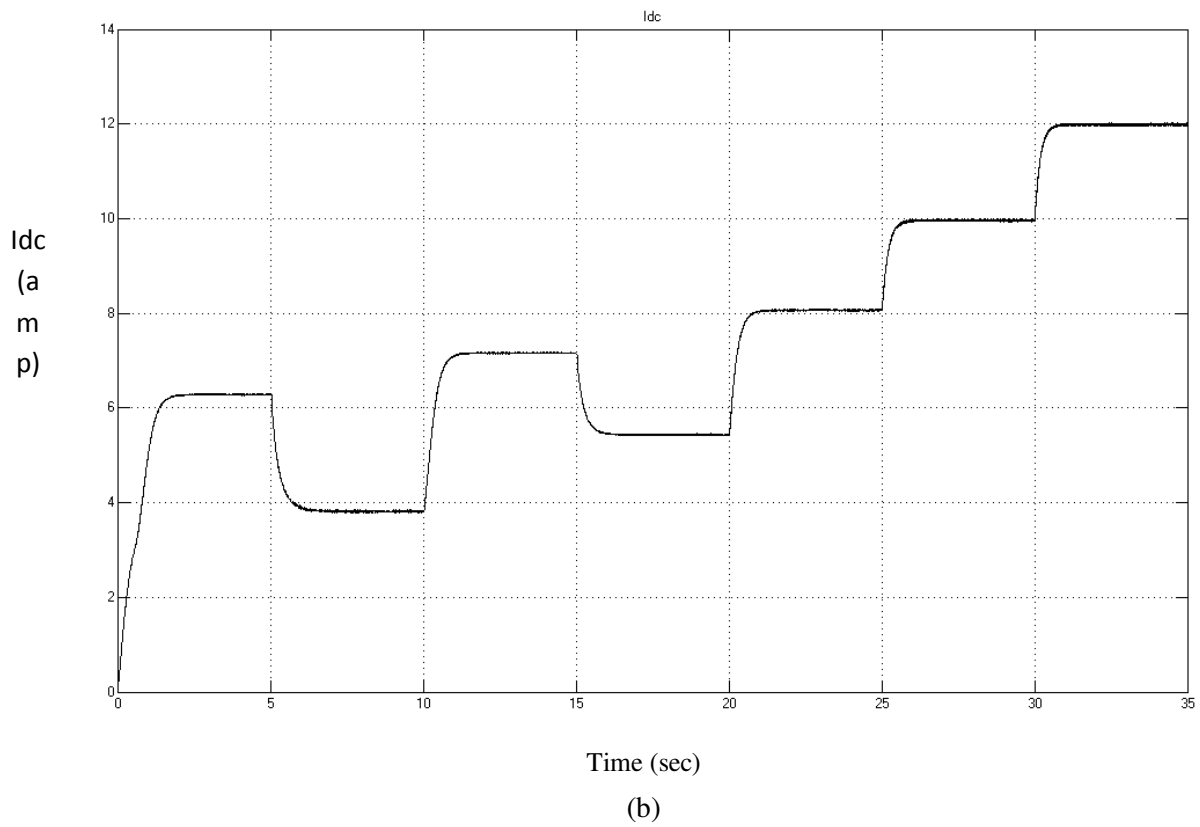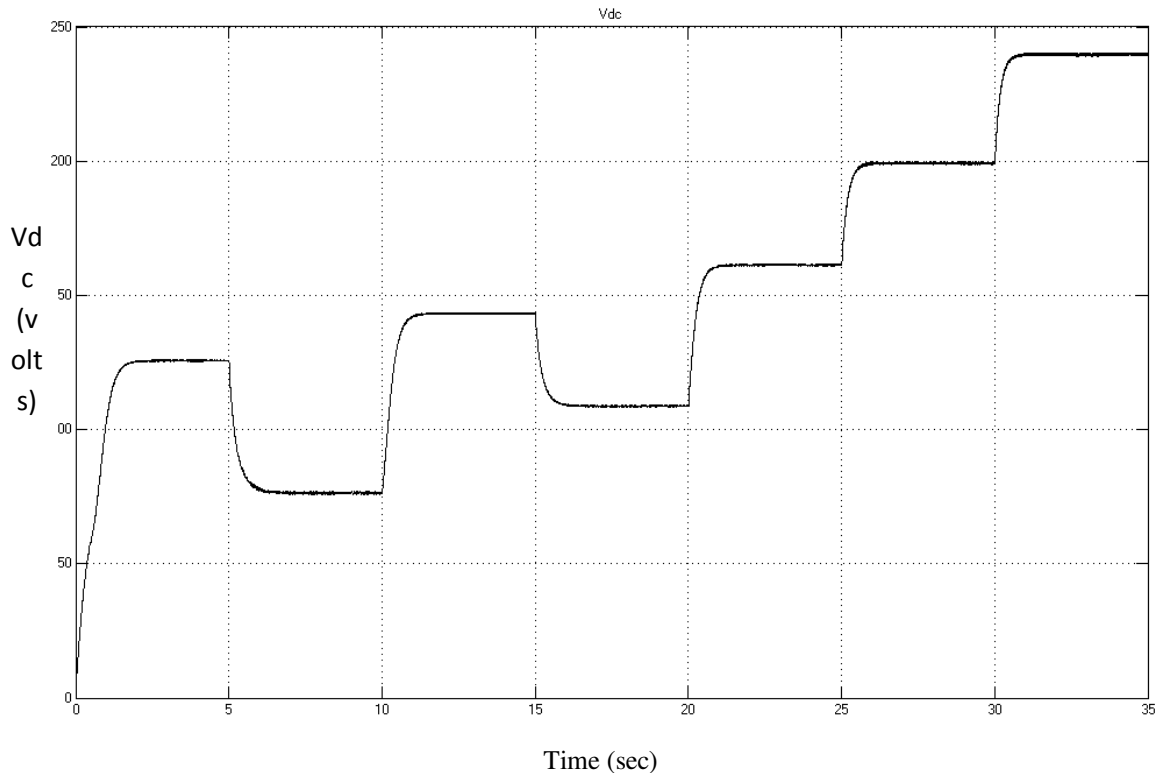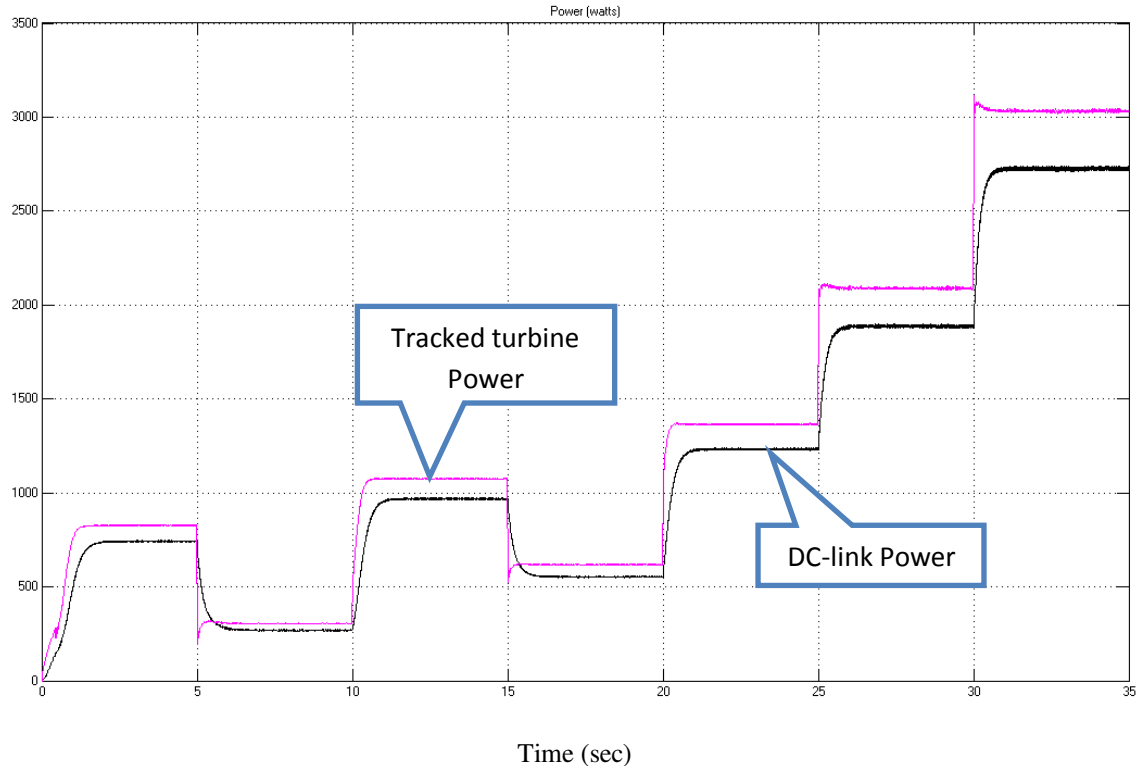
61

Time (sec)

(a)

Time (sec)

(b)

Fig. 3. 11 Responses with step changes in wind speed: (a) steady state three phase voltages (a) zoom-in view of the steady state 3 phase voltages.
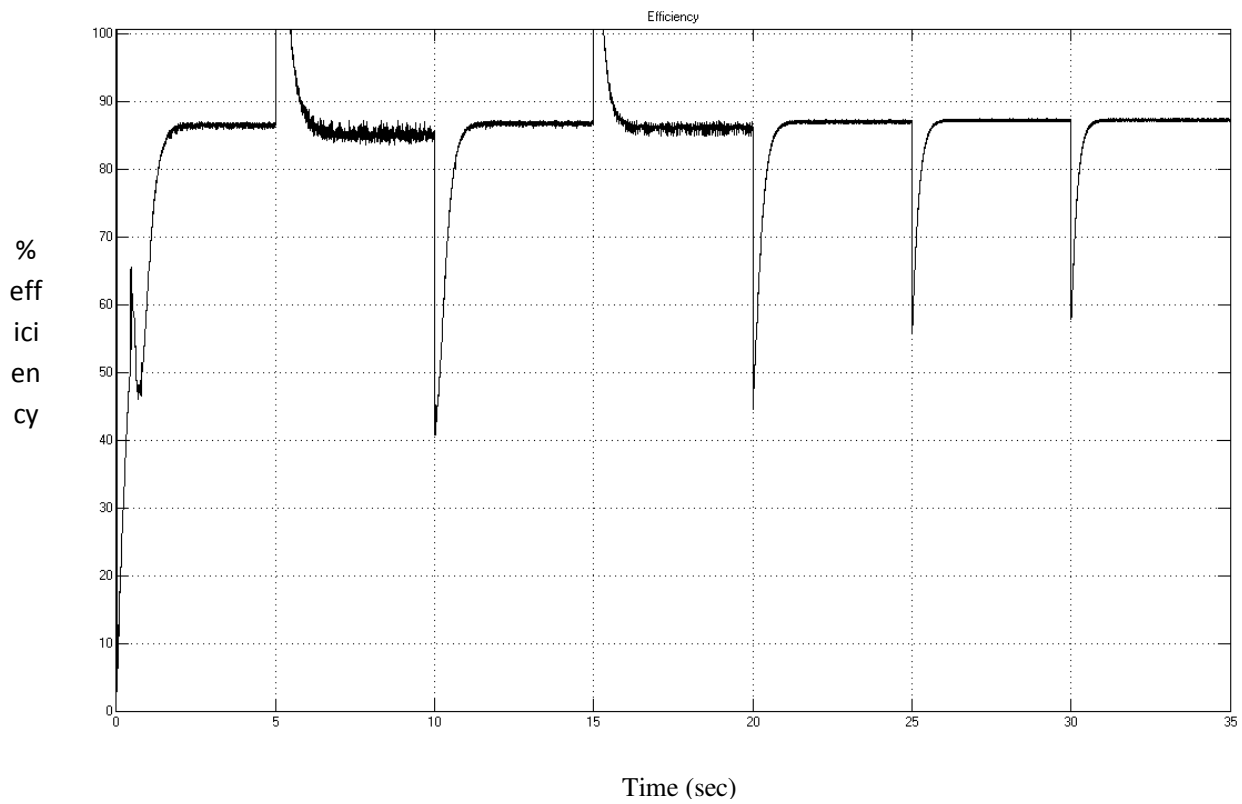
(a)

(b)

Fig. 3. 12 With changing wind speed response of tracked (a) dc-link voltage (Vdc) (b) dc-link current (Idc).

63

Fig. 3. 13 With changing wind speed response of tracked powers mechanical and dc-link power (W).

Fig. 3. 14 Overall % efficiency with step changes in wind speed.
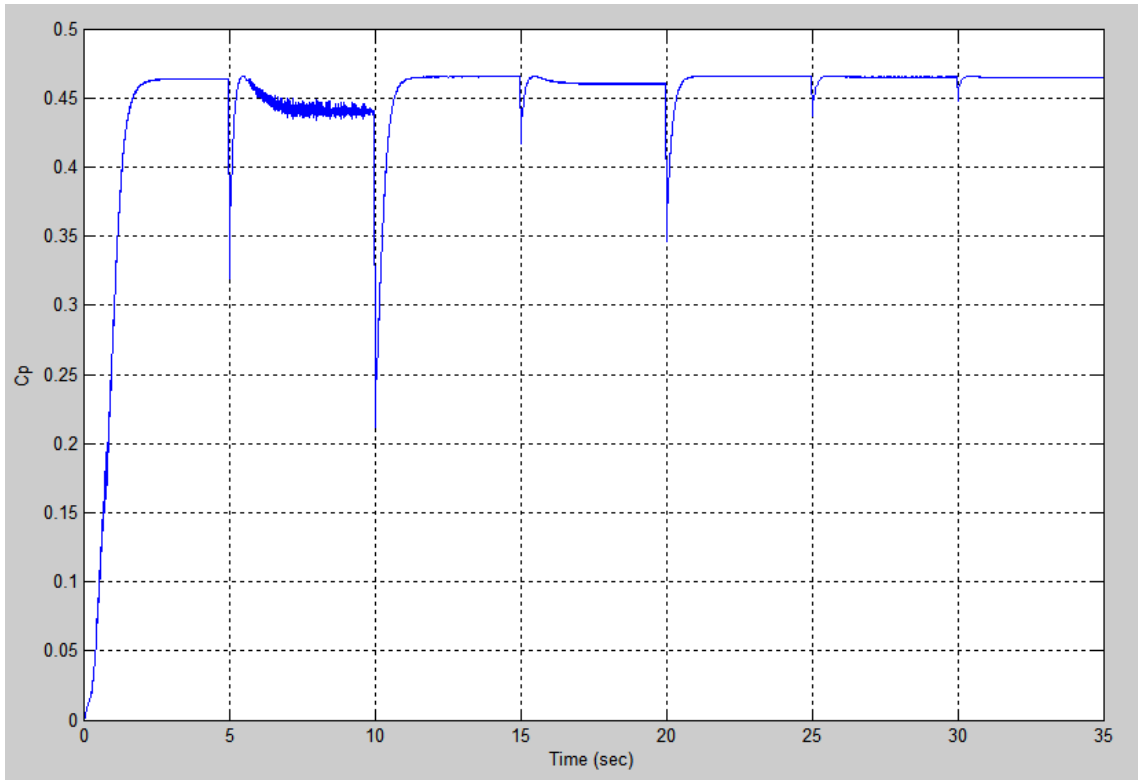
Fig. 3. 15 Turbine power coefficient Cp for proposed control of WECS with step changes in wind speed.
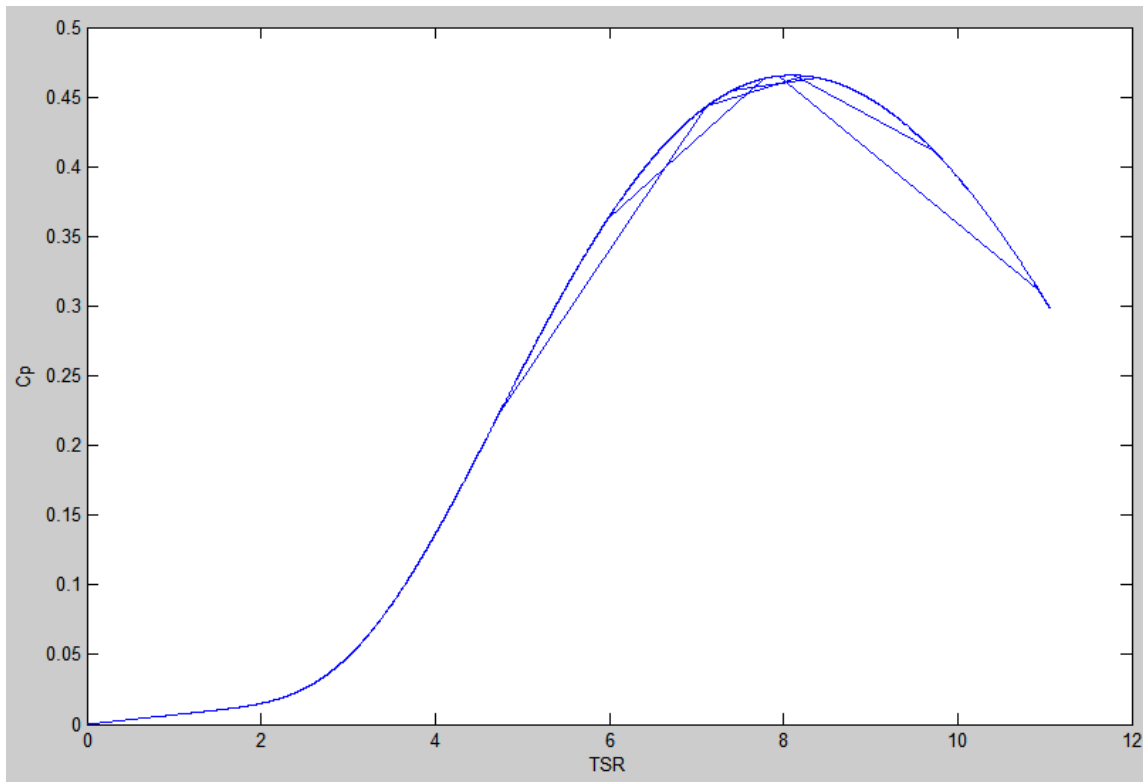
Fig. 3. 16 Power coefficient Cp vs tip speed ratio λ.

65
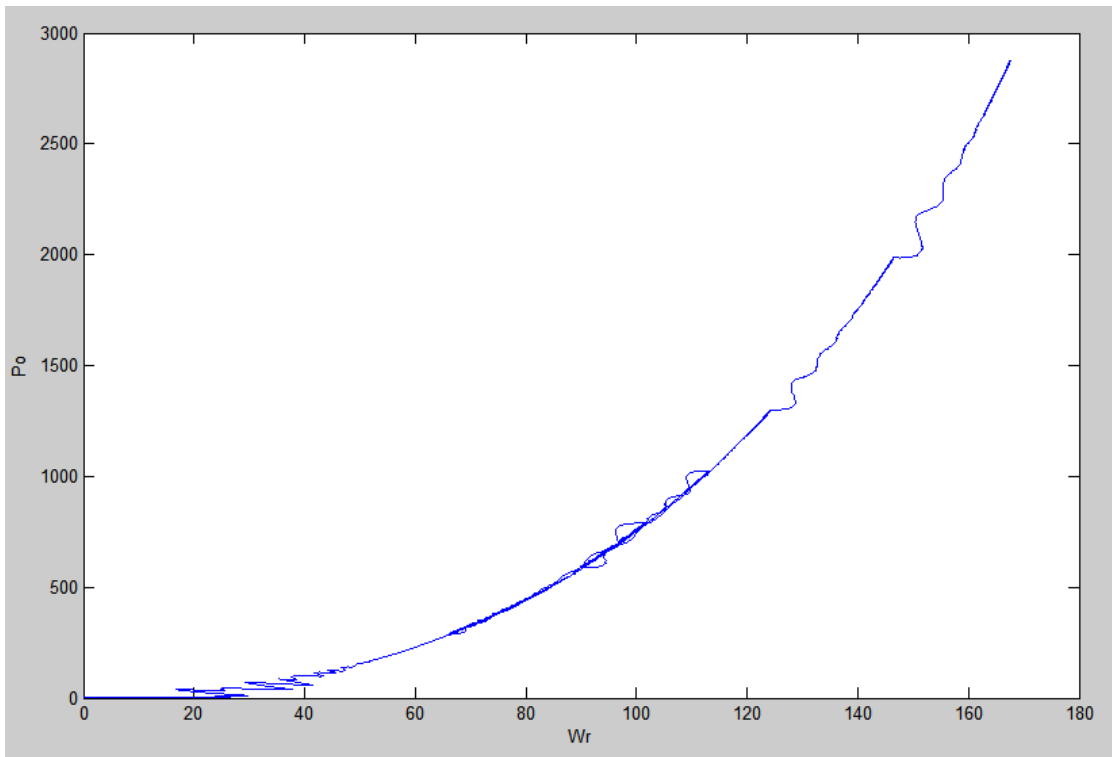
Fig. 3. 17 dc-link power (W) vs Rotor speed (rad/sec).
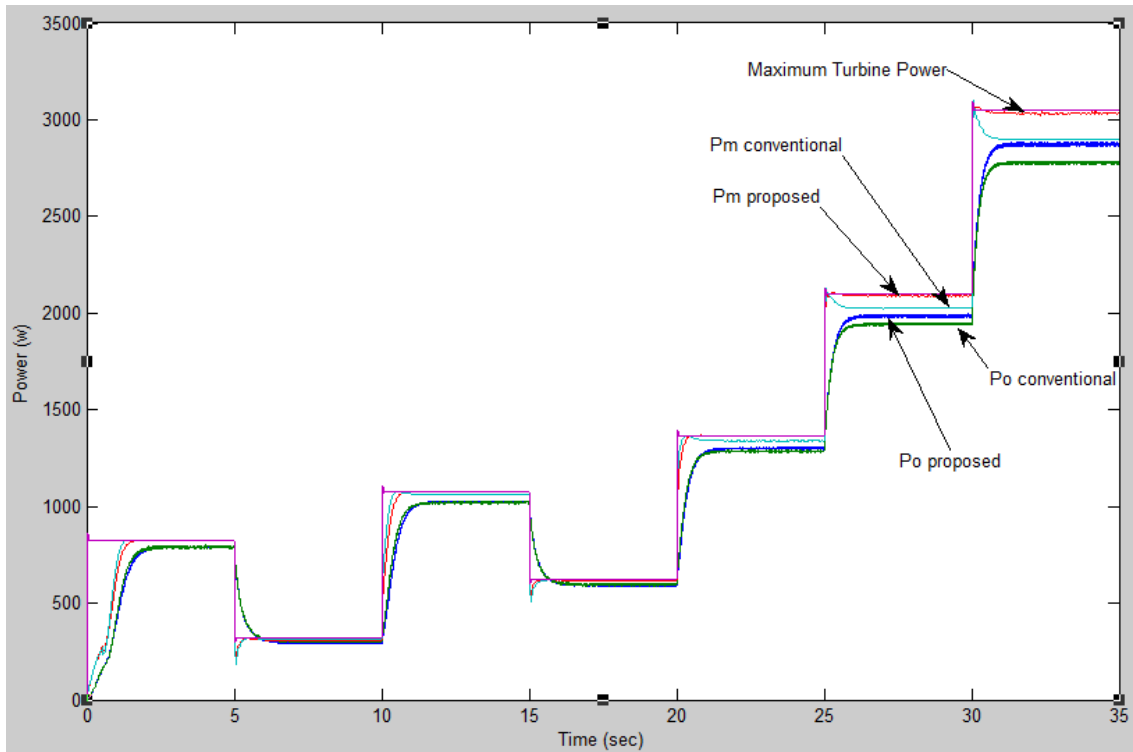
Fig. 3. 18 Power extraction for proposed and conventional WECS with step changes in wind speed.
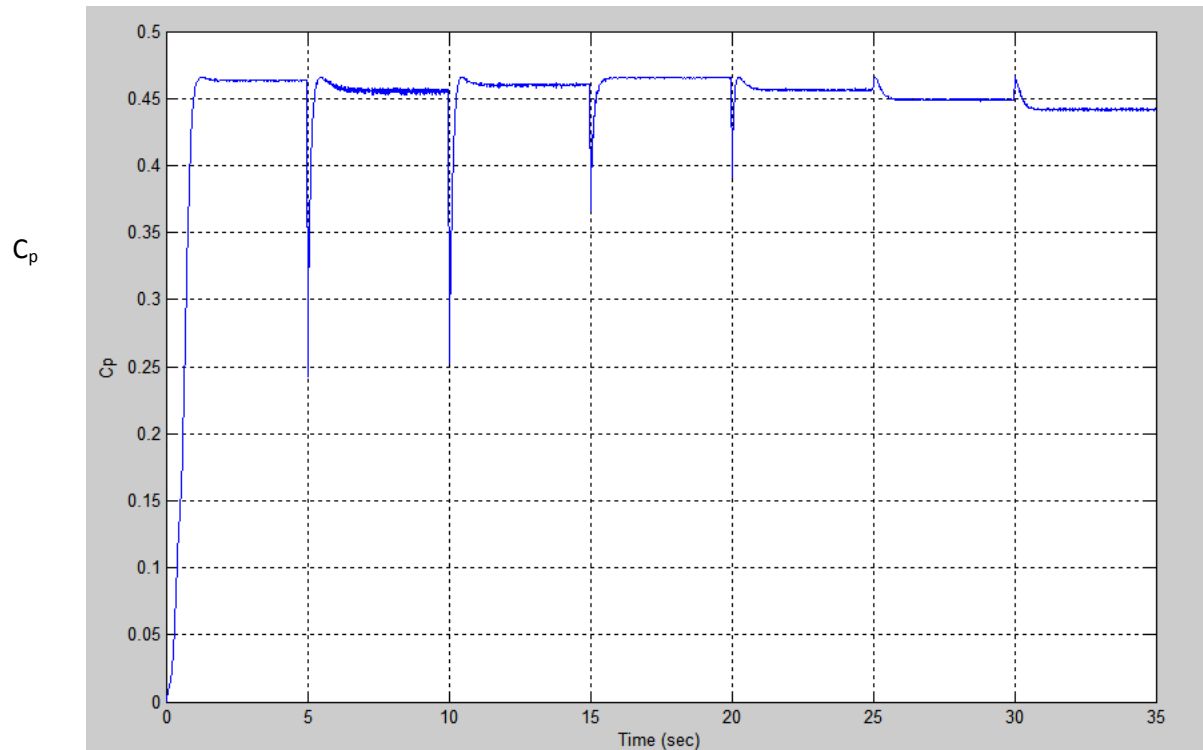
Fig. 3. 19 Turbine power coefficient Cp for conventional control of WECS with step changes in wind speed.

3.5.2 Real Wind Speed Model Based

Fig. (3.21-3.26) show similar responds to previous section for the proposed WECS with real wind speed variation. It is seen from Fig. 3.24 that the proposed control scheme can extract maximum power from wind to turbine output by maintaining almost constant C_p in spite of lot of variation in wind speed. It is also seen from Fig.3.26 that the proposed control can track the maximum power smoothly and stably with real wind model.
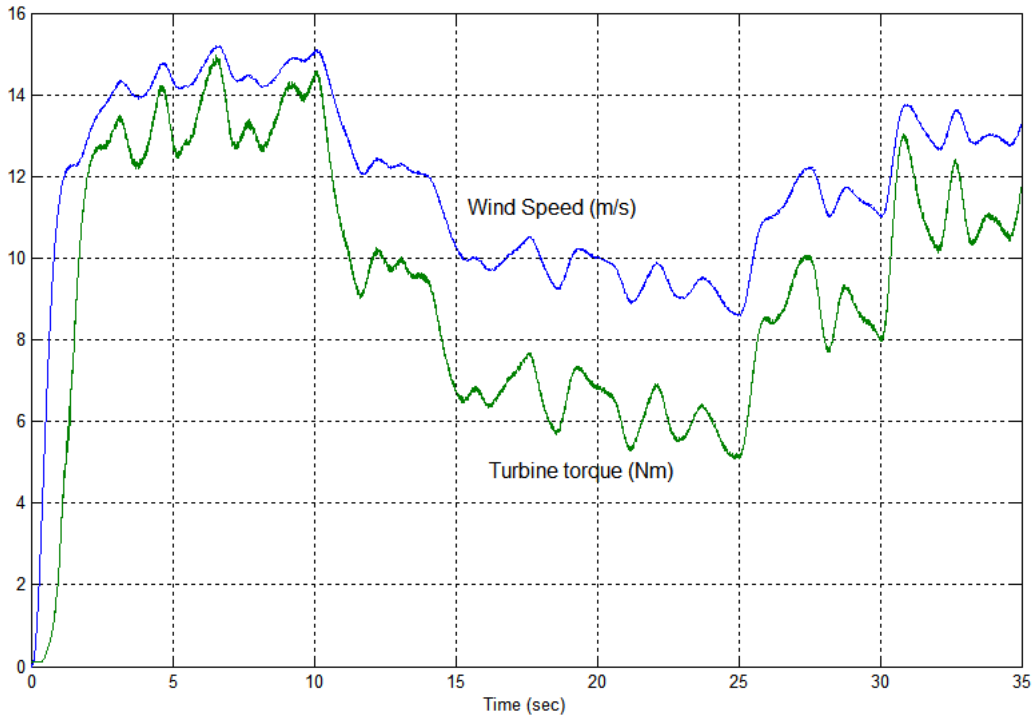
(a)
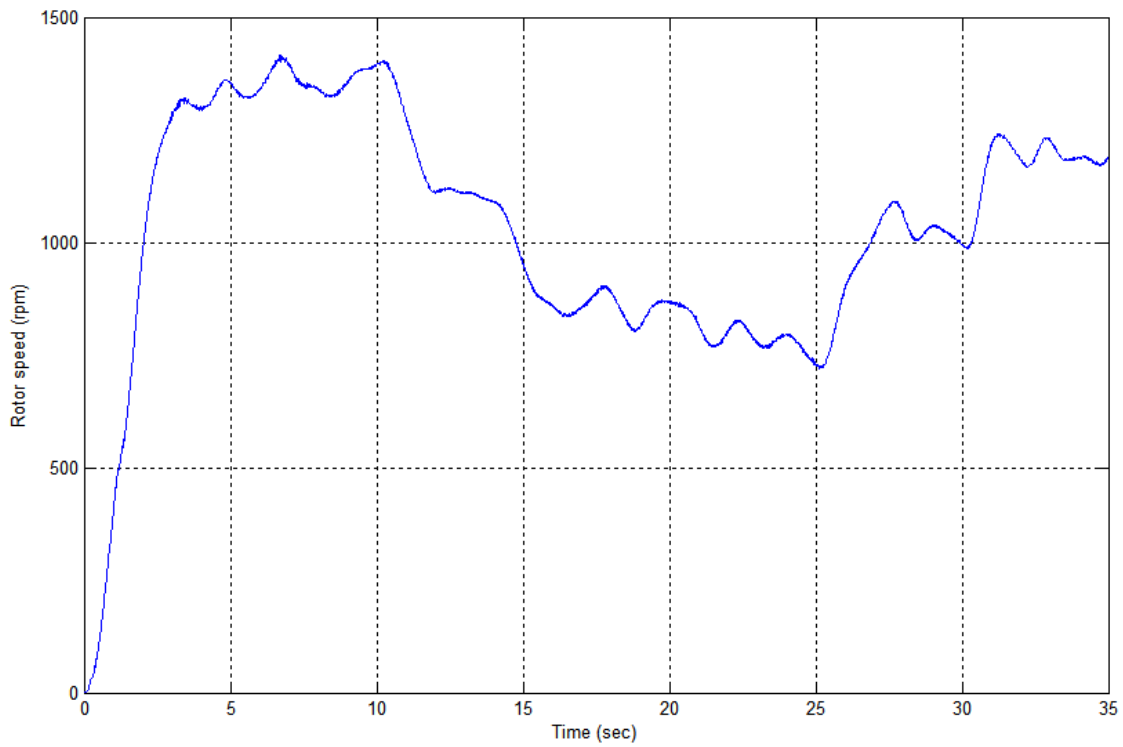
(b)

Fig. 3. 20 Responses of the proposed IPMSG based WECS for real wind speed: (a) wind speed (m/s) and Turbine torque (N.m) (b) rotor Speed (rpm).
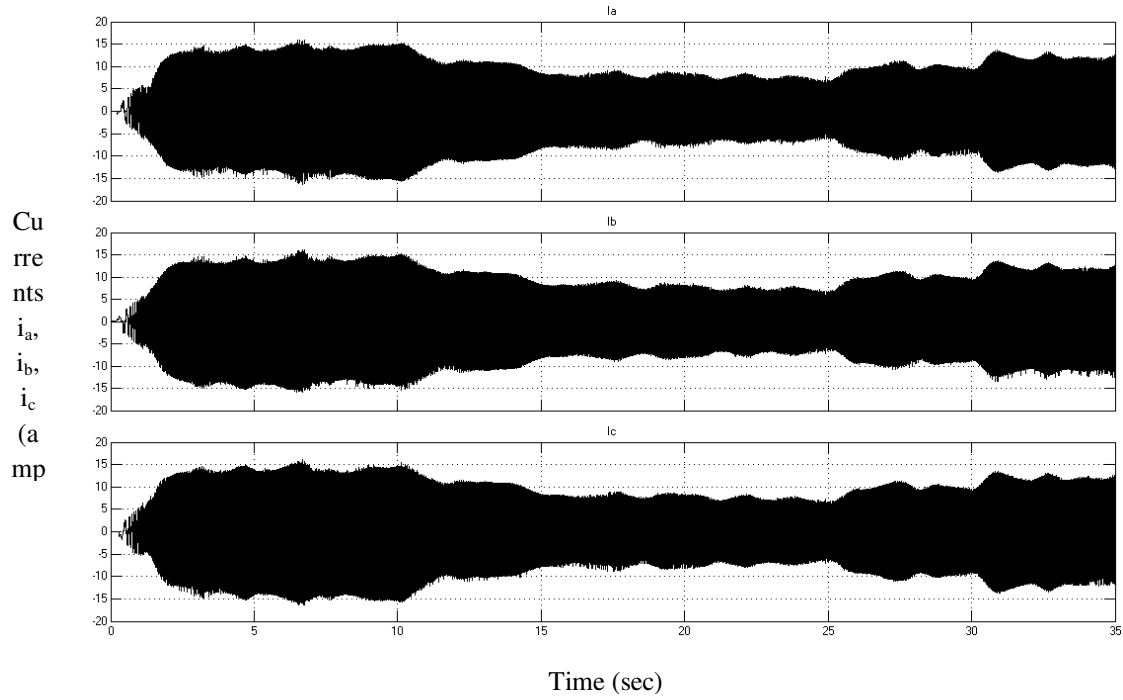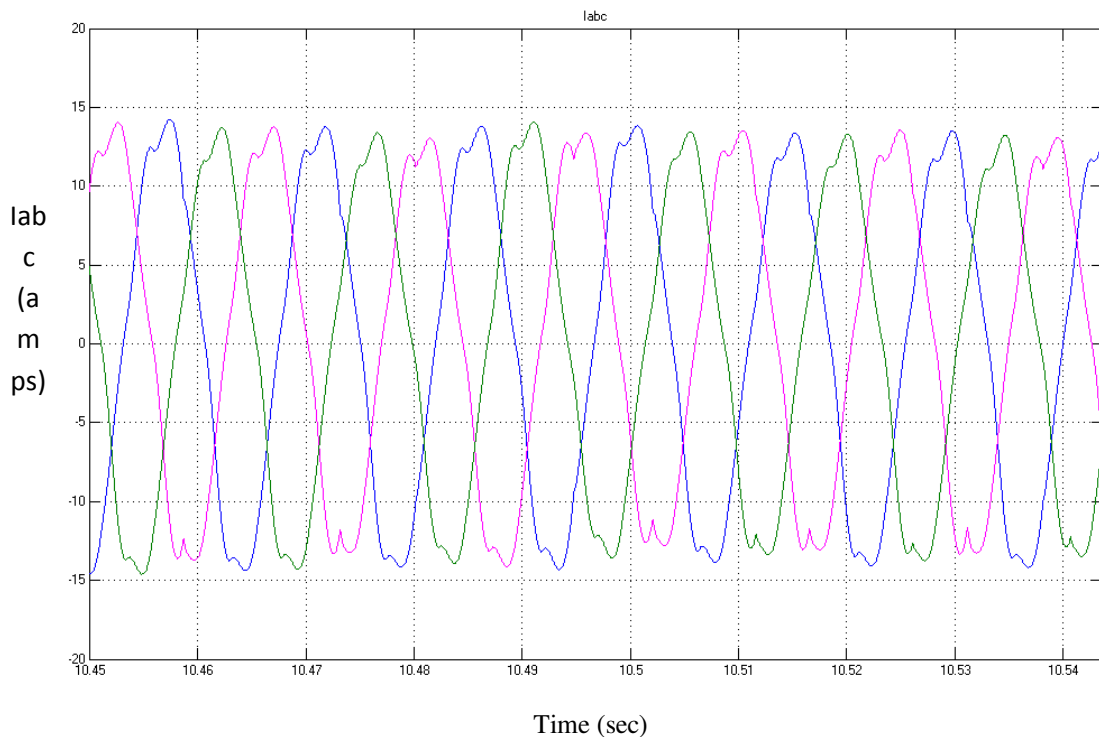
Fig. 3. 21 Responses of proposed WECS for real wind speed model: (a) three phase currents (b) zoom-in view of the 3 phase currents.
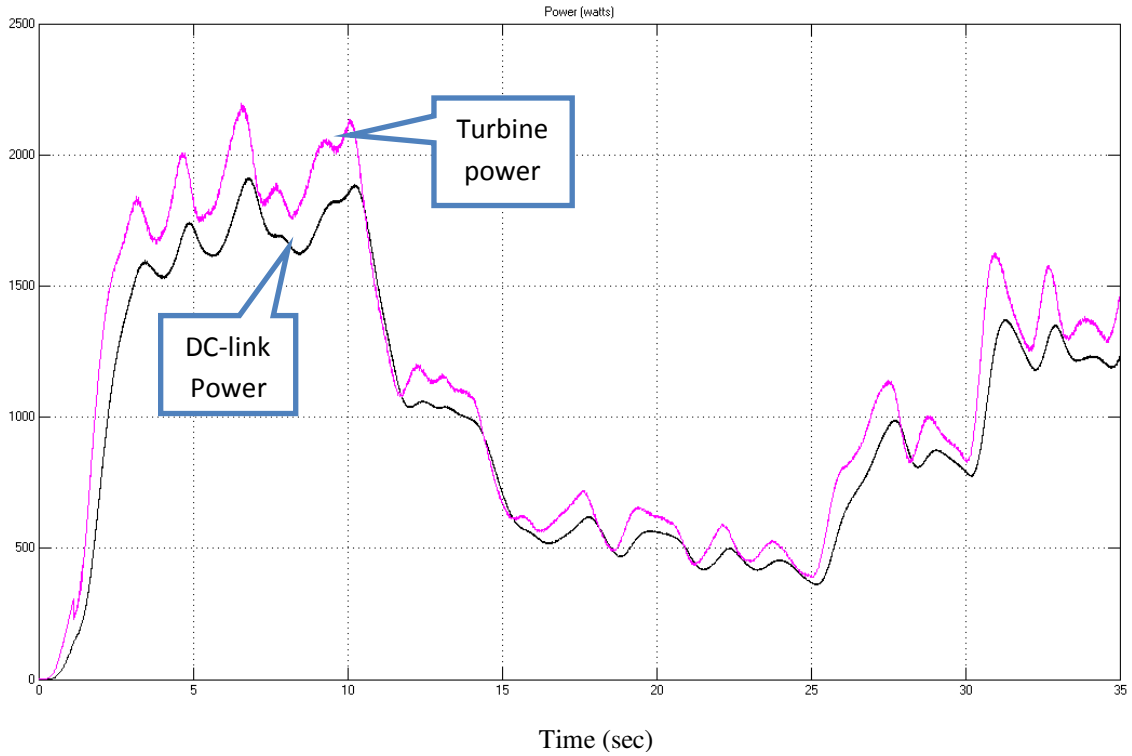
**Fig. 3. 22 With changing wind speed response mechanical and dc-link power (W).**
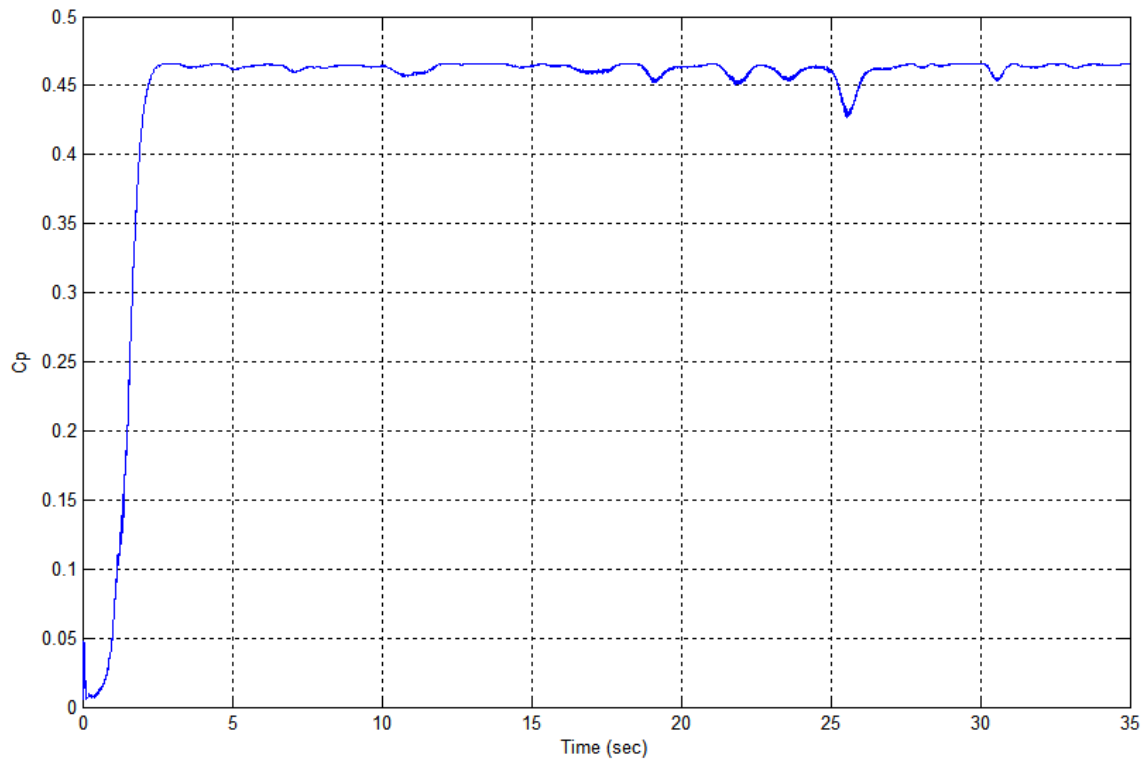
Fig. 3. 23 Turbine power coefficient Cp for proposed control of WECS with real wind speed model.

70
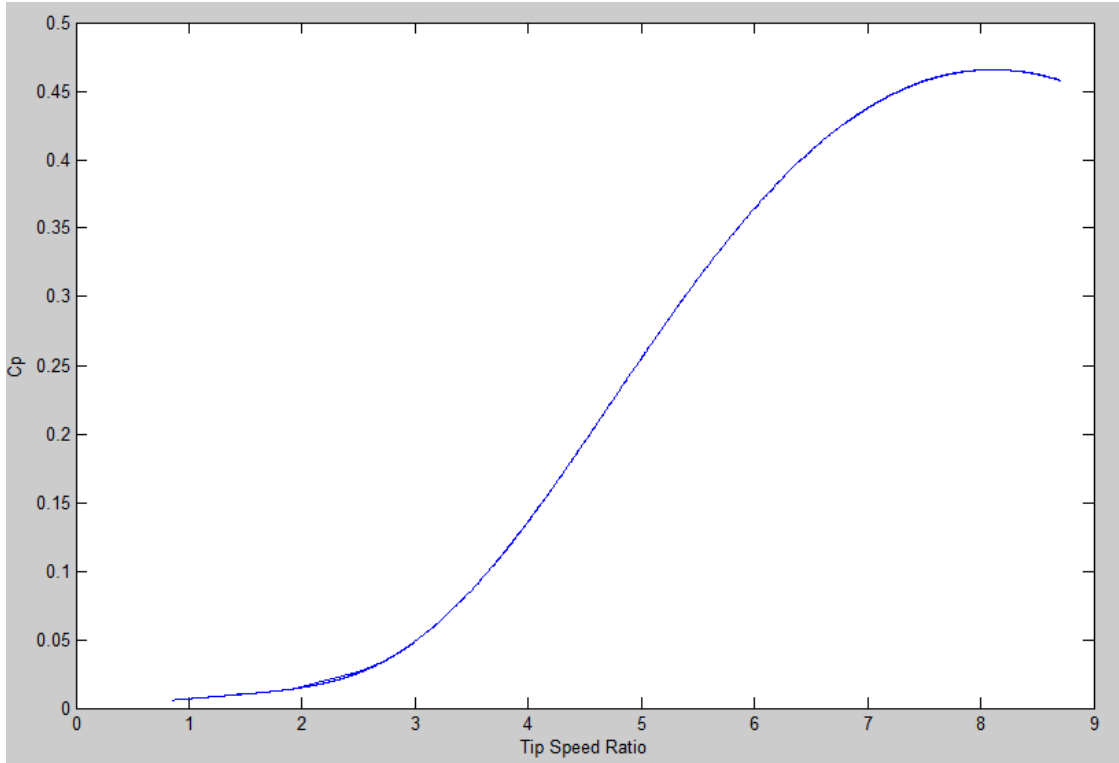
Fig. 3. 24 Power coefficient C_p vs tip speed ratio λ.
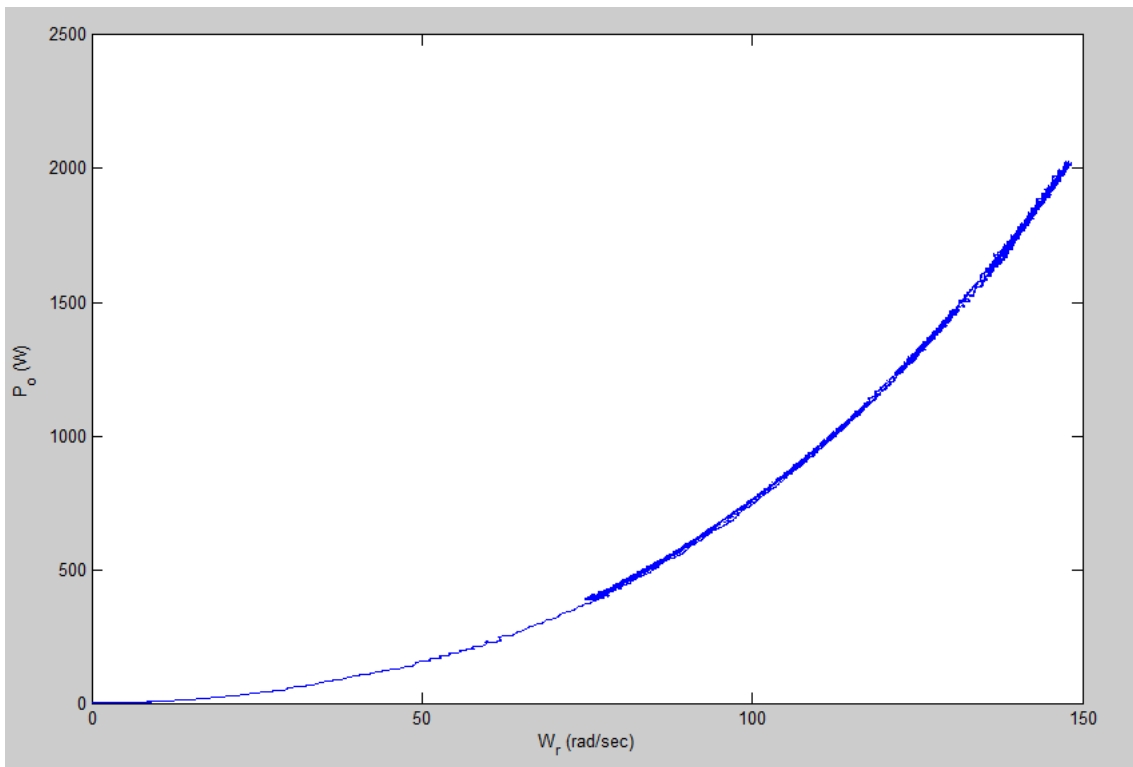
Fig. 3. 25 Rotor speed (rad/sec) vs dc-link power (W).

71

3.5.3 High speed operation

In order to test the proposed flux weakening control technique the IPMSG was operated above the rated speed condition and the corresponding results are shown in Figs. 3.27 and 3.28. It is found that the generator is running at 220 rad/sec. when the wind speed the wind speed is around 22 m/sec. The corresponding adjustment in d-q axis currents are shown in Fig. 3.28. It is seen from this figure that d-axis becomes more negative when the rotor speed exceeds the rated speed due to the proposed FWC. Without the FWC it was not possible to run the generator at such high speed condition safely.
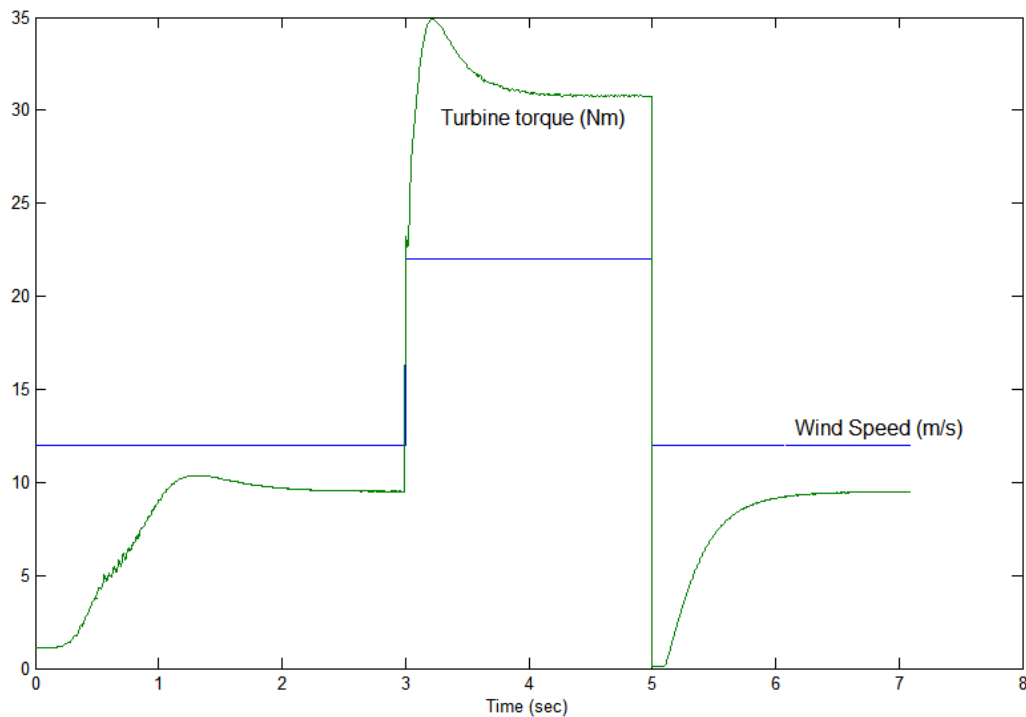
Fig. 3. 26 Responses of the proposed IPMSG based WECS for step change in high wind speed (m/s) and Turbine torque.
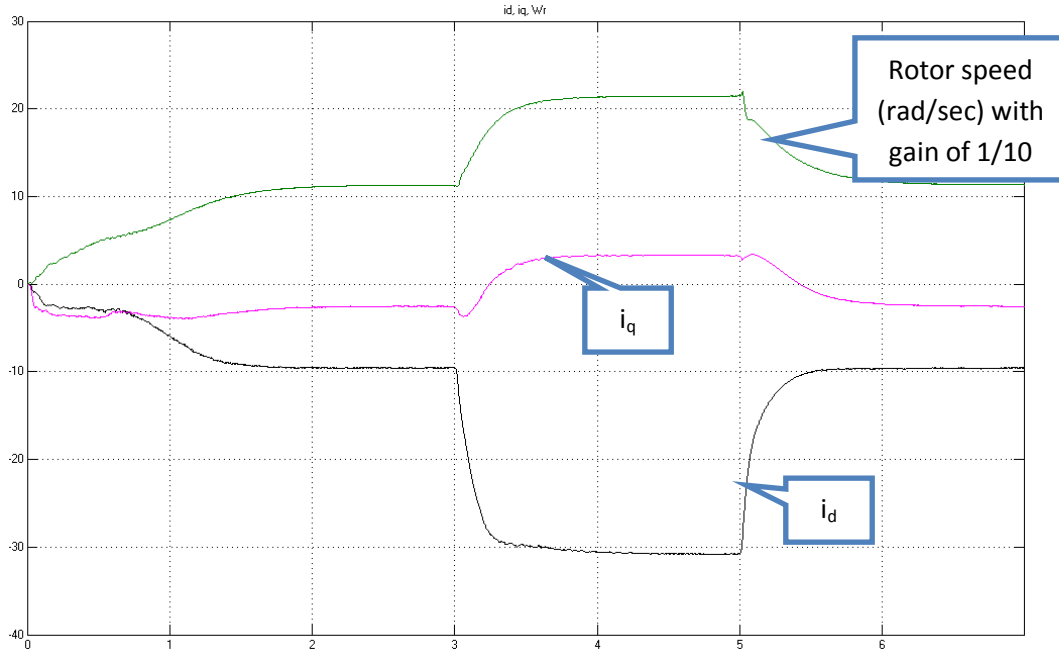
Fig. 3. 27 Response of speed, i_d and i_q current for the proposed flux control.

3.4 Concluding Remarks

An adaptive MPPT algorithm based control of the IPMSG to extract maximum power from wind has been developed. The perturbation and observation based novel MPPT algorithm uses an adaptive constant for fast convergence of power tracking. Flux control of the IPMSG was also implemented for wide speed range operation. The performance of the proposed control technique has been tested in simulation at different operating conditions. Over the wide speed range, the WT power coefficient remained constant which proved the effectiveness of the proposed controller. The results also proved that the stability of the system with sudden disturbances when using proposed control system. The performance of the proposed control technique has been found to be superior when compared with the conventional control of WECS.

Chapter 4

Sensorless Control- Position and Speed Estimation

4.1 Introduction

Speed sensorless control means that the rotor position is not measured by encoder, but estimated online using some algorithms. However, their control still uses some basic sensors, e.g. current sensors, voltage sensors. In recent decade, much research has been done in the area of speed and/ or shaft position sensorless controlled drives [59-83].

The main drawback of a PM-machine is the position sensor, which is vulnerable for electromagnetic noise in hostile environments and has a limited temperature range. For PM machines rated up to 10kW the cost of an encoder is below 10% of the machine manufacturing cost. However, for applications in the automotive industry with the elimination of the position sensor is preferable due to space limitation and cost. Thus, the elimination of the electromechanical sensors reduces the hardware costs, reduces the installation complexity of the system (because of associated wiring), decreases the system inertia, increases the robustness and the reliability and reduces obviously the noise sensitivity of the electrical drive [2],[3].

74

4.2 Strategies for Position and Speed Estimation for IPMSM

In general there are three strategies for position estimation of IPMSM [60], [61]:

1. Model based estimators,

2. Saliency and Signal Injection,

3. Artificial Intelligence.

1. Model based estimators:

The method uses the model of the PM machine and measured electrical quantities to determine the rotor position and speed. The measured electrical quantity is usually the stator current of the PM machine. This method is further classified into two types such as, (a) non-adaptive and (b) adaptive methods.

a) Non-adaptive Methods are divided in the following three categories:

i. Techniques using the measured dc-link current assuming constant dc-link voltage,

ii. Estimators using monitored stator voltages, or currents,

iii. Flux based position estimators,

iv. Position estimators based on back-EMF.

b) Adaptive Methods are divided into the following four categories:

i. Estimator based on Model Reference Adaptive System (MRAS).

ii. Observer-based estimators.

iii. Kalman filter based estimator.

iv.   Estimator which use the minimum error square.

2. Saliency and Signal Injection:

In PM machines, the position dependence is a feature of the rotor. In the case of the interior PMSM there is a measurably spatial variation of inductances or resistances (saliencies) in the d-q direction due to geometrical and saturation effects, which can be used for the estimation of rotor position . In this method, an additional signal (voltage or current) is injected into the machine and the position angle and speed are determined by processing the returning currents or voltages. Based on the signal injection, this method is further divided into the following two groups.

(a) High Frequency Method:

In this estimation of the rotor position, high frequency stator voltage (current) component is added to machine and the effects of the machine saliency (anisotropy) is evaluated on the amplitude of the correspondent stator voltage (current) component. In the literature the frequency of the injection signal is from a few hundred Hz to KHz region.

(b) Low Frequency Method:

This estimators are based on the mechanical vibration of the rotor. The injected frequency is usually from few Hz to few hundred Hz.

3. Artificial Intelligence:

Artificial intelligence methods use neural network, fuzzy logic based systems or neuro – fuzzy systems to estimate the rotor position. These kind of methods do not require a mathematical model of the drive, exhibit good noise rejection properties, can easily be extended and modified, can be robust to parameter variations and are computationally less intensive.

Fuzzy logic estimators are based on linguistic rules determined by experts. Neural network estimators learn the properties of the particular machine using predetermined training data. The inputs of the neural network are currents and voltages. Neuro-fuzzy technique has an advantage of fuzzy logic and neural network which has self-learning, self-organizing and self-tuning capabilities.

These techniques require high bandwidth and high precision measurement, and fast signal processing capability, which may increase the complexity and cost of control system. The injected high-frequency voltages may also cause more torque ripple, shaft vibration and audible noises. On the other hand, MRAS scheme offer simpler implementation and require less computational effort compared to other methods, and it is widely accepted for speed estimation. Mathematical model of MRAS is discussed in following section.

4.2 Model Reference Adaptive System Based Speed Estimation

The model reference adaptive system includes two models: the reference model and the adaptive model. The external excitation for the two models is the same, and the difference state vector between the outputs of the two models is used as the input of adaptive unit. Based on this input the parameters of the adaptive model should be modified so that the output state vector of the adaptive model approaches toward the reference model fast and stably. For the current of PMSG can be directly measured, current model of PMSG is usually used as adjustable model. In

d-q reference frame, the mathematical model of IPMSM Eqns. (2.18-2.19) can be rewritten in current model form as:

$$
p\begin{bmatrix} i_d \\ i_q \end{bmatrix} = \begin{bmatrix} \dfrac{-R_s}{L_d} & \omega \dfrac{L_q}{L_d} \\ -\omega \dfrac{L_d}{L_q} & \dfrac{-R_s}{L_q} \end{bmatrix} \begin{bmatrix} i_d \\ i_q \end{bmatrix} + \begin{bmatrix} \dfrac{v_d}{L_d} \\ \dfrac{v_q - \omega \psi_m}{L_q} \end{bmatrix}
\tag{4.1}
$$

Where p is derivative operator. Eqn. (4.1) can be rewritten as [12],

$$
p\begin{bmatrix} i_d + \dfrac{\psi_m}{L_d} \\ i_q \end{bmatrix} = \begin{bmatrix} \dfrac{-R_s}{L_d} & -\omega \dfrac{L_q}{L_d} \\ \omega \dfrac{L_d}{L_q} & \dfrac{-R_s}{L_q} \end{bmatrix} \begin{bmatrix} i_d + \dfrac{\psi_m}{L_d} \\ i_q \end{bmatrix} + \begin{bmatrix} \dfrac{v_d L_d + R_s \psi_m}{L_d{}^2} \\ \dfrac{v_q}{L_q} \end{bmatrix}
\tag{4.2}
$$

Let's assume,

$$
x = \begin{bmatrix} x_1 \\ x_2 \end{bmatrix} = \begin{bmatrix} i_d + \dfrac{\psi_m}{L_d} \\ i_q \end{bmatrix}
$$

$$
A = \begin{bmatrix} \dfrac{-R_s}{L_d} & -\omega \dfrac{L_q}{L_d} \\ \omega \dfrac{L_d}{L_q} & \dfrac{-R_s}{L_q} \end{bmatrix}
$$

$$
u = \begin{bmatrix} \dfrac{v_d L_d + R_s \psi_m}{L_d{}^2} \\ \dfrac{v_q}{L_q} \end{bmatrix}
$$

The state Eqn. (4.2) would be

$$
px = Ax + u
\tag{4.3}
$$

So the adaptive model can be written as,

$$p\hat{x} = \hat{A}\hat{x} + u \tag{4.4}$$

Where,

$$\hat{A} = \begin{bmatrix} \dfrac{-R_s}{L_d} & -\hat{\omega}\dfrac{L_q}{L_d} \\ \hat{\omega}\dfrac{L_d}{L_q} & \dfrac{-R_s}{L_q} \end{bmatrix}$$

Now suppose error vector is given by,

$$e = x - \hat{x} = \begin{bmatrix} x_1 - \hat{x}_1 \\ x_2 - \hat{x}_2 \end{bmatrix} = \begin{bmatrix} i_d + \dfrac{\psi_m}{L_d} \\ i_q \end{bmatrix} \tag{4.5}$$

From Eqns. (4.3)(4.4), there would be,

$$pe = Ae - H \tag{4.6}$$

And in Eqn. (4.6),

$$H = (\hat{\omega} - \omega) = \begin{bmatrix} 0 & \dfrac{L_q}{L_d} \\ -\dfrac{L_d}{L_q} & 0 \end{bmatrix} \hat{x}$$

According to Popov's hyperstability criterion [100], the adaptive law could be obtained as:

$$\hat{\omega} = C_1(N) + C_2 \int (N)d\tau + \hat{\omega}(0) \tag{4.8}$$

$$\hat{\theta} = \int (\hat{\omega})d\tau \tag{4.9}$$

Where, $N = -\dfrac{L_d}{L_q}\left(\hat{i}_d + \dfrac{\psi_m}{L_d}\right)\left(i_q - \hat{i}_q\right) + -\dfrac{L_q}{L_d}\hat{i}_q\left(i_d - \hat{i}_d\right)$, $\hat{\omega}(0)$ is initial speed and C_1, C_2 are proportional and integral gains respectively.

Eqn (4.8) represents a PI controller. Thus, the error between reference and adaptive model is processed through the PI controller, which gives the estimated speed as output.

The estimating performance of rotor speed is designed only by the PI coefficients. The proposed SVPWM using MRAS-based speed estimation for sensorless MPPT control of IPMSG drive was shown in Fig. 3.7.

4.3 Simulation Results

The complete simulation model for the proposed sensorless MPPT and flux controller based WECS is built in Matlab/simulink. The generator parameters are given in appendix A. Simulation blocks are shown in Appendix B. Estimation of rotor speed and position is achieved for IPMSG with 3 pole pairs. Fig 4.1(a) shows the rotor position estimation and phase 'a' current during steady state, whereas Fig. 4.1(b) shows the rotor position estimation and phase 'a' current during step change in wind speed. The angle in both these figures corresponds to electrical frequency of generator and has maximum amplitude of 2π rad for each cycle which confirms the accuracy and stability of the rotor position estimation.

Fig 4.2(a) and 4.2 (b) shows the comparative measured and estimated rotor speed for real wind profile and step changes in wind, respectively. It is clearly seen that the estimated speed is same as the measured rotor speed for both wind speed disturbances. The corresponding speed estimation errors are shown in Fig. 4.3 (a) and 4.2(a) for both wind speed profiles. As the wind speed was changed from very low to high as shown in Fig. 3.11(a), the high accuracy has been

maintained over wide speed range. The experimental test has also been performed which is discussed in next chapter.
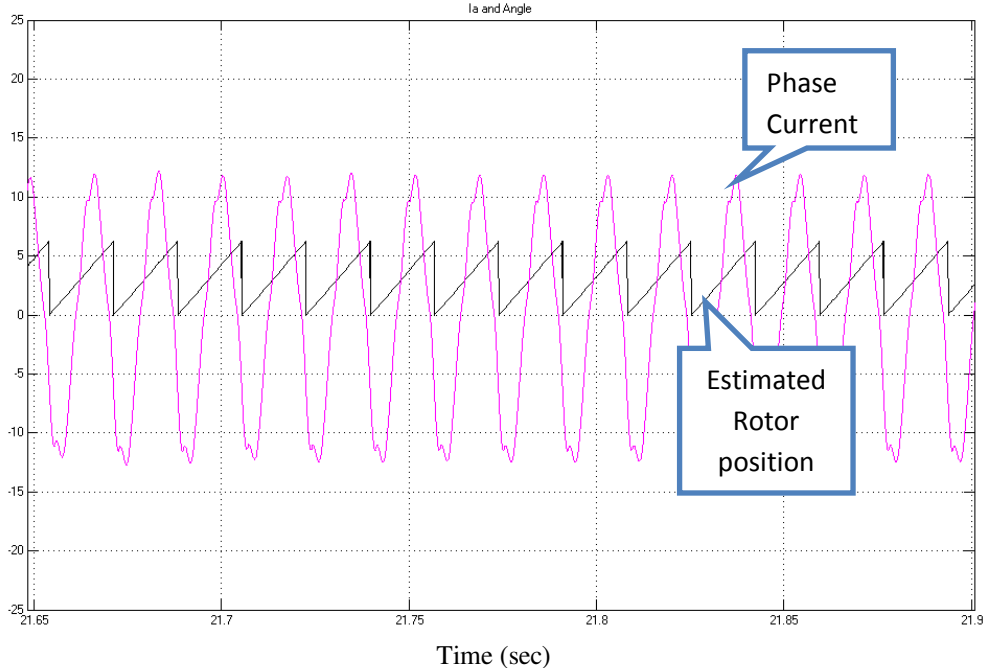
(a)
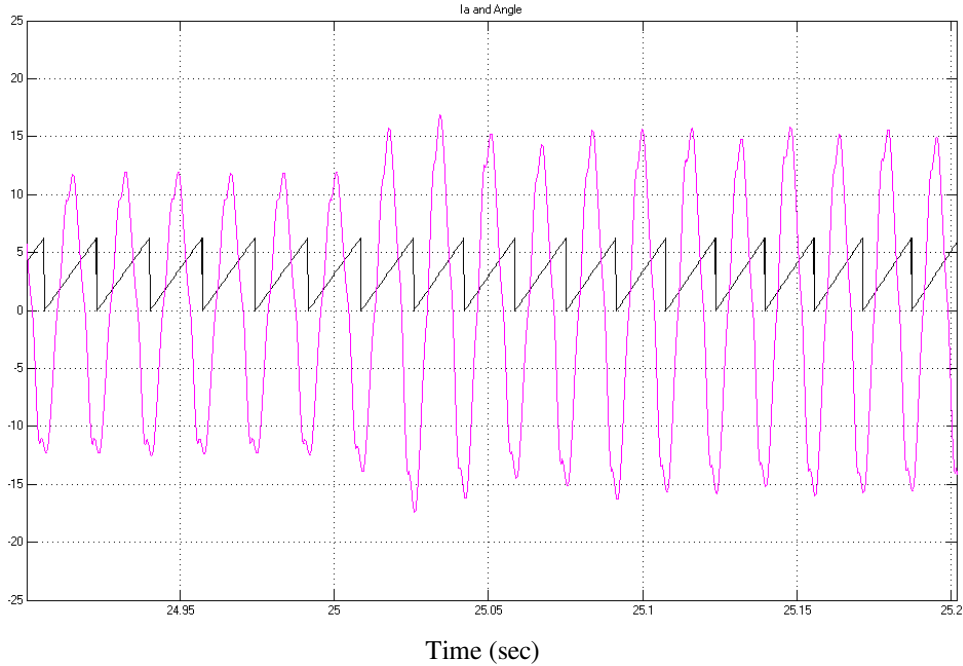
(b)

Fig. 4. 1 Estimated rotor position (electrical) and Phase 'a' current at (a) steady state and, (b) step change of wind speed at t=25 sec.
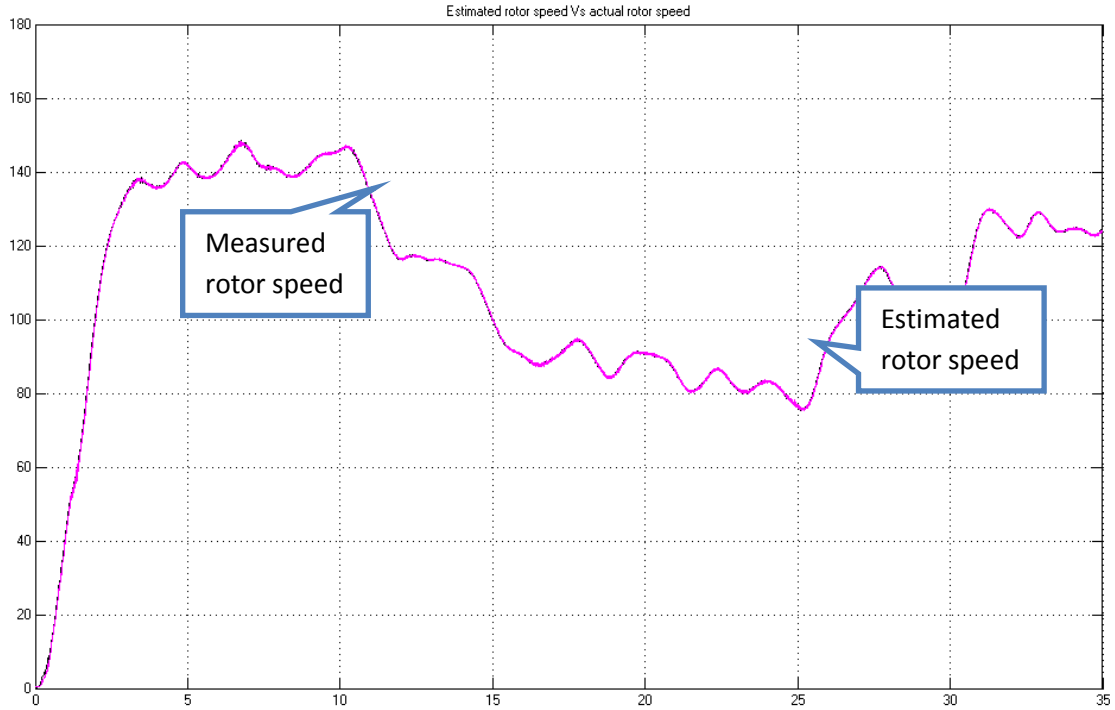
(a)
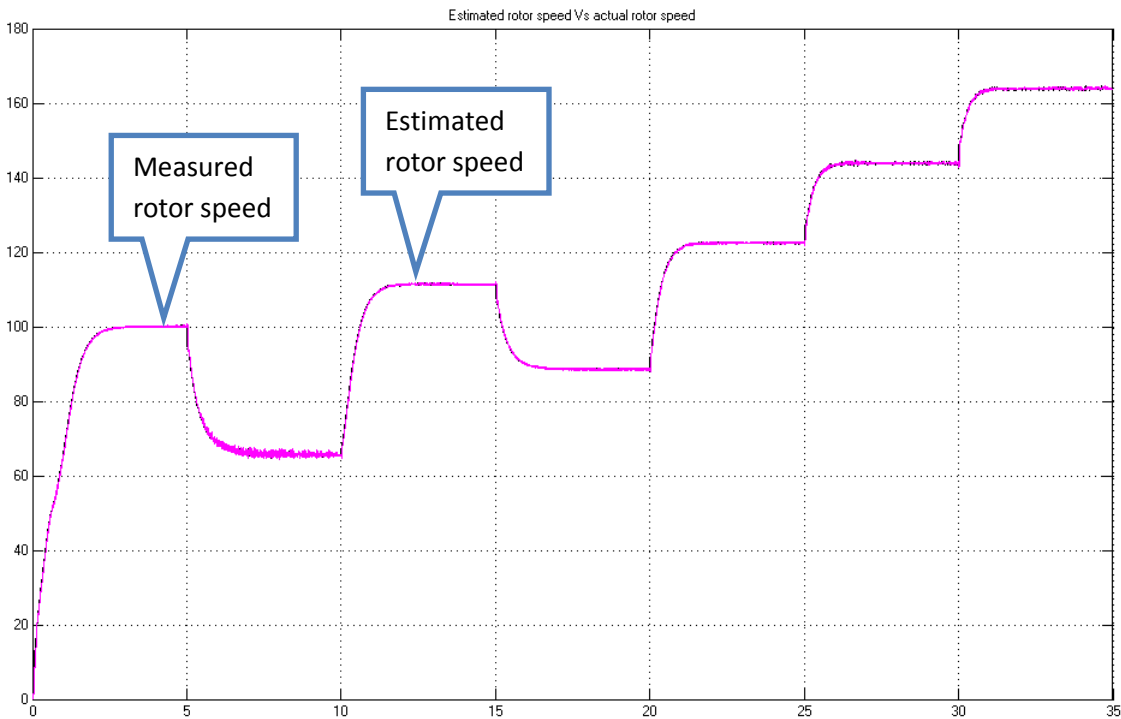
(b)

Fig. 4. 2 Comparison of estimated and the real rotor speed (rad/sec): (a) real wind profile and (b) step change in wind speed.
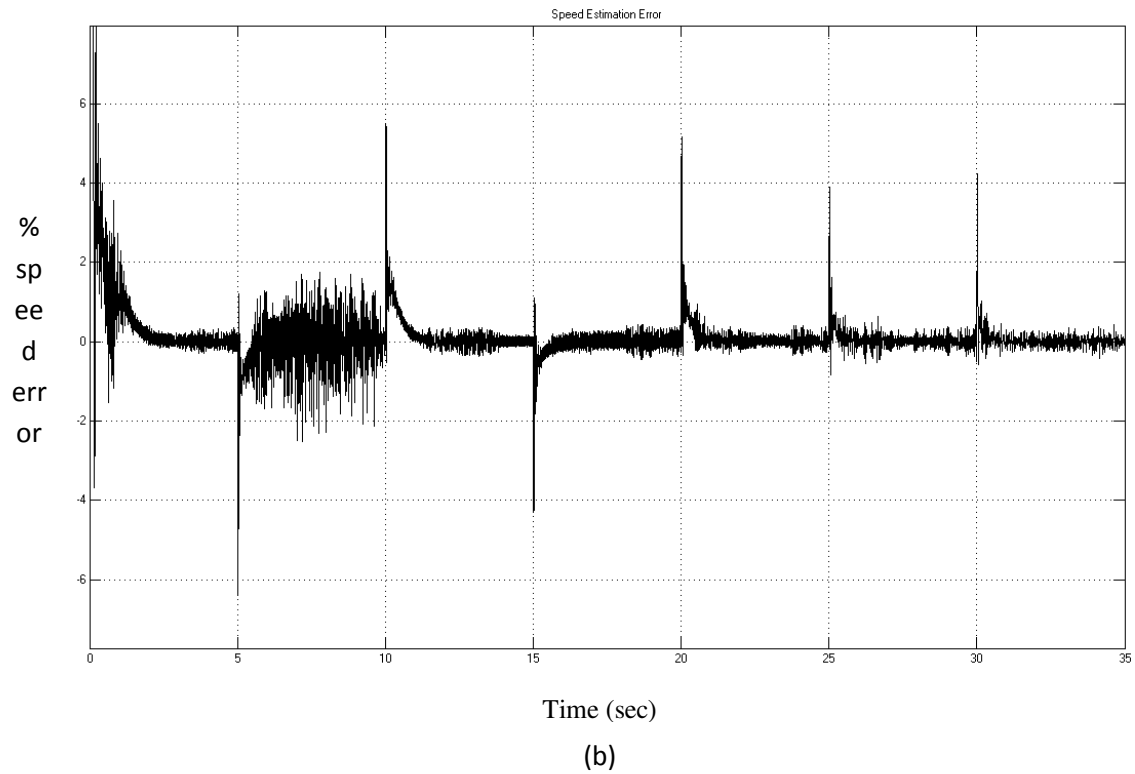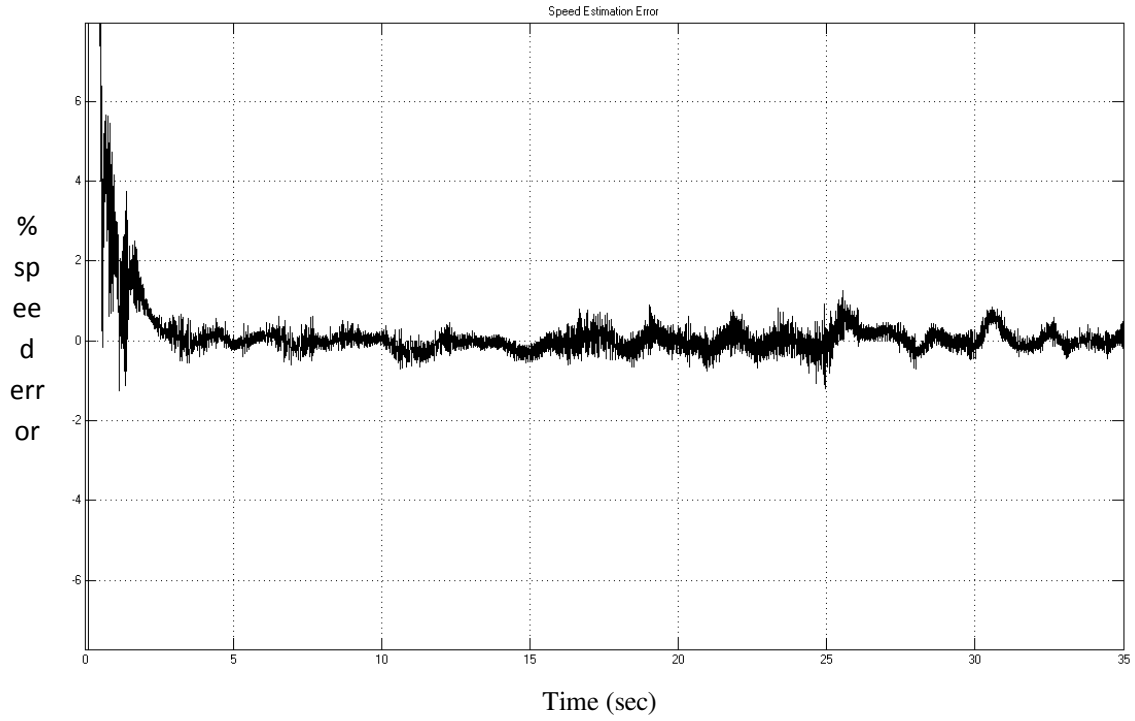
Fig. 4.3 Rotor speed estimation percentage error (a) real wind profile (b) step change in wind speed.

4.4 Concluding Remarks

The MRAS based speed and position estimations have been proposed in this Chapter. As compared to the others, the proposed MRAS technique is relatively simple and therefore, has low computational burden. The results proved the effectiveness of position estimation in both steady-state and transient conditions. It has also been found from results that the proposed MRAS tracks the rotor speed without significant error at variable wind speed conditions. The simulation results showed that the speed estimation error was maintained below $\pm 2\%$ at different rotor speeds. The real-time implementation of the proposed MPPT and MRAS based speed and position estimation techniques for IPMSG based WECS is shown in Chapter 5.

Chapter 5

Real-time Implementation

5.1 Introduction

The performance of the proposed drive was tested in real-time after getting some promising results in simulation. The complete sensorless vector control scheme of IPMSG incorporating the proposed MPPT based algorithm is successfully implemented in real-time using DSP board controller board DS 1104. The dSPACE DS1104 board is a very flexible and powerful system both for high computational capability and comprehensive I/O periphery. The detailed real-time implementation is described in this chapter.

5.2 Experimental Setup

The experimental setup for the prototype 5 HP IPMSG based WECS is shown in Fig. 5.1 and 5.2. The test IPMSG is labelled as 'G'. The rotor speed of the test machine is measured by an optical incremental encoder which is labelled as 'E'. The measured speed is only used for comparison purpose with the estimated rotor speed. The encoder is directly connected to the rotor shaft. The IPMSG is coupled with a PM-DC machine (M), which works as a separately excited motor to drive the generator. Thus, the DC motor replaces the wind turbine in a laboratory environment. The actual motor currents are measured by Hall-effect current transducers.
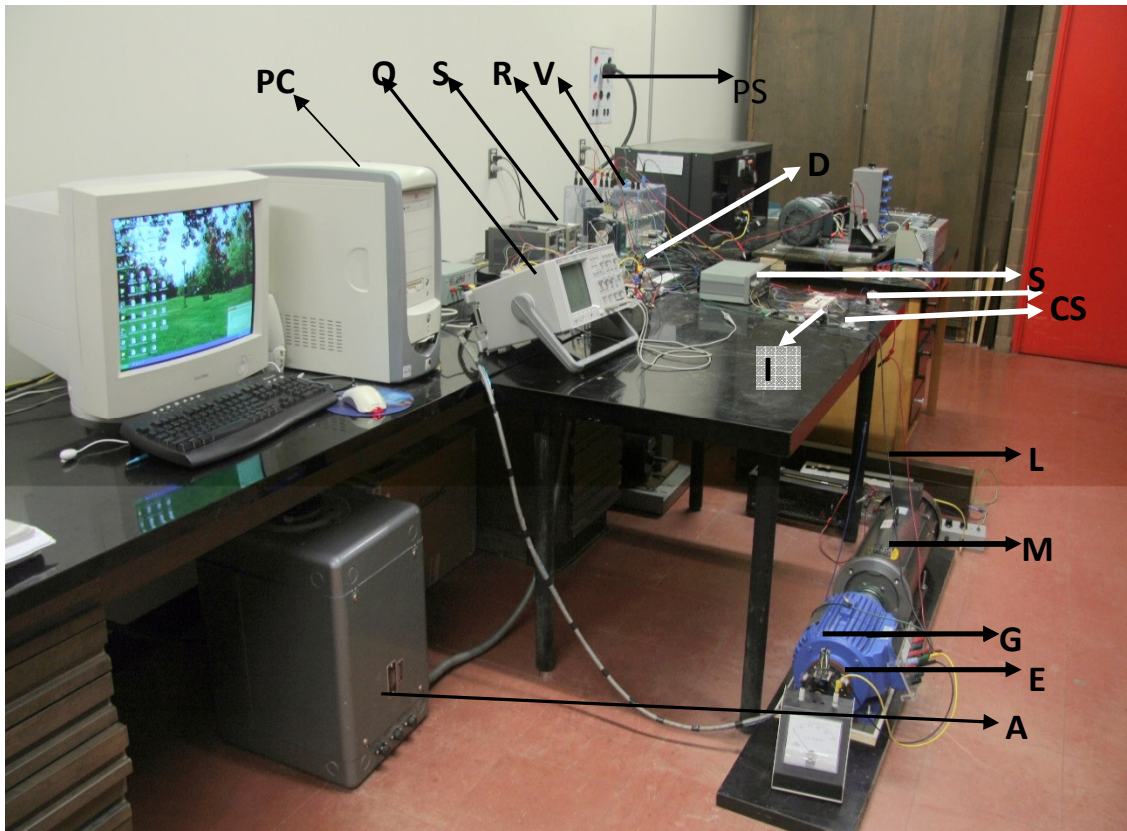
Fig. 5. 1 : Experimental setup of the proposed IPMSG based WECS (DC motor replaces wind turbine).
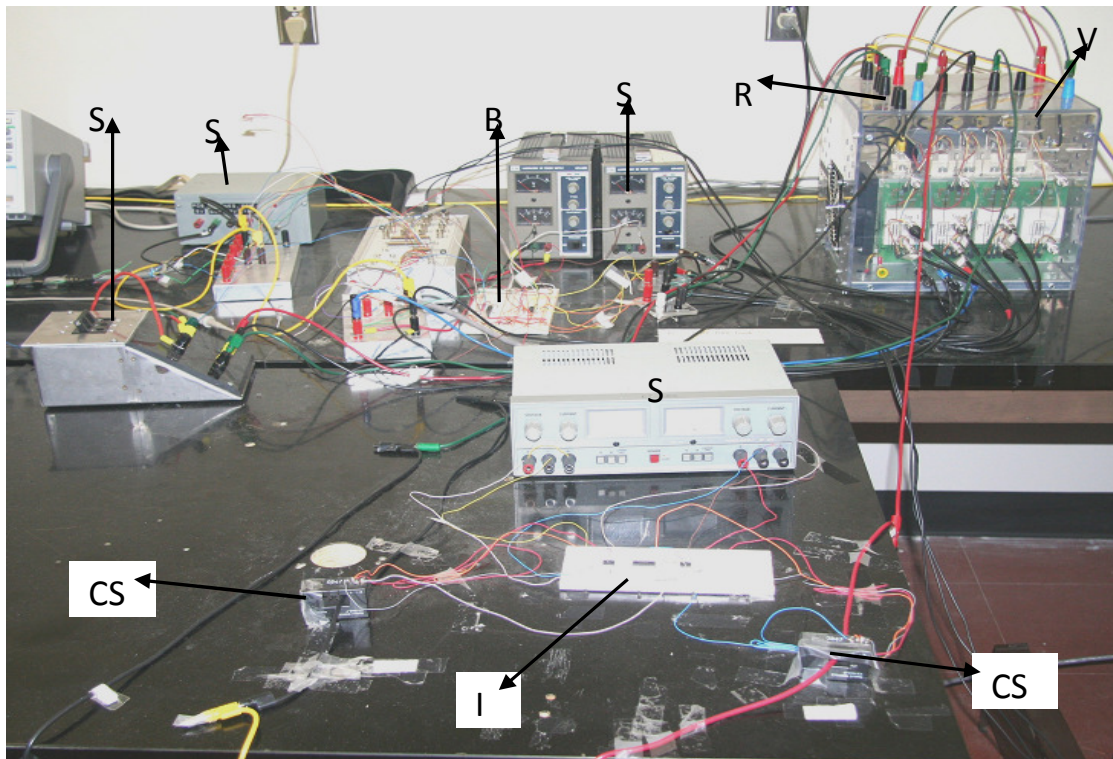
Fig. 5. 2 Experimental setup of the proposed WECS controller (zoom-in view).

The interface circuit (I) is located between the Hall-effect sensor and the A/D channel of DSP board. These transducers are labelled as 'CS'. These current sensors (CS) have a linear response over wide range of frequencies (up to 250 kHz). Another gate drive circuit is used to increase the power level of the firing pulses so that these are sufficient to drive the converter insulated gate bipolar transistor (IGBT) switches. The gate drive circuit also provides isolation between low power control and the high power supply circuits. The gate drive circuit is labelled as 'D'. The power circuits consist of a 3-phase variable ac autotransformer (A), power supply (PS), rectifier (R) and IGBT converter (V). The ac voltage is supplied by the power supply through autotransformer which is rectified by uncontrolled rectifier to supply DC motor. The speed of the motor is changed by varying the input ac voltage to the rectifier. Thus, it simulates the variable wind speed conditions. The rectifier enclosed within 3-phase (6 pulses) IGBT converter is labelled as 'V'. This converter has active security feature against short circuit, under voltage of power
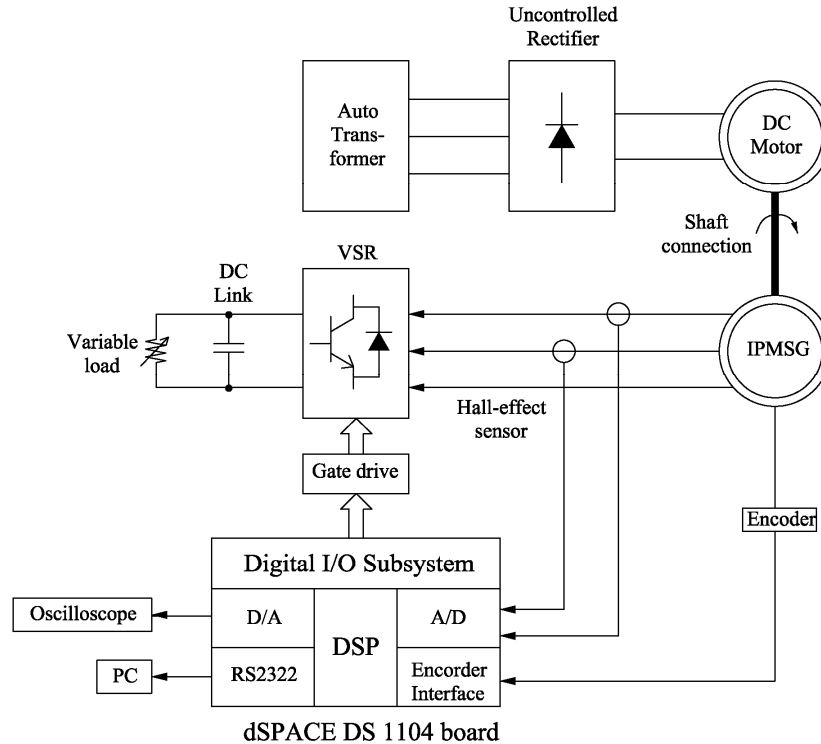
Fig. 5. 3 Block diagram of hardware schematic of VSI fed IPMSM drive.

supply as well as built in thermal protection, which prohibits destructive heat sink temperatures. The variable ac power of the uncontrolled rectifier is supplied by autotransformer (A) through a single pole single throw (SPST) switch (SW). The personal computer, in which the DSP board DS1104 is installed, is labelled as 'PC'. A digital storage oscilloscope is used to capture the desired analog signal coming out through D/A port of the DSP board. The oscilloscope is labelled as 'O'. The complete drive has been implemented through both hardware and software which are discussed below.

5.2.1 Hardware implementation of the drive

The block diagram of hardware schematic of voltage source rectifier (VSR) fed IPMSG drive is shown in Fig.5.3. The DSP board DS1104 board is installed in an Intel PC with uninterrupted communication through dual port memory to implement the control scheme in real-time. The DS1104 board is mainly based on a Texas Instrument MPC8240 64-bit floating

point digital signal processor. The block diagram of the DSP board is shown in Fig.5.4. The DS1104 board uses a PowerPC type PPC603e processor which operates at the clock of 250 MHz with 32 KB cache. This board has a 32 MB of SDRAM global memory and 8 MB of flash memory. The DSP is supplemented by a set of on-board peripherals used in digital control systems including analog to digital (A/D), digital to analog (D/A) converters and digital incremental encoder interfaces. This board is also equipped with a TI TMS320F240 16-bit micro controller DSP that acts as a slave processor and provides the necessary digital I/O ports configuration and powerful timer functions such as input capture, output capture and PWM generation. In this work, the slave processor is used for only digital I/O subsystem configuration. The block diagram of the hardware schematic is shown in Fig. 5.3. Rotor position is sensed by an optical incremental encoder mounted at the rotor shaft and is fed back to the DSP board through the encoder interface. The encoder used in this work generates 1024 pulses per revolution. By using a built-in 4-fold pulse multiplication the output of the encoder is increased to 4x1024 pulses per revolution in order to get a better resolution. So the resolution of the encoder is 0.087890625°. These pulses are fed to the one of two digital incremental encoder interface channels of the board. A 24-bit position counter is used to count the encoder pulses and is read by a calling function in the software. The counter is reset in each revolution by the index pulse generated from the encoder. The generator speed is computed from the measured rotor position angles using discrete difference equation. The measured speed is used to compare estimated speed. The actual generator currents are measured by the Hall-effect sensors, which have current range of 0 ~ ±200A and a frequency range of 0~250 KHz. The current signals are fed back to DSP board through A/D channels. The output current signal of these sensors is converted to a voltage across the resistor connected between the output terminal of the sensor and ground. One

89

can scale the output voltage by selecting the value of the resistors. These resistors can be within the range 0~100Ω. As the output voltages due to these current sensors are low, interface circuit is used to amplify the output of the sensor and it also reduces the noises. The interface circuit consists of non-inverting amplifier with operational amplifier LM741CN as shown in Appendix C. As the generator neutral is not grounded, only two phases current are measured and third phase current is calculated using Kirchoff's Current Law in software. The command voltages are generated from the proposed controller and compared with the triangular carrier wave. This generates the logic signals which act as firing pulses for the converter switches. Thus, these six logic signals are the output of the DSP Board and fed to the base drive circuit of the IGBT converter power module. The outputs of the digital I/O subsystem of the DS 1104 are six pulses with a magnitude of 5 V. This voltage level is not sufficient for the gate drive of IGBTs. Therefore, the voltage level is shifted from +5 V to +15V through the base drive circuit with the chip SN7407N as shown in Appendix C. At the same time it also provides isolation between low power and high power circuits.
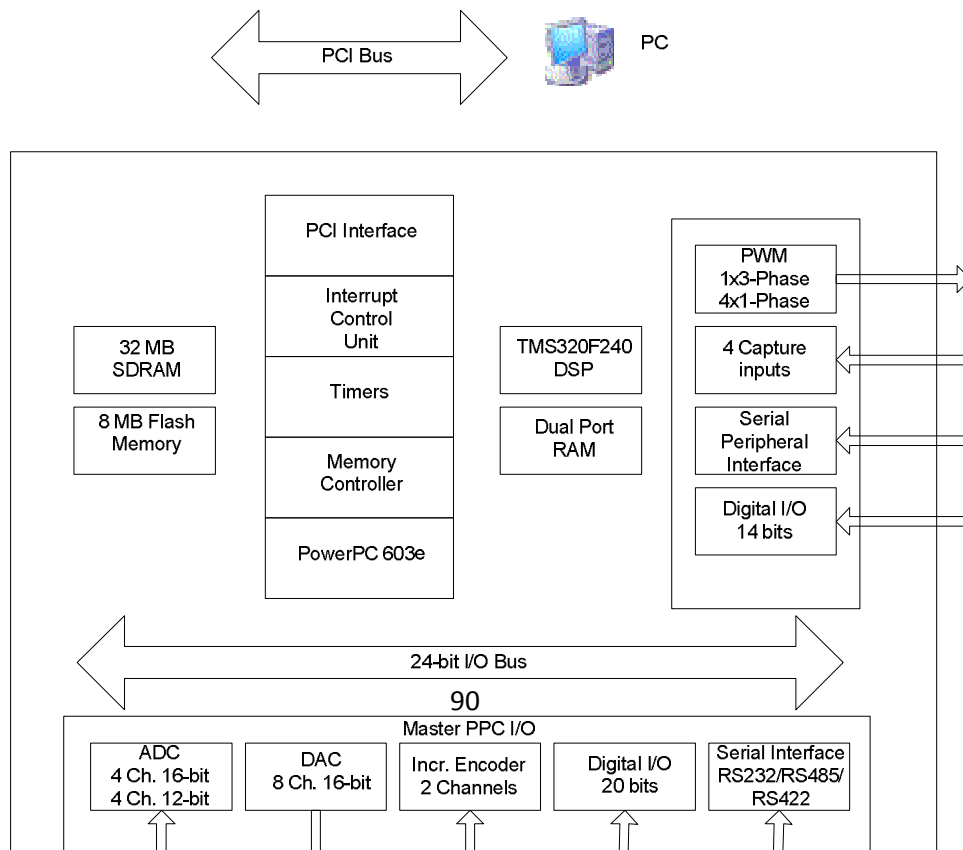
5.3.2 Software implementation of the drive

The dSPACE DS1104 board is a self-contained system, not an embedded system. This means the board installed in the lab computer through a PCI slot is its own entity and the host PC does none of the processing for a system implemented on the board. As a result, the board requires that software to be created and downloaded to the board for the system to function.

The ControlDesk software is used to download software to the DSP board, start and stop the function of the DS1104 as well as create a layout for interfacing with global variables in dSPACE programs. The sampling frequency used in this work is found to be 5 kHz. If the sampling frequency that is higher than 5 kHz is chosen, the 'overrun error' occurs, which indicates too much computational burden for the processor. The simulink blocks used for real-time implementations is shown in Appendix D.

5.3 Experimental Results

In order to verify the effectiveness and the dynamic performances of the proposed sensorless MPPT control of IPMSG based WECS, experimental tests have been carried out. Sample results are presented below. Fig. 5.5 illustrates the rotor position estimation using MRAS

model. As the IPMSG is 3 pole pair machine, one cycle of rotor position angle corresponds to three cycle of phase 'a' current. Fig. 5.6 shows the performance of the MRAS observer tracking the rotational speed under various speed conditions. It can be observed that the estimated speed tracks the actual rotor speed very well and the estimation error is very small during the transient state. Thus, the effectiveness of the proposed speed sensorless scheme is verified. Fig. 5.7 shows three phase output voltages and currents of IPMSG under fixed speed condition. The voltage and current waveform validate the balanced operation of the system.

To conform the maximum power point tracking control, couple of experimental tests have been carried out. As the IPMSG is driven by 5 HP DC machine, the WT parameter is unavailable for conventional controller. For this reason, the testing using conventional control is not available. This is also the main drawback of conventional controller that it requires WT information.
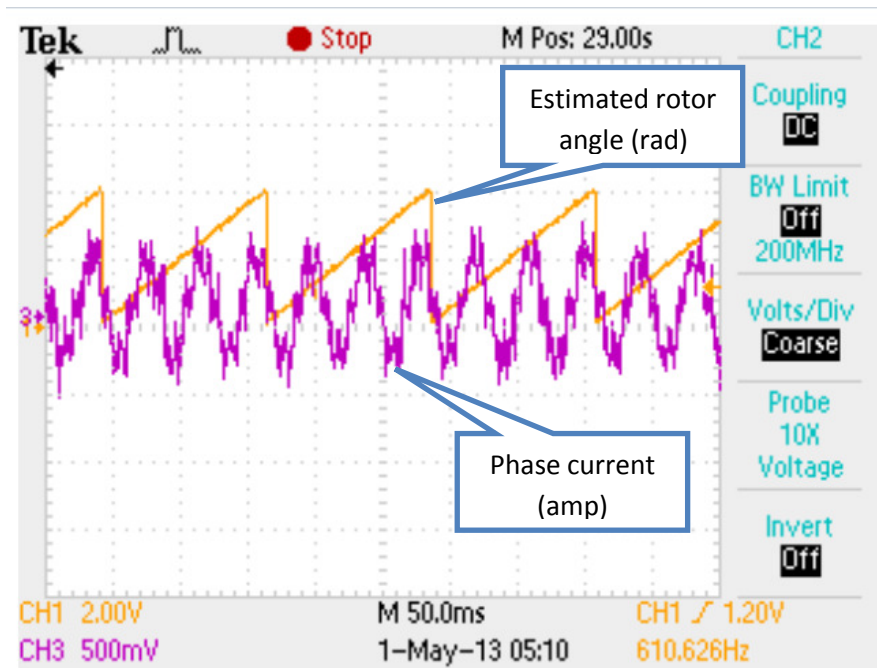
Fig. 5. 5 Phase 'a' current and estimated rotor position angle.

92
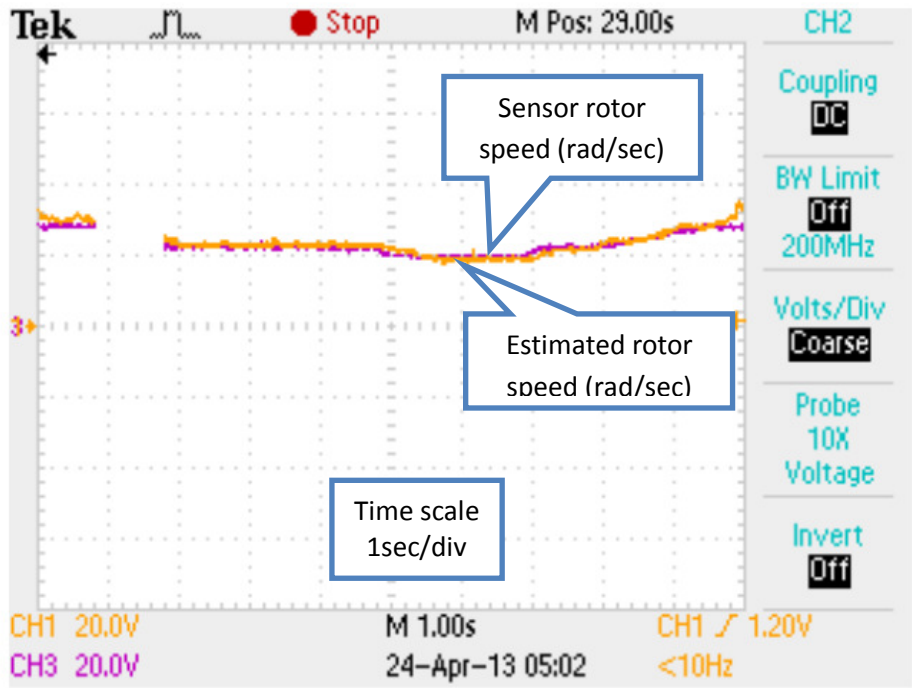
Estimated Speed and sensor speed

Fig. 5. 6 Real and estimated rotor speed tracking.

Va
bc
(vo
lts)

Vabc

(a)

93

Ia
bc
(a
~
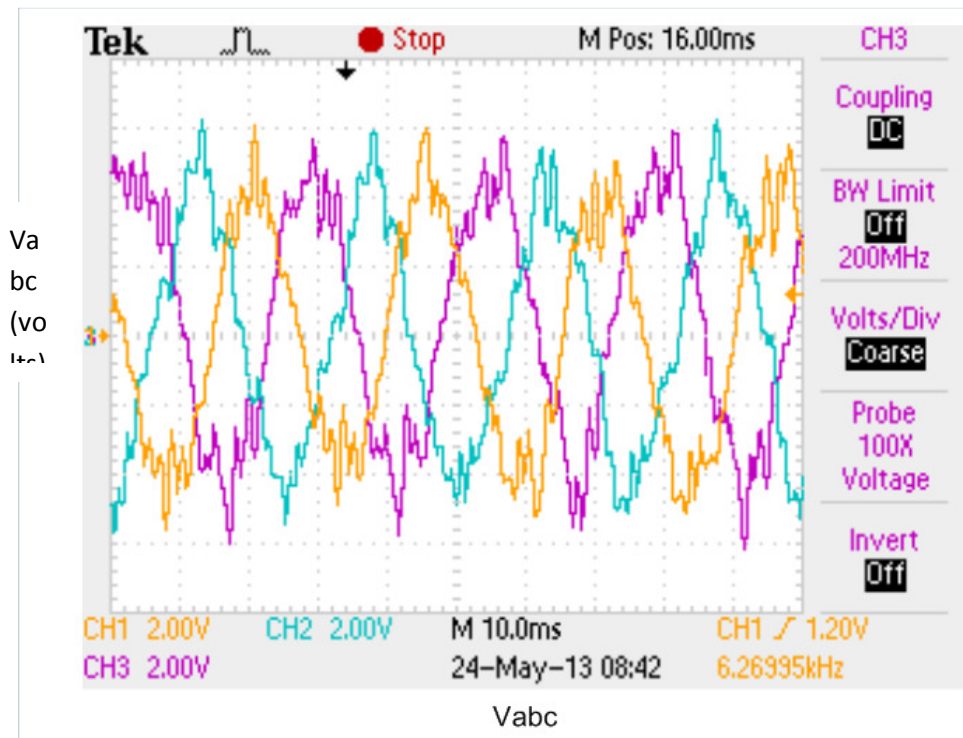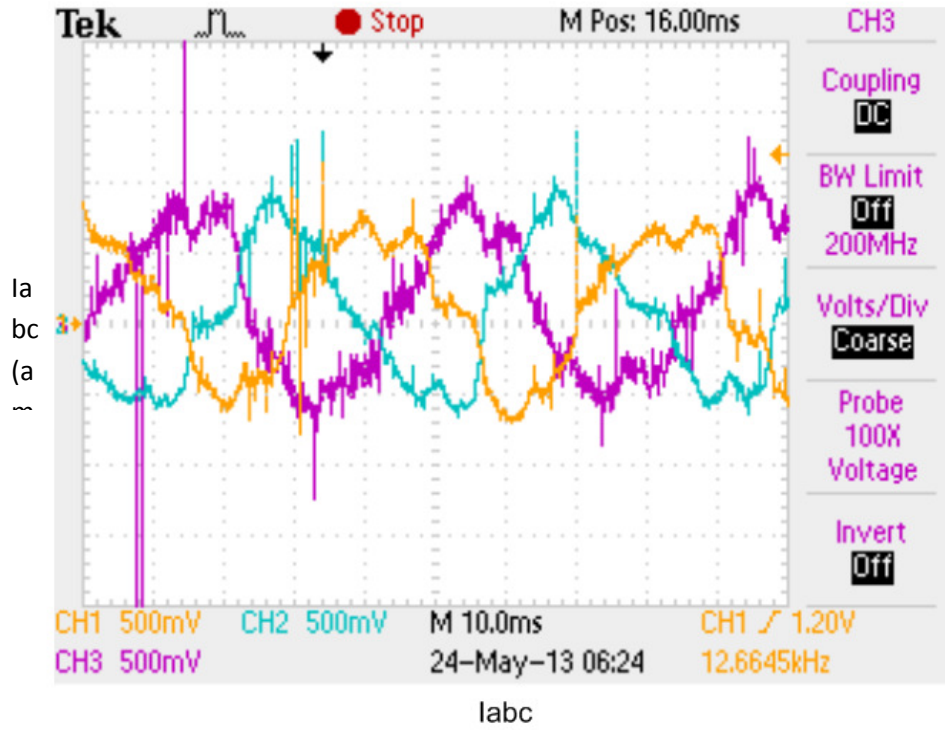
Iabc

(c)

Fig. 5. 7 During steady state (a) Vabc (V), (b) Iabc (amps).
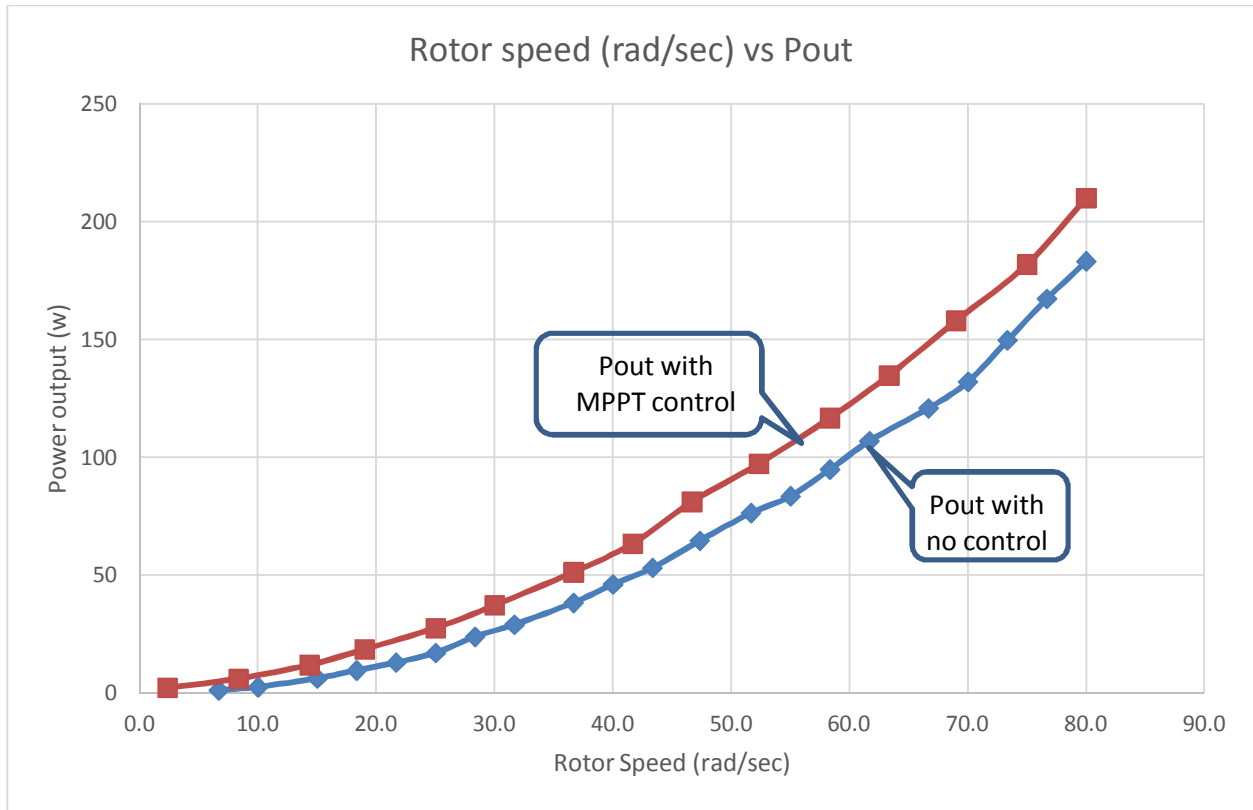
Fig. 5. 8 Rotor speed (rad/sec) vs Pout with and without MPPT algorithm.

Fig. 5.8 shows dc-link power with and without the proposed adaptive MPPT technique. DC-link power first measured based on voltmeter and ammeter readings at steady-state condition and then plotted against the rotor speed. It is clearly seen that the proposed MPPT transfer more power from generator to the dc-link as compared to without any control. In the lab, due to the limitation of rating conditions of capacitors and load resistors, the generator was running up to a speed of 80 rad/sec.

5.5 Concluding Remarks

The detailed experimental implementation of the proposed sensorless control of IPMSG based in MPPT technique using dSPACE DSP board DS1104 has been presented in this Chapter. The performance of the proposed drive has been tested in real-time at different operating rotor speed. In order to prove the superiority, the performance of the proposed MPPT based technique has been compared with a no controller tracking condition. Due to MPPT algorithm extracted power has been increased. Due to simplicity of MRAS sensorless technique, it was possible to implement it in real-time. Position estimation comparison with phase current showed the effectiveness of MRAS technique. Speed estimation has been also tested at various speed conditions. It was noticed that speed was tracked with minimum speed error.

Chapter 6

Conclusions

6.1 Concluding Remarks

An improved control technique for variable-speed WECS using an IPMSG to extract maximum power over wide operating speed range has been proposed in this thesis. A novel adaptive MPPT with sensorless scheme have been proposed to maximize generated output power. Additionally, flux weakening control technique has been also implemented to extend the operating speed range. The MPPT algorithm generates optimum speed reference to track maximum power without the knowledge of wind speed, turbine parameter or generator parameters. The proposed control system incorporated flux weakening controller above rated speed. In Matlab/Simulink control system was tested with sudden disturbance in wind speed varying from 8m/s to 17m/s, and maximum power coefficient C_p was maintained almost constant during wide speed operating range. The proposed controller has also been tested with real wind speed model which conformed maximum power transfer maintaining high stability and high controllability of the IPMSG.

A sensorless MPPT control of IPMSG and the SVPWM rectifier has been implemented in real time using DSP board DS1104. The speed sensorless technique has been developed based on model reference adaptive system (MRAS) algorithm. In real time, a 5 HP variable speed DC

motor has been used to replace the WT. The experimental results verified the effectiveness of sensorless and MPPT technique for the proposed IPMSG based WECS.

6.2 Future work

➢ During continuous operation of IPMSG, it may increase internal temperature, so online parameter adaptation technique could be incorporated in the system.

➢ The effect of magnetic saturation, which causes highly non-linear characteristic of the IPMSG, needs to be considered in control scheme design.

➢ Fuzzy logic controller can be implemented in sensorless MRAS scheme to replace the PI controller.

➢ Loss minimization technique can be implemented in order to improve the efficiency of the system

References

[1]   S. Morimoto, H. Kato, M. Sanada and Y. Takeda, "Output Maximization Control for Wind Generation System with Interior Permanent Magnet Synchronous Generator", in 41st IAS Annual Meeting IEEE Industry Applications Conference, Tampa, FL, 2006.

[2]   S. Morimoto, M. Sanada and Y. Takeda, "Optimum control of IPMSG for wind generation system", in PCC Osaka Power Conversion Conference, Osaka, 07 August 2002.

[3]   J. S. Thongam, P. Bouchard, H. Ezzaidi and M. Ouhrouche, "Wind Speed Sensorless Maximum Power Point Tracking Control of Variable Speed Wind Energy Conversion Systems", in IEEE IEMDC, Miami, FL, 3-6 May 2009.

[4]   N. Srighakollapu and P. Sensarma, "Sensorless maximum power point tracking control in wind energy generation using permanent magnet synchronous generator", in 34th Annual Conference of IEEE Industrial Electronics, Orlando, FL, 10-13 Nov. 2008.

[5]   J. S. Thongam, P. Bouchard, R. Beguenane and I. Fofana, "Neural network based wind speed sensorless MPPT controller for variable speed wind energy conversion systems", in IEEE Electric Power and Energy Conference, Halifax, NS, Aug 25-27, 2010.

[6]   J. S. Thongam, P. Bouchard, R. Beguenane, I. Fofana, and M. Ouhrouche, "Sensorless Control of PMSG in Variable Speed Wind Energy Conversion Systems", in IPEC 2010, pp. 2254 - 2259, Sapporo, 21-24 June 2010.

[7]   A. M. O. Haruni, M. E. Haque, A. Gargoom and M. Negnevitsky, "Control of a Direct

Drive IPM Synchronous Generator Based Variable Speed Wind Turbine with Energy Storage", IECON 2010 - 36th Annual Conference on IEEE Industrial Electronics Society, Glendale, AZ, Nov 2010.

[8]   V. Quaschning, "Understanding Renewable Energy Systems, London", UK & Sterling, VA: Earthscan, 2005.

[9]   "2012 Half year report", The World Wind Energy Association, Bonn, Germany, October, 2012.

[10]   A. Merabet, R. Beguenane, J. S. Thongam and I. Hussein, "Adaptive Sliding Mode Speed Control for Wind Turbine Systems", in 37th Annual Conference on IEEE Industrial Electronics Society, Melbourne, VIC, 2011.

[11]   X. Yang, X. Gong and W. Qiao, "Mechanical sensorless maximum power tracking control for direct-drive PMSG wind turbines", in IEEE Energy Conversion Congress and Exposition (ECCE), Atlanta, GA, 2010.

[12]   W. Liu, L. Chen, J. Ou and S. Cheng, "Simulation of PMSG wind turbine system with sensor-less control technology based on model reference adaptive system", in International Conference on Electrical Machines and Systems, Beijing, 2011

[13]   H. Polinder , "Overview of and trends in wind turbine generator systems", IEEE Power and Energy Society General Meeting, pp. 1-8, San Diego, CA, July 2011

[14]   F. Blaabjerg, Chen, Z., Teodorescu, R. E., & Iov, F. "Power Electronics in Wind Turbine Systems". IEEE 5th International IPEMC 2006 CES, pp. 1-11. Shanghai, Aug

2006.

[15]   S. Diaz, C. A. Silva, J. Juliet, & J. J. Miranda, "Indirect sensorless speed control of a
        PMSG for wind application. IEEE International Electric Machines and Drives
        Conference", 2009, pp. 1844-1850, Miami, FL, May 2009.

[16]   J. Marques, H. Pinheiro, H. Grundling, J. Pinheiro, and H. Hey, "A survey on variable-
        speed wind turbine system," Proceedings of Brazilian conference of electronics of
        power, vol. 1, pp. 732 -738, 2003.

[17]   A. M. O. Haruni, M. E. Haque, A. Gargoom and M. Negnevitsky, "Control of a Direct
        Drive IPM Synchronous Generator Based Variable Speed Wind Turbine with Energy
        Storage," in 36th Annual Conference on IEEE Industrial Electronics Society, Glendale,
        AZ, 7-10 Nov. 2010.

[19]   A.M. De Broe, S. Drouilhet, and V. Gevorgian, "A peak power tracker for small wind
        turbines in battery charging applications," IEEE Trans. Energy Convers., vol. 14, no. 4,
        pp. 1630-1635, Dec. 1999.

[20]   M. Chinchilla, S. Arnaltes, and J.C. Burgos, "Control of Permanent Magnet Generators
        Applied to Variable-Speed Wind-Energy Systems Connected to the Grid", IEEE Trans.
        Energy Convers., vol. 21, no. 1, Mar. 2006, pp. 130-135.

[21]   S. Morimoto, H. Nakayama, M. Sanada, and Y. Takeda, "Sensorless output
        maximization control for variable-speed wind generation system using
        IPMSG," Industry Applications Conference, 2003. 38th IAS Annual Meeting.

Conference Record of the , pp.1464-1471, vol.3, 12-16 Oct. 2003

[22]   J. Thongam, P. Bouchard, R. Beguenane, A. Okou, and A. Merabet, "Control of variable speed wind energy conversion system using a wind speed sensorless optimum speed MPPT control method. 37th Annual Conference on IEEE Industrial Electronics Society", pp. 855-860. Melbourne, VIC, Nov. 2011.

[23]   R. Datta and V.-T. Ranganathan, "A method of tracking the peak power points for a variable speed wind energy conversion system", IEEE Transactions on Energy Conversion, vol. 18, pp. 163-168, March 2003.

[24]   W. Qiao, L. Qu and R. G. Harley, "Control of IPM Synchronous Generator for Maximum Wind Power Generation Considering Magnetic Saturation," *IEEE Industry Applications Society,* vol. 45, pp. 1095-1105, May- June 2009.

[25]   A. Miller, E. Muljadi, D.S. Zinger, "A variable speed wind turbine power control" Energy Conversion, IEEE Transaction on power electronics, Volume: 12 Issue: 2, pp: 181 -186, June 1997.

[26]   N. Horiuchi, T. Kawahito, "Torque and power limitations of variable speed wind turbines using pitch control and generator power control". Power Engineering Society Summer Meeting, Vol. 1, pp: 638 –643, 2001.

[27]   H. Camblog, I. Mart´ınez de Alegr´ıa, M. Rodr´ıguez, and G. Abab, "Experimental evaluation of wind turbines maximum power point tracking controllers" Energy Conversion Management, vol. 47, no 18-19, pp.2846-2858, 2006.

[28] Y. Zhang and S. Ula, "Comparison and Evaluation of Three Main Types of Wind Turbines", in IEEE/PES Transmission and Distribution Conference and Exposition, Chicago, IL, pp. 21-24, April 2008.

[29] Y. Errami, M. Benchagra, M. Hilal, M. Maaroufi, and M. Ouassaid, "Control strategy for PMSG wind farm based on MPPT and direct power control", pp. 1125- 1130, Tangier, May 2012.

[30] A. Hamadi, S. Rahmani, A. Ndtoungou, K. Al-Haddad, and H. Kanaan, "A new Maximum Power Point Tracking with indirect current control for a three-phase grid-connected inverter used in PMSG-based wind power generation systems", 38th Annual Conference on IEEE Industrial Electronics Society- IECON, pp. 916- 923. Montreal, QC, Oct. 2012.

[31] T. Isobe, T. Kawaguchi, T. Sakazaki, and R. Shimada, "A simple and reliable rectifier for PMSG wind turbines by using series reactive compensator named MERS", 15th International Conference on Electrical Machines and Systems (ICEMS), 2012.

[32] F. Kendouli, K. Abed, K. Nabti, H. Benalla, and B. Azoui, "High performance PWM converter control based PMSG for variable speed wind turbine", First International Conference on Renewable Energies and Vehicular Technology (REVET), pp. 502- 507. Hammamet, 2012.

[33] S. Li, T. Haskew, R. Swatloski, and W. Gathings, "Optimal and Direct-Current Vector Control of Direct-Driven PMSG Wind Turbines", IEEE Transactions on Power Electronics, pp. 2325- 2337, May 2012.

[34]   K. Qu, Q. Niu, and J. Li, "A MPPT vector control method for wind power PMSG system", 7th International Power Electronics and Motion Control Conference (IPEMC), 2012 , (pp. 1264- 1267). Harbin, China, June, 2012.

[35]   M. Rosyadi, S. Muyeen, R. Takahashi, & J. Tamura, "New controller design for PMSG based wind generator with LCL-filter considered", XXth International Conference on Electrical Machines (ICEM), pp. 2112- 2118. Marseille, Sept. 2012.

[36]   S. Yang, & L. Zhang, "Modeling and Control of the PMSG Wind Generation System with a Novel Controller", Third International Conference on Intelligent System Design and Engineering Applications (ISDEA), (pp. 946- 949). Hong Kong, 2013.

[37]   Z. Zhang, Y. Zhao, W. Qiao, & L. Qu , "A space-vector modulated sensorless direct-torque control for direct-drive PMSG wind turbines", IEEE IAS . Las Vegas, NV, Oct, 2012.

[38]   S. Vaez-Zadeh, M. Zamanifar and J. Soltani, "Nonlinear Efficiency Optimization Control of IPM Synchronous Motor Drives with Online Parameter Estimation," in IEEE Power Electronics Specialists Conference, Jeju, June 2006.

[39]   K. Tan and S. Islam, "Optimum control strategies in energy conversion of PMSG wind turbine system without mechanical sensors", IEEE Trans. Energy Convers., vol. 19, no. 2, pp.392 -399 2004.

[40]   D. Xu, Z Luo, "A Novel AC-DC Converter for PMSG Variable Speed Wind Energy Conversion Systems," Power Electronics and Motion Control Conference, IPEMC '09,

IEEE 6th International, pp. 1117-1122, 2009.

[41]   A.O. Di Tommaso, R. Miceli, G.R. Galluzzo, M. Trapanese, "Optimum performance of permanent magnet synchronous generators coupled to wind turbines," Power Engineering Society General Meeting, IEEE, pp. 1-7, 2007.

[42]   Z. Xinyin, H. Minqiang, C. Xiaohu, W. Zaijun, "The research on grid-connected wind-power generation system of variable speed permanent magnet synchronous wind generator," Electric Utility Deregulation and Restructuring and Power Technologies,. DRPT 2008, Third International Conference on , pp. 2640-2646.

[43]   S. Bhowmik, R. Spee, and J. H. R. Enslin, "Performance optimization for doubly fed wind power generation systems", IEEE Trans. Ind. Appl., Vol. 35, No. 4, pp. 949-958, July/Aug. 1999.

[44]   H. Li, K. L. Shi and P. G. McLaren, "Neural-network-based sensorless maximum wind energy capture with compensated power coefficient," IEEE Trans. Ind. Appl., vol. 41, no. 6, pp. 1548-1556, Nov./Dec. 2005.

[45]   B. Boukhezzar and H. Siguerdidjane, "Nonlinear control of variable speed wind turbines without wind speed measurement," Proc. of 44th Conf. on Decision and Control, and the European Control Conference, Serville, Spain, pp. 3456-3461, 12-15 Dec. 2005.

[46]   T. Senjyu, S. Tamaki, E. Muhando, N. Urasaki, H. Kinjo, T. Funabashi, H. Fujita, and H. Sekine, "Wind velocity and rotor position sensorless maximum power point tracking

control for wind generation system," Renewable Energy, Vol. 31, pp. 1764-1775, 2006.

[47]   M. Ermis, H. B. Ertan, E. Akpinar, and F. Ulgut, "Autonomous wind energy conversion systems with a simple controller for maximum-power transfer," Proc. Inst. Elect. Eng. B, vol. 139, pp. 421-428, Sept. 1992.

[48]   X. Gong, X. Yang and W. Qiao, "Wind Speed and Rotor Position Sensorless Control for Direct Drive PMG Wind Turbines," IEEE Industry Applications Society, vol. 48, no. 1, pp. 3- 11 , Jan.-Feb. 2012.

[49]   J. H. R. Enslin and J. D. Van Wyk, "A study of a wind power converter with micro-computer based maximal power control utilizing an oversynchronous electronic Scherbius cascade," Renewable Energy, vol. 2, no. 6, pp. 551-562, 1992.

[50]   A. G. Abo-Khalil, D. C. Lee, and J. K. Seok, "Variable speed wind power generation system based on fuzzy logic control for maximum power output tracking", in Proc. 35th Annual IEEE-PESC'04, vol. 3, pp. 2039-2043, 2004.

[51]   T. Tanaka and T. Toumiya, "Output control by hill-climbing method for a small scale wind power generating system", Renewable Energy, vol. 12, no. 4, pp. 387-400, 1997.

[52]   Q. Wang and L. Chang, "An intelligent maximum power extraction algorithm for inverter-based variable speed wind turbine systems," IEEE Trans. Power Electron., vol. 19, no. 5, pp. 1242-1249, Sept. 2004.

[53]   K. Tan and S. Islam, "Optimum control strategies in energy conversion of PMSG wind turbine system without mechanical sensors," IEEE Trans. Energy Conv., vol. 19, no. 2,

pp. 392-399, June 2004

[54]   M. G. Simoes, B. K. Bose, and R. J. Spiegal, "Fuzzy logic-based intelligent control of a variable speed cage machine wind generation system", IEEE Trans. Power Electron., vol. 12, no.1, pp. 87-95, Jan. 1997.

[55]   E. Koutroulis, K. Kalaitzkis, "Design of a maximum power tracking system for wind-energy-conversion applications", IEEE Trans. on Ind. Electronics, Vol.53, No.2, pp.486-494, April 2006.

[56]   Y. Jia, Z. Yang, B. Cao, "A new maximum power point tracking control scheme for wind generation", POWERCON 2002, Proceedings of International Conference on Power System Technology, Vol.1, 1 pp. 144 - 148, Oct. 13-17, 2002, Kunming, China.

[57]   M. G. Simoes, B. K. Bose, and R. J. Spiegal, "Fuzzy logic-based intelligent control of a variable speed cage machine wind generation system", IEEE Trans. Power Electron., vol. 12, no.1, pp. 87-95, Jan. 1997.

[58]   A. G. Abo-Khalil, D. C. Lee, and J. K. Seok, "Variable speed wind power generation system based on fuzzy logic control for maximum power output tracking", in Proc. 35th Annual IEEE-PESC'04, vol. 3, pp. 2039-2043, 2004.

[59]   K. Rajashekara, & A. Kawamura, "Sensorless control of permanent magnet AC motors. 20th International Conference on Industrial Electronics, Control and Instrumentation", 1994. IECON '94., (pp. 1589- 1594 vol.3). Bologna.

[60]   O. Benjak and D. Gerling, "Review of position estimation methods for IPMSM drives

without a position sensor part II: Adaptive methods", in Electrical Machines (ICEM), XIX International Conference on, Rome, 6-8 Sept, 2010.

[61]   O. Benjak and D. Gerling, "Review of position estimation methods for IPMSM drives without a position sensor part I: Nonadaptive methods", in Electrical Machines (ICEM) XIX International Conference on, Rome, 6-8 Sept 2010.

[62]   M. Tursini, R. Petrella and F. Parasiliti, "Initial rotor position estimation method for PM motors", IEEE Trans. Ind. Applicat., vol. 39, pp. 1630-1640, Nov./Dec., 2003.

[63]   J. Jang, J. Ha and A. Testa, "Analysis of permanent-magnet machine for sensorless control based on high-frequency signal injection", IEEE Trans. Ind. Applicat., vol. 40, pp. 1595-1603, Nov./Dec., 2004.

[64]   A. Qiu and B. Wu, "Sensorless control of permanent magnet synchronous motor using extended Kalman filter", in Proc. Conf. Of CCECE 2004, Niagara Falls, pp.1557-1562.

[65]   Y. Yamamoto, Y. Yoshida and T. Ashikaga, "Sensorless control of PM motor using full order flux observer", IEEJ Trans. Ind. Applt., vol. 124, pp. 743-749, Aug. 2004.

[66]   M. Elbuluk and C. Li, "Sliding mode observer for wide-speed sensorless control of PMSM drives", in Conf. Rec. IEEE-IAS Annu. Meeting, vol. 1, 2003, pp. 480–485.

[67]   Z. Yan and V. Utkin, "Sliding mode observers for electric machines-an overview," in Conf. Rec. IEEE-IES 28th Annu. Meeting IECON02, vol. 3, 2002, pp. 1842–1847.

[68]   R. G. Berstecher, R. palm and H. D. Unbehauen, "An adaptive fuzzy sliding mode controller", IEEE Trans. Power Electron., vol. 48, pp. 18-31, 2001

[69]   M. J. Corley, and R. D. Lorenz, "Rotor position and velocity estimation for permanent magnet synchronous machine at standstill and high speed", in Conf. Rec. IEEE-IAS Annu. Meeting, vol. 1, 1996, pp. 36-41.

[70]   A. Consoli, G. Scarcella and A. Testa, "Industry application of zero-speed sensorless control techniques for PM synchronous motors", IEEE Trans. Ind. Applicat., vol. 37, pp. 513-521, March/April, 2001.

[71]   Y. S. Han, J. S. Choi and Y.S. Kim, "Sensorless PMSM drive with a sliding mode control based adaptive speed and stator resistance estimator", IEEE Trans. Magnetics, vol. 36, pp. 3588-3591, Sept. 2000.

[72]   Z. M. Peixoto, et al., "Speed control of permanent magnet motors using sliding mode observers for induced emf, position and speed estimation", in Conf. Rec. IEEE-IAS Annu. Meeting, vol. 2, 1995, pp. 1023–1028.

[73]   G. el Murr, D. Giaouris, and J.W. Finch, "Universal PLL strategy for sensorless speed and position estimation of PMSM", IEEE Region 10 Colloquium and the Third International Conference on Industrial and Information Systems, pp.1-6, 2008

[74]   R. P. Burgos, P. Kshirsagar, A. Lidozzi, J. Jang, "Design and Evaluation of a PLL-Based Position Controller for Sensorless Vector Control of Permanent-Magnet Synchronous Machine", IEEE Industrial Electronics, pp.5081-5086, 2006.

[75]   M. Preindl and E. Schaltz, "Sensorless Model Predictive Direct Current Control Using Novel Second Order PLL-Observer for PMSM Drive Systems", IEEE Transactions on

Industrial Electronics, vol.99 ,2010.

[76]   Z. Zhang and J. Feng, "Sensorless Control of Salient PMSM with EKF of Speed and Rotor Position", International Conference on Electrical Machines and Systems, pp.1625-1628, 2008.

[77]   A. Wang, Q. Wang and C. Hu," An EKF for PMSM Sensorless Control Based on Noise Model Identification Using Ant Colony Algorithm," International Conference on Electrical Machines and Systems, pp.1-4, 2009.

[78]   X. Xiang and Y. He," Sensorless Vector Control Operation of a PMSM by Rotating High-Frequency Voltage Injection Approach," International Conference on Electrical Machines and Systems, pp.752-756.

[79]   T. Halkosaari, "Speed Sensorless Vector Control of a Redundant Permanent Magnet Wind Power Generator," Industrial Electronics, pp.2595-2600, 2007.

[80]   Y. Li and H. Zhu, "Sensorless control of permanent magnet synchronous motor–a survey," in Proc. of IEEE Vehicle Power and Propulsion Conf., Harbin, China, Sept. 2008, pp. 1-8.

[81]   C. Nitayotan and S. Sangwongwanich," A Filtered Back EMF Based Speed-Sensorless Induction Motor Drive," Industry Applications Conference, vol.2, pp.1224-1231, 2001.

[82]   Y. Liang and Y. Li, "Sensorless control of PM synchronous motors based on MRAS method and initial position estimation," in Proc. of IEEE International Conf. on Electrical Machines and Systems, Beijing, China, Nov. 2003, vol. 1, pp. 96-99.

[83] Y. S. Kim, S. K. Kim, and Y. A. Kwon, "MRAS based sensorless control of permanent magnet synchronous motor," in Proc. of IEEE Annual Conf. of the Society of Instrument and Control Engineers of Japan, Fukui, Japan, Aug. 2003, vol. 2, pp. 1632-1637.

[84] Y. Sozer and D. A. Torrey, "Adaptive flux weakening control of permanent magnet synchronous motor," in Conf. Rec. IEEE-IAS Annu. Meeting, vol. 1, St. Louis, MO, 1998, pp. 475–482

[85] E. Nipp, "Alternative to field-weakening of surface-mounted permanent-magnet motors for variables-speed drives," in Conf. Rec. IEEE-IAS Annu. Meeting, vol. 1, 1995, pp. 191–198.

[86] Uddin, M.N.; Azizur Rahman, M., "High-Speed Control of IPMSM Drives Using Improved Fuzzy Logic Algorithms," Industrial Electronics, IEEE Transactions on , vol.54, no.1, pp.190,199, Feb. 2007

[87] J. A. Tapia, F. Leonardi, and T. A. Lipo, "Consequent-pole permanent-magnet machine with extended field-weakening capability," IEEE Trans. Ind. Applicat., vol. 39, pp. 1704-1709, Nov./Dec., 2003.

[88] R. Dhaouadi and N. Mohan, "Analysis of current-regulated voltage-source inverters for permanent magnet synchronous motor drives in normal and extended speed ranges," IEEE Trans. Energy Conv., vol. 5, pp. 137-144, Mar. 1990.

[89] S. D. Sudhoff, K. A. Corzine and H. J. Hegner, "A flux-weakening strategy for current-regulated surface-mounted permanent-magnet machine drives," IEEE Trans. Energy

Conv., vol. 10, pp. 431-437, Sept. 1995.

[90]   B. Bae, N. Patel, S. Schulz, and S. Sul, "New Flux Weakening Technique for High Saliency Interior Permanent Magnet Motor", industry application conference, 2003.38th IAS Annual Meeting. Conference Record of the, Vol.2, Oct 12-16, 2003, pp. 898-905.

[91]   L. Dongyun, N.C. Kar, "A review of flux-weakening control in permanent magnet synchronous machines", Vehicle Power and Propulsion Conference (VPPC), 2010 IEEE, pp: 1 - 6

[92]   S. Campbell and H. A. Toliyat, "DSP-Based Electromechanical Motion Control", CRC Press, 2003

[93]   T.A. Lipo, "Comparative Analysis of Permanent Magnet AC Machines in Variable Speed Applications." University of Wisconsin-Madison, ECE Dept., WEMPEC Research Report No. 82-12, Sept. 1982.

[94]   R.S. Colby, "Classification of Inverter Driven Permanent Magnet Synchronous Motors." Conference Record of IEEE Industry Applications Society Annual Meeting, Vol.1, pp.1– 6, 2-7 Oct. 1988.

[95]   K. Zhou and Danwei Wang, "Relationship Between Space-Vector Modulation and Three-Phase Carrier-Based PWM: A Comprehensive Analysis," IEEE trans. on IE, vol. 49, no. 1, pp. 186-196, FEB, 2002.

[96]   B. K. Bose, "Pulse Width Modulation Techniques," in Modern Power Electronics and AC Drives, Prentice Hall, pp. 210-239.

[97]   M. Konghirun, "A three-phase space vector based PWM rectifier with power factor control", Proc. Power Conversion conference 2-5 April, Nagoya, Japan, pp. 57-61, 2007

[98]   W. Ke-xin, & W. Shui-ming, "Modeling and Simulation of Three-Phase Voltage Source PWM Rectifier", International Conference on Advanced Computer Theory and Engineering, (pp. 982- 986). Phuket, 2008.

[99]   V. Blasko, V. Kaura, "A new mathematical model and control of a three-phase AC-DC voltage source converter", IEEE Trans. on Power Electronics, vol. 12, no. 1, pp. 116-122, January 1997.

[100]   H. M. Kojabadi, and M. Ghribi, "MRAS-based adaptive speed estimator in PMSM drives," Proceedings of Advanced Motion Control Conference, pp. 569–572, Istanbul, Turkey, 27–29 March 2006.

[101]   Md. M. I. Chy, "Development and Implementation of Various Speed Controllers for Wide Speed Range Operation of IPMSM Drive", MSc. Thesis, Lakehead Univeristy, Thunder Bay, July 2007

Appendix –A

IPMSM Parameters

Number of phases = 3

Number of poles = 6

Rated Frequency = 87.5 Hz

Rated power = 5 HP

Rated input line-to-line voltage = 183 V

q-axis inductance, L_q = 6.42 mH

d-axis inductance, L_d = 5.06 mH

Stator resistance per phase R = 0.242 ohm

Inertia constant J = 0.013 kg.m^2

Rotor damping constant B_m = 0.001 Nm/rad/sec

Permanent magnet flux linkage = 0.24 volts/rad/sec

Appendix –B
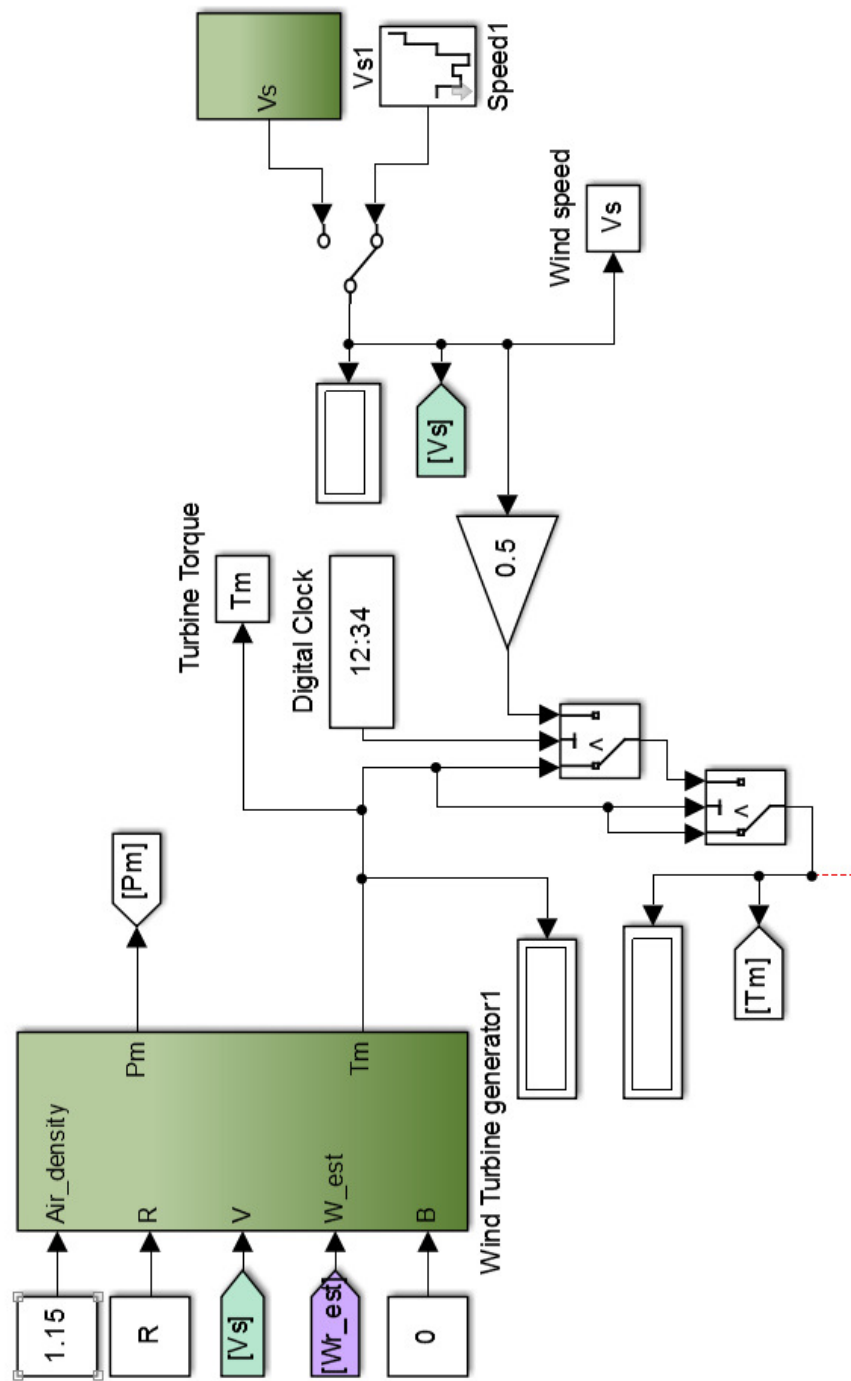
Simulink Blocks for Simulation

App. B. 1 Overall WT model.
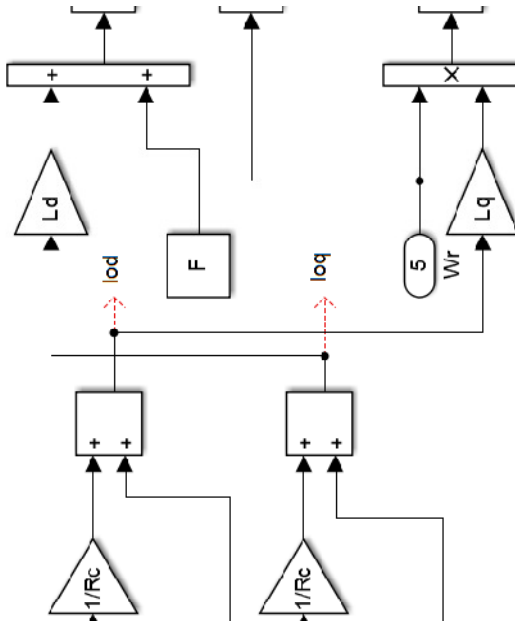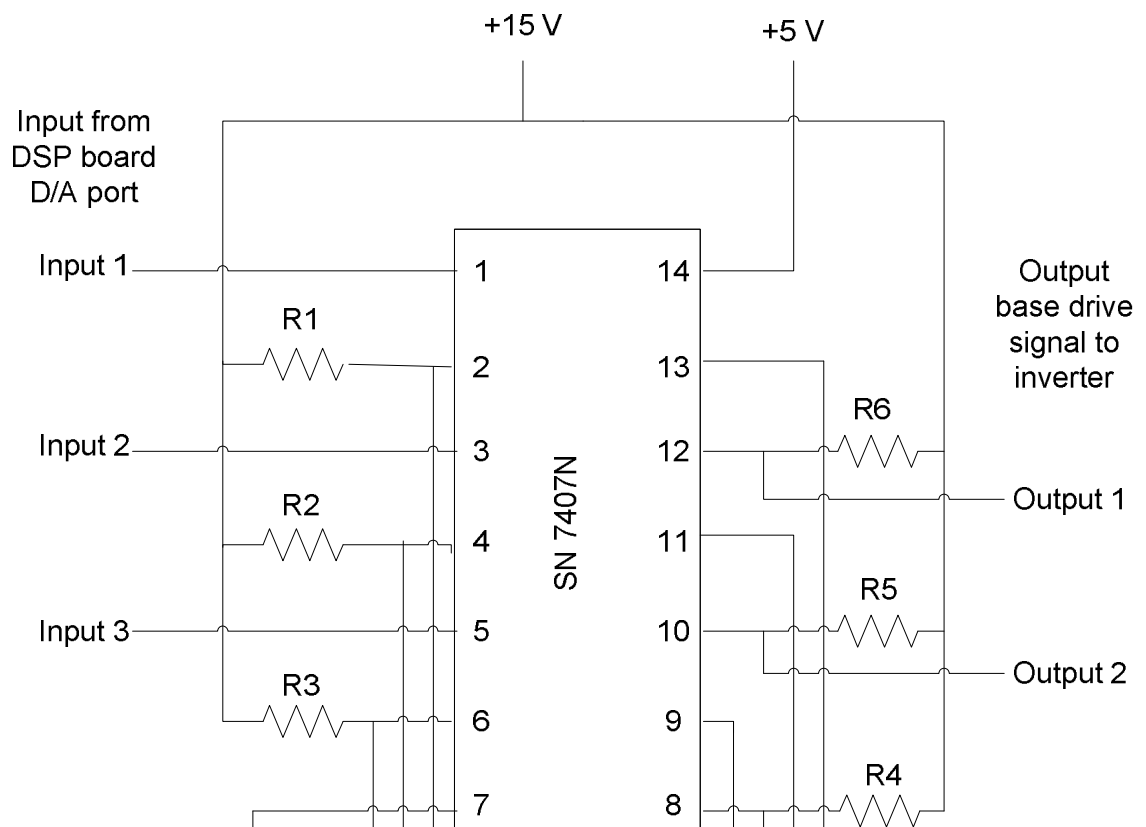
118
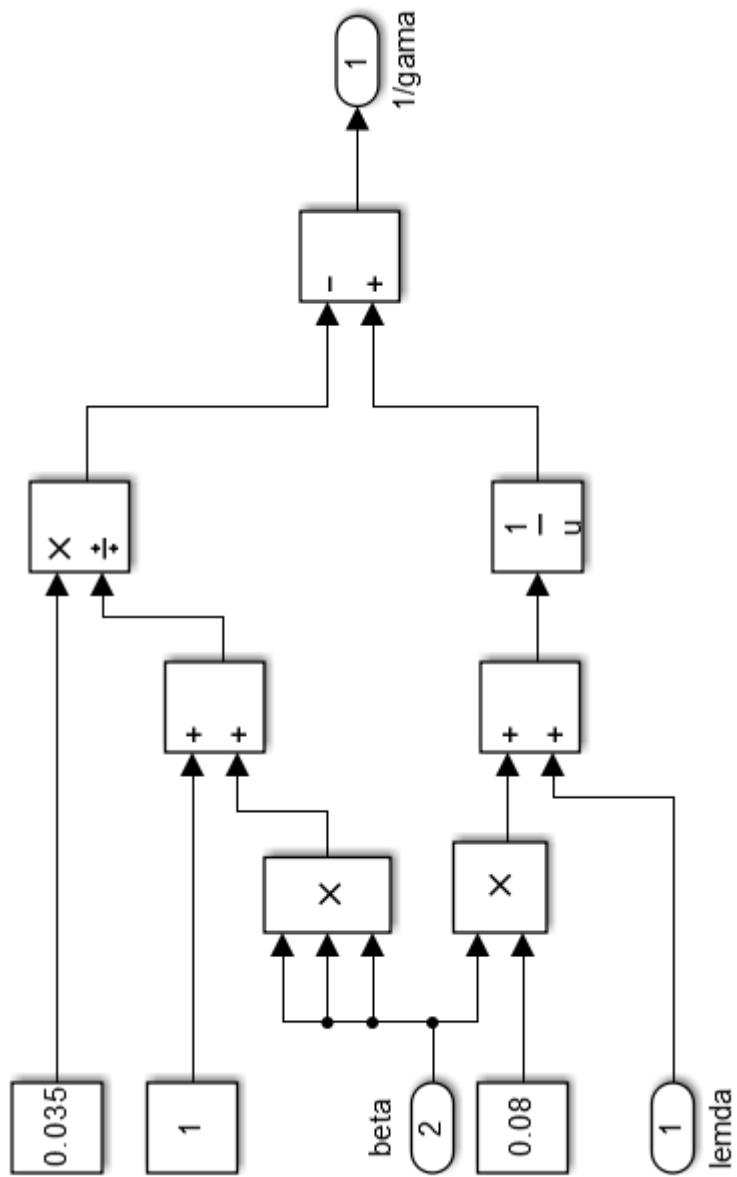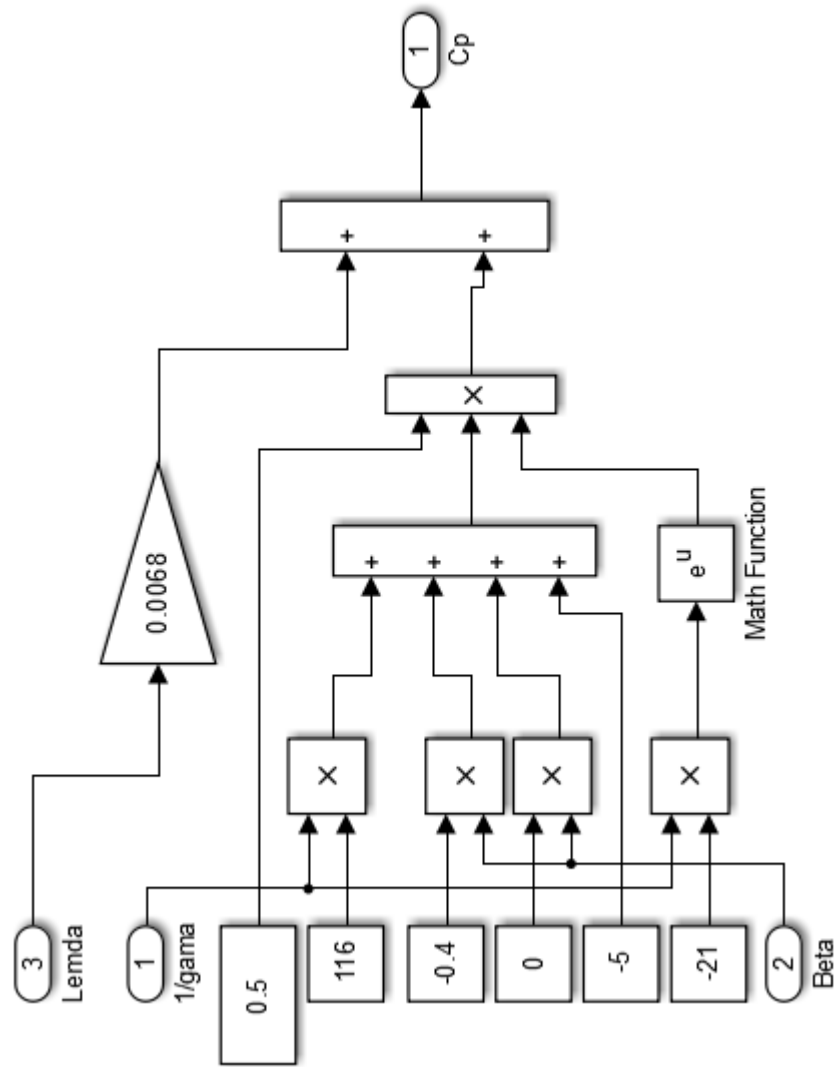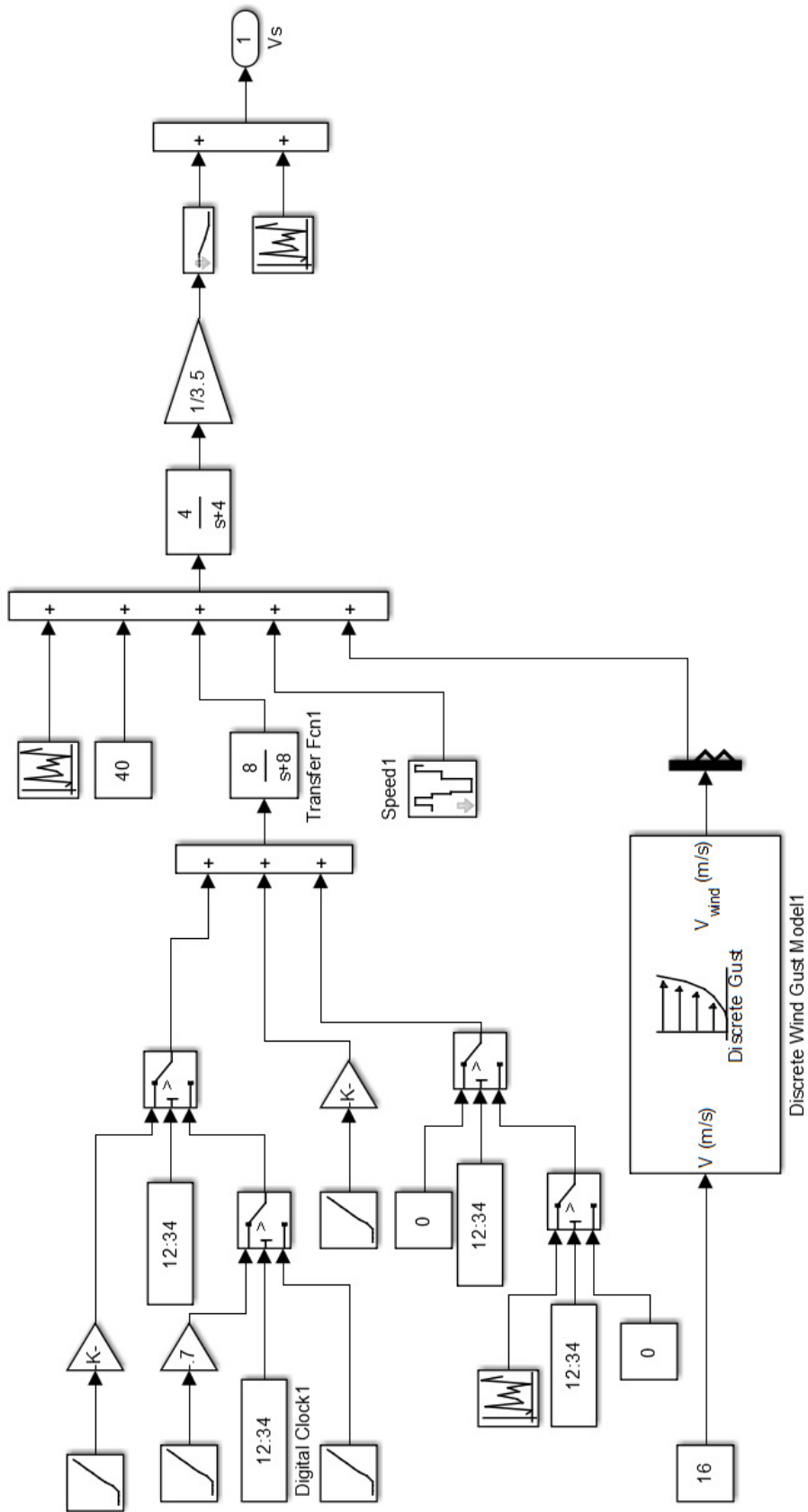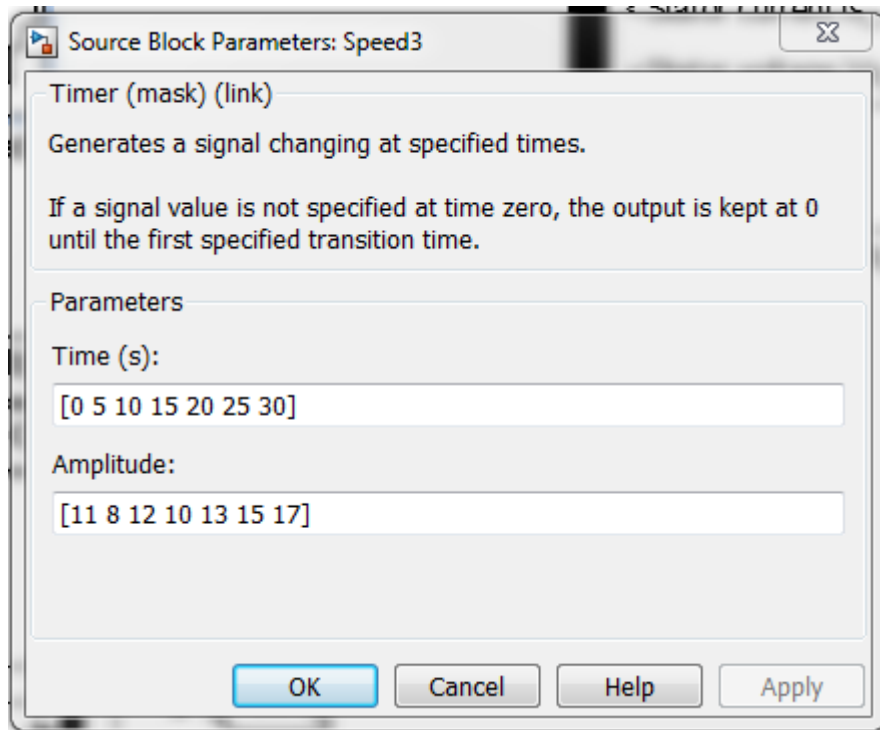
App. B. 6 Wind speed step changes.

123
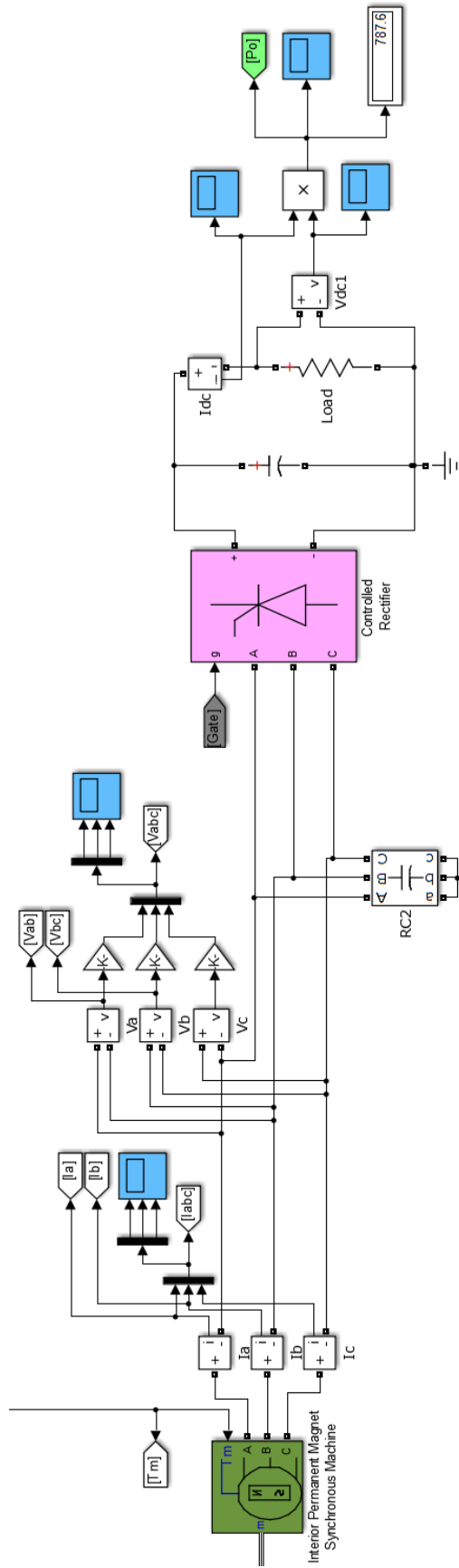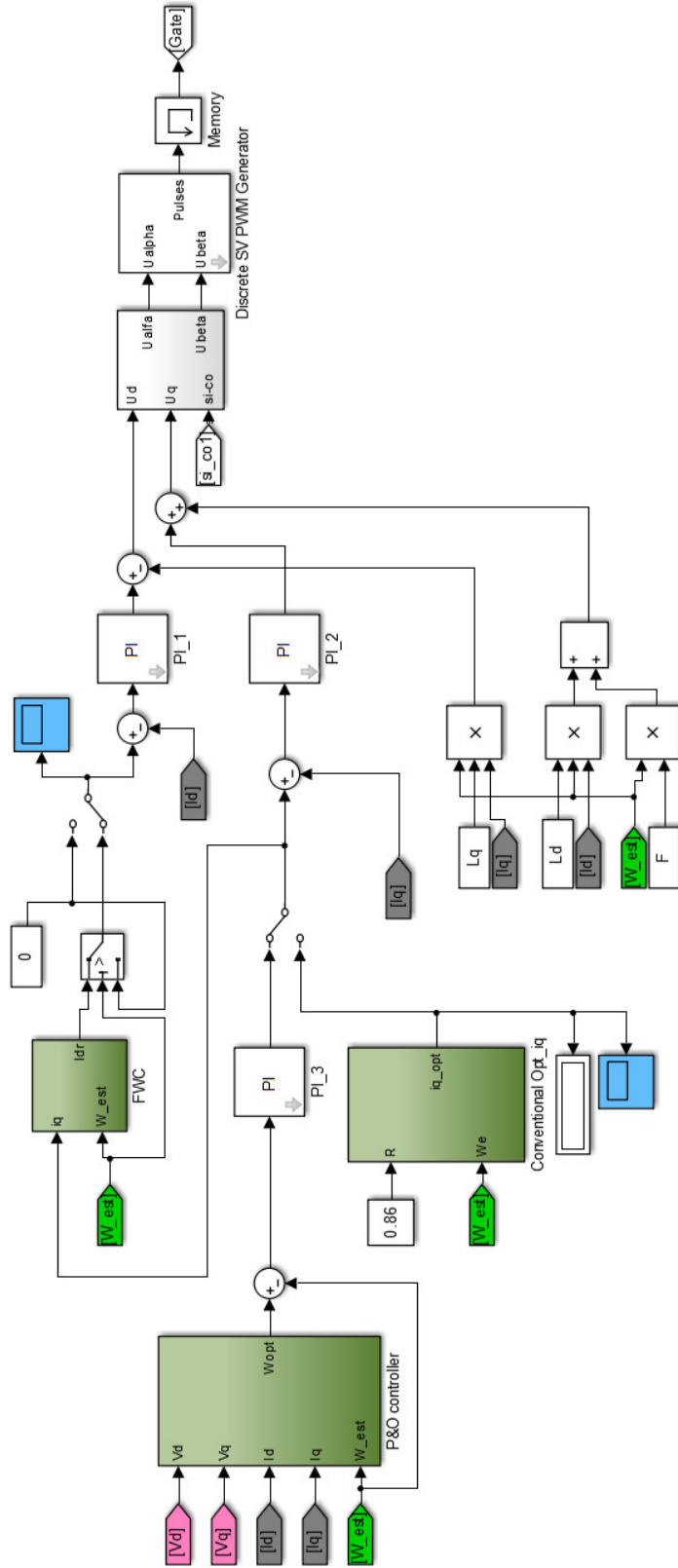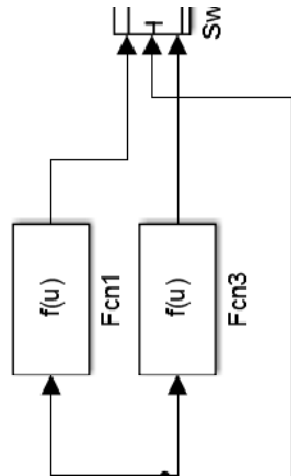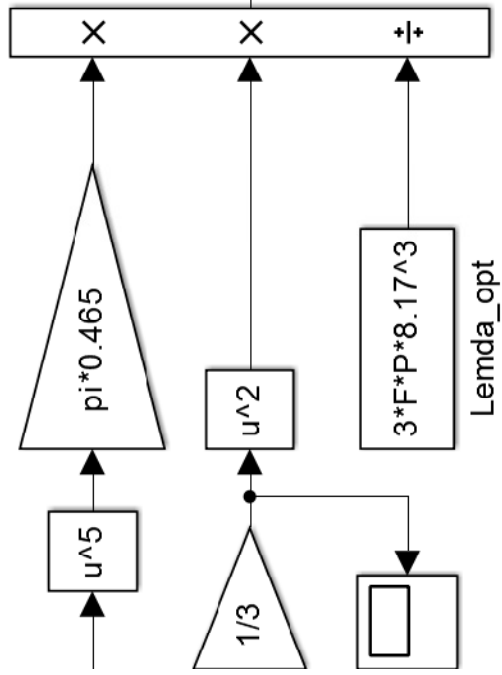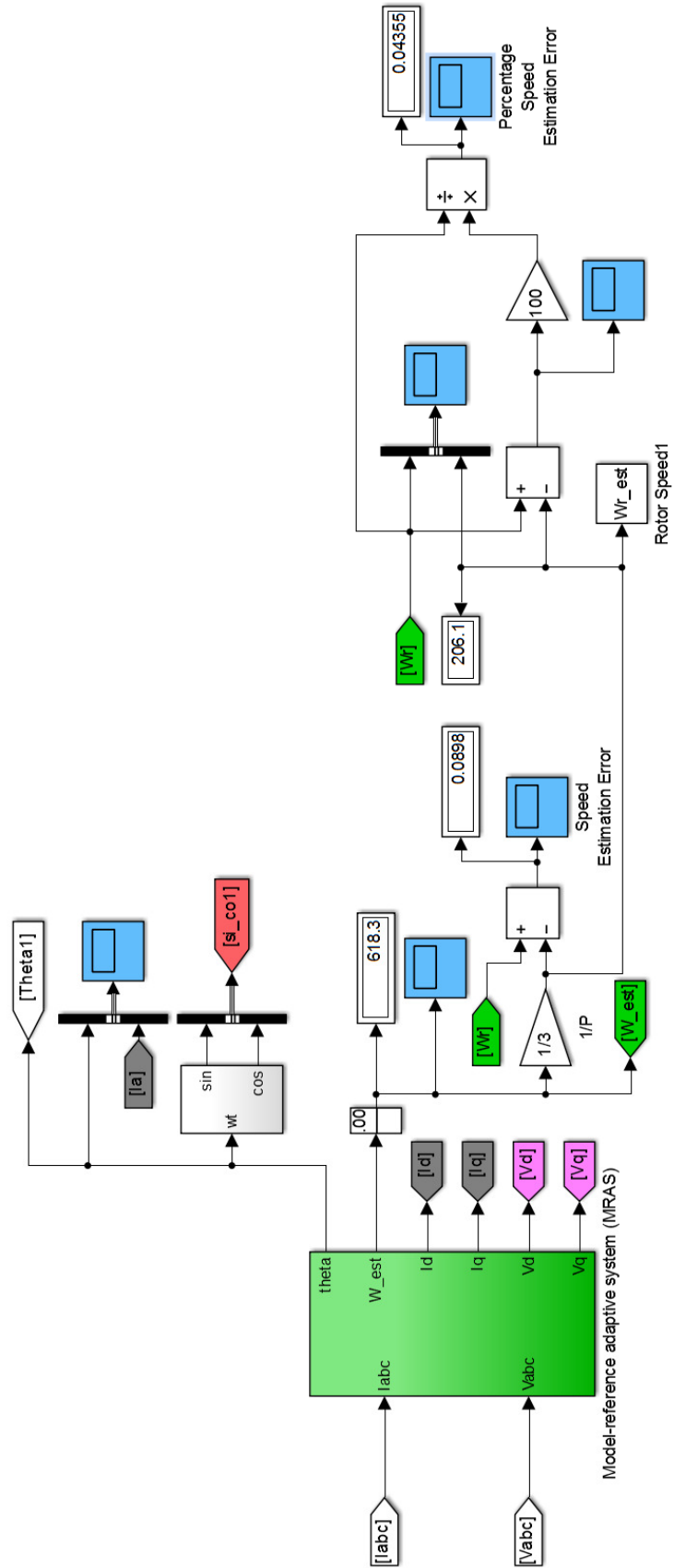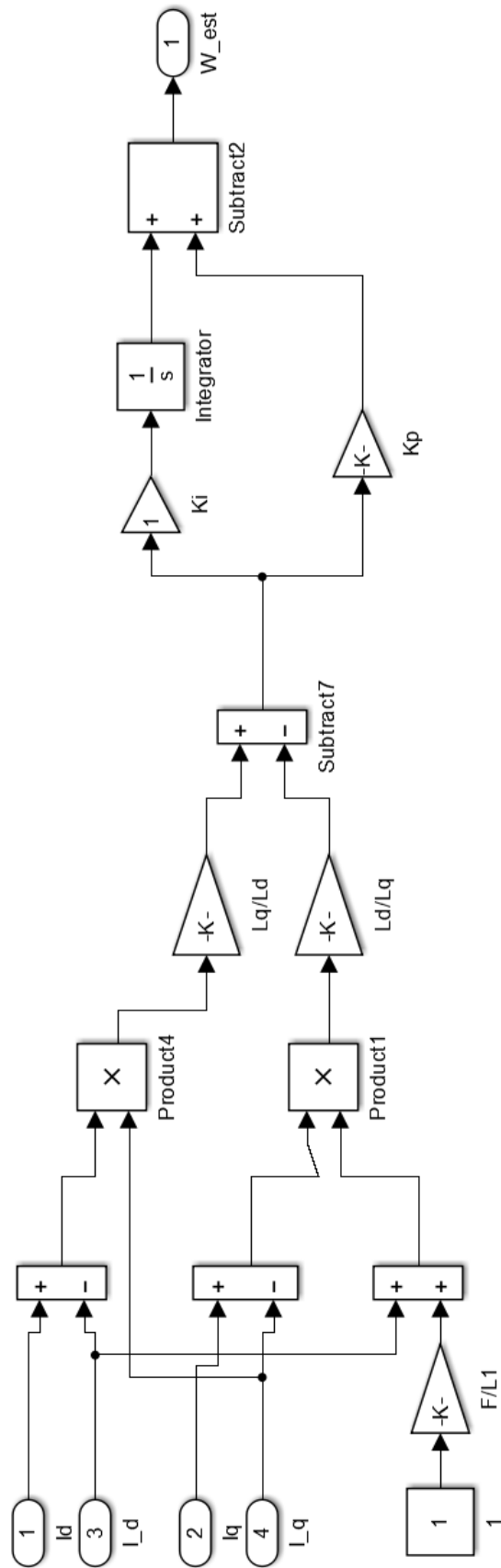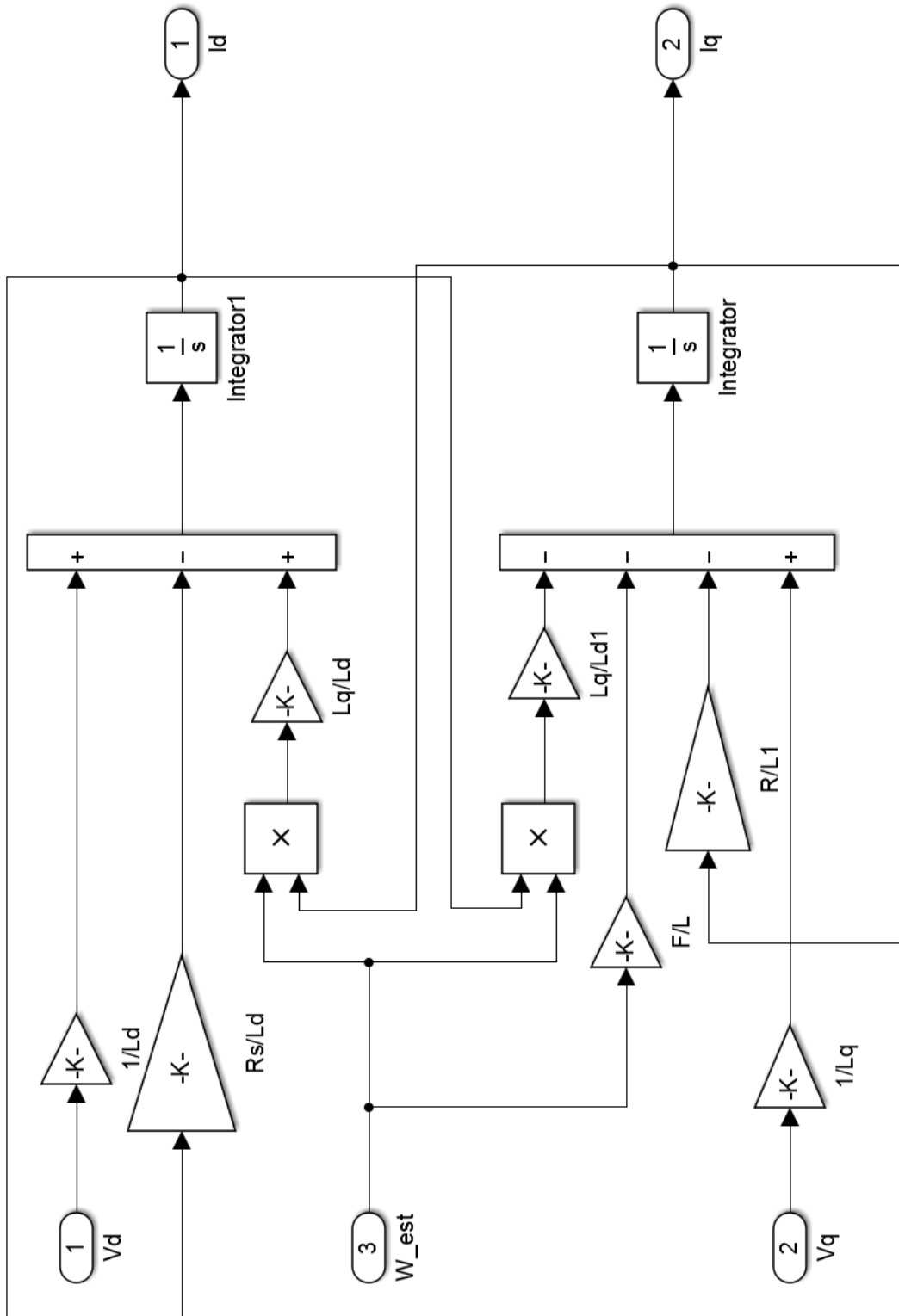
Appendix C

Drive and Interface Circuit

Base drive circuit for the inverter and interface circuit for the current sensor
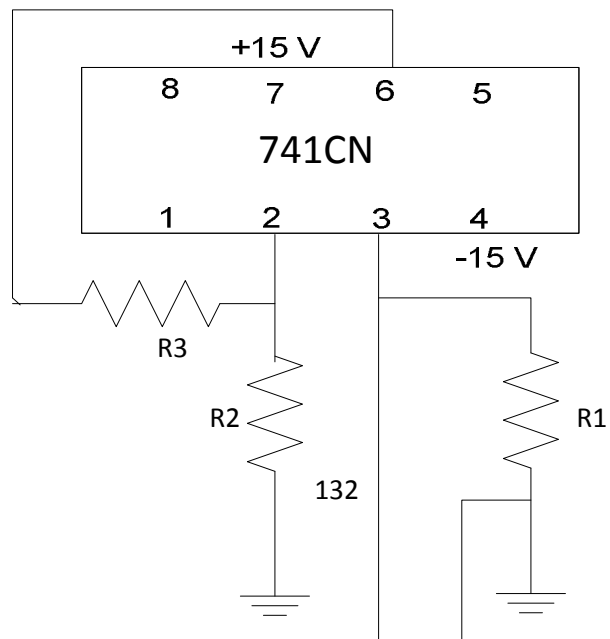
R1= R2 = R3 = R4 = R5 = R6 = 1.5k

Gain of Op-Amp (741CN) = 1+R3/R2

Magnitude of resistors:

	Current sensor for phase 'a'	Current sensor for phase 'b'
R1	98.7 ohm	99 ohm
R2	1.8 k	2 k
R3	5.5 k	5.1 k

Appendix D

Real-Time Simulink Model